약학박사학위논문

핵 수용체 RORα의 미토콘드리아 역동성 및 자가포식 작용에 대한 연구

The roles of hepatic nuclear receptor RORα in mitochondrial dynamics and autophagy

2019년 8월

서울대학교 대학원

약학과 병태생리학전공

김 현 지

핵 수용체 RORα의 미토콘드리아 역동성 및 자가포식 작용에 대한 연구

The roles of hepatic nuclear receptor RORα in mitochondrial dynamics and autophagy

지도교수 이 미 옥

이 논문을 약학박사 학위논문으로 제출함

2019년 8월

서울대학교 대학원

약학과 병태생리학 전공

김 현 지

김현지의 박사학위논문을 인준함

2019년 7월

위 원 장 이 호 영 (인)

부위원장 이 정 원 (인)

위 원 김 명 미 (인)

위 원 이 윤 희 (인)

위 원 이 미 옥 (인)

ABSTRACT

The roles of hepatic nuclear receptor RORα in mitochondrial dynamics and autophagy

Hyeon-Ji Kim
Department of Pathology & Physiology
College of Pharmacy
The Graduate School
Seoul National University
Advisor: Prof. Mi-Ock Lee

Nonalcoholic fatty liver disease ranges from simple steatosis to nonalcoholic steatohepatitis (NASH), which can eventually progress to irreversible cirrhosis and to hepatocarcinoma. About 10% to 20% of patients with hepatic steatosis develop NASH, a disease stage that is characterized by increased oxidative stress and lipotoxicity and leads to cellular injury and chronic inflammation. Mitochondrial dysfunction may play a key role in the progression of steatosis to NASH; however, the molecular mechanism that

controls the structure and function of mitochondria in NASH is not clearly understood. Here, I demonstrated that the orphan nuclear receptor retinoic acid-related orphan receptor α (RORα) is a regulator of mitochondrial fission and autophagy thereby contributes to mitochondrial quality control.

First, I observed that liver-specific RORα knockout mice (RORα-LKO) were more susceptible to high-fat diet (HFD)-induced NASH. Results from an RNA-seq analysis combined with public ChIP-seq data (GSE59486) revealed that RORα-mediated transcription was significantly associated with electron transport chain and ATP synthesis. Concordantly, mitochondrial structure was defective, mitochondrial fission was abnormal, and the fission proteins Bnip3 and phospho-Drp1 were downregulated in the hepatocytes of RORα-LKO. RORα enhanced the oxygen consumption rate and expression of genes associated with mitochondrial quality control. Finally, I observed the positive correlation of the expression levels of Bnip3 and PGC-1α with those of RORα in patients with steatohepatitis. These results suggest that the induction of mitochondrial fission of RORα in hepatocytes can protect against development of NASH.

Next, I investigated the effects of RORα on autophagy including mitophagy and lipophagy in progression of NASH. In HFD-induced NASH model, autophagosomes were less in the livers of RORα-LKO with accumulation of LC3-Ⅱ, NBR1, and lysosome-specific enzyme procathepsin D. Number of

autophagic puncta co-stained with mitochondria and lipid were decreased after treatment with bafilomycin A1 in the hepatocytes of RORα-LKO. Using the ratio of mcherry-LC3 to GFP-LC3, I found that the autophagic flux was downregulated in the hepatocytes of RORα-LKO. In addition, deletion of RORα decreased co-localization of mitochondria and lipid droplets with lysosomes, suggesting decreased mitophagy and lipophagy with lysosomal defects in the hepatocytes. Overexpression of RORα in the primary hepatocytes increased autophagic flux and expression of genes associated with autophagy and lysosomal function with inactivation of mTOR pathway. In addition, mTOR pathway was activated in HFD-induced RORα-LKO mouse model.

Together, I demonstrated that RORα mediates mitochondrial fission and autophagy under nutrient-overloaded conditions and propose RORα as a potential therapeutic target in treatment of NASH.

keywords : NASH, mitochondrial dynamics, autophagy, RORα

Student Number **: 2011-21714**

CONTENTS

LIST OF TABLES

LIST OF FIGURES

Ⅰ. INTRODUCTION

1. Non-alcoholic steatohepatitis (NASH)

1.1. Pathogenesis of NASH

Nonalcoholic fatty liver disease (NAFLD) ranges from simple steatosis to nonalcoholic steatohepatitis (NASH), which can eventually progress to irreversible cirrhosis and to hepatocarcinoma (HCC). Nonalcoholic fatty liver disease is caused by dietary factors, drugs, genetic factors, and is one of the systemic metabolic diseases, which is likely to accompany diabetes, hyperlipidemia, and cardiovascular disease. About 10% to 20% of patients with hepatic steatosis develop NASH. Increased serum fatty acids due to abdominal obesity cause liver lipid accumulation and also activation of hepatic stellate cells and kupffer cells through adipokines. NASH occurs due to inflow of persistent and complex pathological factors (Byrne and Targher, 2015; Cohen et al., 2011). NASH is a disease stage that is characterized by increased oxidative stress and lipotoxicity and leads to cellular injury and chronic inflammation (Fuchs and Sanyal, 2012; Koek et al., 2011; Schattenberg and Schuppan, 2011). However, the molecular mechanism underlying the development of NASH from steatosis remains unclear. Therefore, it is necessary to study the molecular mechanisms involved in the pathogenesis of nonalcoholic steatohepatitis. This may lead to more effective therapeutic strategy for cure of nonalcoholic steatohepatitis

1.2. Need of drug development for NASH

Unlike alcoholic fatty liver disease, the onset of nonalcoholic fatty liver disease is increasing over time. Despite the increasing incidence of nonalcoholic fatty liver disease and the severity of liver cirrhosis and liver cancer due to disease progression, there is currently no drug for the treatment of nonalcoholic fatty liver disease. Currently, hyperlipemia therapy, diabetes therapy, insulin resistance therapy and anti-inflammatory drugs, which improve non-alcoholic fatty liver disease through the correction of risk factors and antioxidants such as vitamin E, are recommended as drugs for treating non-alcoholic fatty liver disease. However, there is a need for further study of adverse effects in long-term treatment, appropriate dosing periods, treatment doses, and there are safety concerns for long-term administration of vitamin E (Hamishehkar et al., 2016).

PPAR agonists are the drugs of choice for the treatment of nonalcoholic steatohepatitis. However, as a PPARα agonist, fibrates are used to treat hypertriglyceridemia but have no significant effect on NAFLD treatment. In the case of PPARβ/δ agonist (GW501516), it was withdrawn due to stability problems. The PPARγ agonist, pioglitazone, did not effectively reduce liver fibrosis and showed side effects such as weight gain and increased risk of cardiovascular disease. In addition, lipid-altering agents and incretin-based

therapies have been used to treat NASH (Oseini and Sanyal, 2017; Sumida and Yoneda, 2018).

Currently, obeticholic acid, a farnesoid X receptor agonist has been shown to reduce NAFLD activity in a randomized phase IIb FLINT trial and are likely to be marketed after approval (Neuschwander-Tetri et al., 2015). However, as side effects, pruritus is present and there is a limit for treatment to the patients because of the decrease of high-density lipoprotein cholesterol and the increase of low-density lipoprotein. There is a need to develop drugs for the treatment of nonalcoholic fatty liver disease that can overcome these side effects.

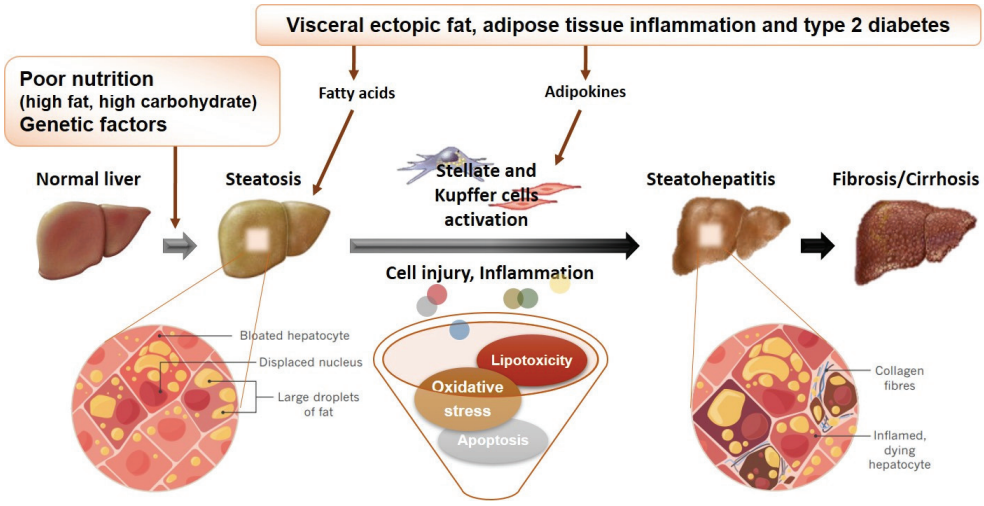

Figure 1. Pathogenesis of NAFLD

NAFLD is caused by dietary factors, drugs, genetic factors, and is one of the systemic metabolic diseases. Increased serum fatty acids due to abdominal obesity cause liver lipid accumulation and also activation of hepatic stellate cells and kupffer cells through adipokines (Byrne and Targher, 2015; Cohen et al., 2011; Drew, 2017).

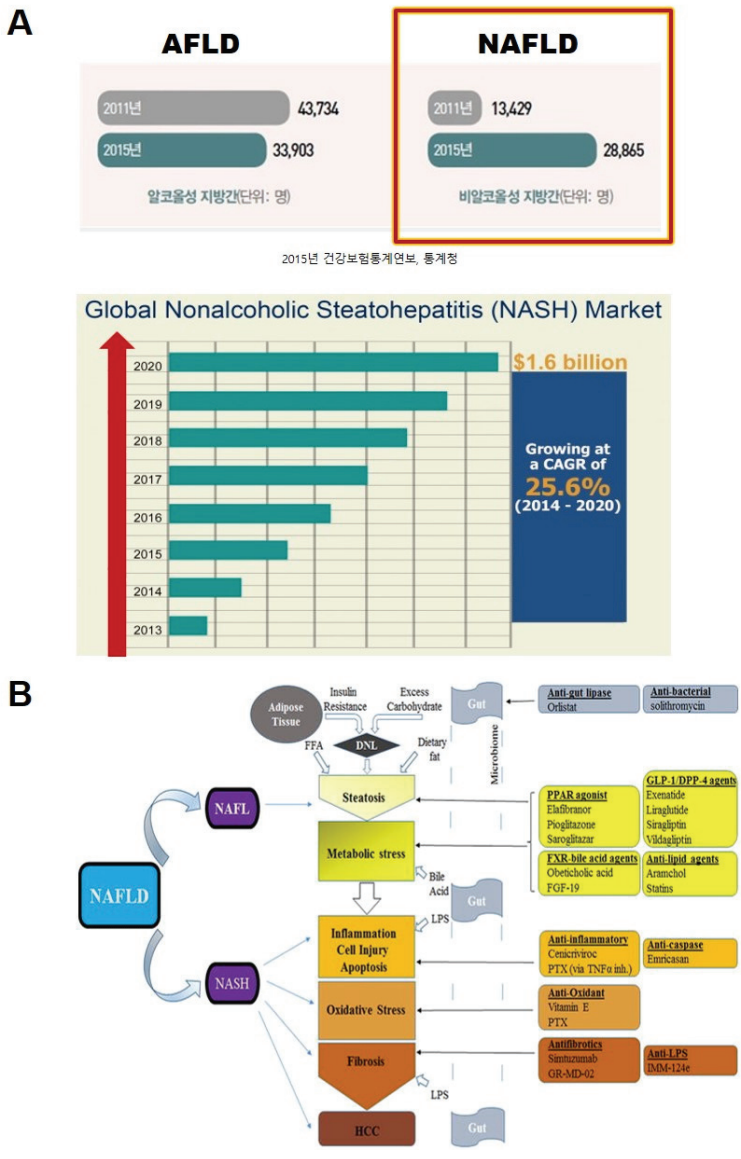

Figure 2. Need of drug development for NAFLD

(A) The onset of nonalcoholic fatty liver disease and global NASH market are increasing over time.

(B) Therapies in NAFLD/NASH (Oseini and Sanyal, 2017; Sumida and Yoneda, 2018).

2. Role of mitochondria in NASH

2.1. Mitochondrial dysfunction in NASH

Oxidative stress, lipid toxicity, and cell death, all of which are due to malfunction of the mitochondria (Fuchs and Sanyal, 2012; Koek et al., 2011; Schattenberg and Schuppan, 2011). Actually, the features that distinguish NASH from steatosis include defects in mitochondrial structure and function, as the mitochondria in the hepatocytes of patients with NASH are swollen and have an abnormal morphology with a loss of cristae, and the activities of mitochondrial respiratory complexes are impaired in these patients (Perez-Carreras et al., 2003; Sanyal et al., 2001). Thus, mitochondrial dysfunction is considered as a central cause of the development of steatosis to NASH, and the identification of the molecular mechanisms that control the structure and function of mitochondria will contribute to the understanding of the progression of NAFLD.

2.2. Mitochondrial quality control (Fission, Fusion, Biogenesis, Mitophagy)

Mitochondria are the main organelles that are required for energy-yielding metabolism via the oxidative phosphorylation (OXPHOS) of

glucose and lipids. Maintaining mitochondrial quality is critical for cellular survival, because mitochondria are frequently vulnerable to reactive oxygen species (ROS), a side product of electron transfer. Multiple quality control mechanisms contribute to the maintenance of mitochondrial activity and function, including biogenesis, fission, fusion, and mitochondria-selective autophagy (mitophagy) (Palikaras and Tavernarakis, 2014). New mitochondria are generated by mitochondrial fission resulting from a fragmentation of the mitochondrial network, especially to reduce oxidative stress in nutrient-overloaded conditions. In contrast, mitochondrial fusion is stimulated by energy demand, to increase metabolic efficiency. The core machineries of mitochondrial dynamics include the dynamin-1-like protein (Drp1), fission 1 homolog (Fis1), mitochondrial fission factor, BCL2/adenovirus E1B 19 kDa interacting protein 3 (Bnip3), mitofusin 1, 2 (Mfn1, 2), and optic atrophy 1 (Opa1) (Westermann, 2010). Mitochondrial biogenesis is regulated by a nuclear - mitochondrial network (Finley and Haigis, 2009). In this network, the peroxisome proliferator-activated receptor γ coactivator (PGC-1α) acts as a master regulator that modulates the activity and expression of nuclear respiratory factors, followed by the induction of the transcription factor A, mitochondrial (TFAM), which stimulates mitochondrial gene expression (Scarpulla, 2008). Nuclear receptors, such as the estrogen-related receptor (ERR) and peroxisome proliferator-activated receptor

(PPAR), are also reported to play a role in connecting the nutrient influx status to mitochondrial gene expression (Hock and Kralli, 2009).

2.3. The regulation of autophagy by mTOR signaling

Autophagy is a lysosomal degradation process in the turnover of cytosolic components, or damaged organelles. As an adaptive pathway, autophagy could maintain homeostasis in nutrient-rich conditions through removal activity. Autophagy is accomplished through initiation and vesicle nucleation, vesicle elongation, fusion with lysosome, and degradation. Activation of the Ulk1 complex leads to the activation of the Beclin1-Vps34 complex. Subsequently, autophagosomes are formed starting from the recruitment of DFCP1 and WIPI. The modification of Atg8 by phosphatidylethanolamine results in the elongation of the autophagosome, followed by fusion with the lysosome to form an autolysosome, where sequestered substrates are degraded (Kim and Lee, 2014). mTOR signaling is an upstream signaling that inhibits autophagy and acts by phosphorylating the Ulk1 complex. In addition, ATG14L, a component of the Vps34 complex, is phosphorylated to inhibit autophagosome formation. In addition, direct phosphorylation of TFEB is known to inhibit the expression of genes associated with autophagy and lysosome biogenesis. Especially, mTOR signaling is known to suppress mitochondria-selective autophagy regulated by

Bnip3, Fundc1, PINK1 and lipid-selective autophagy (Han and Wang, 2018, Lee et al., 2017).

2.4. Mitochondrial quality control defects in NASH

In NASH, defects appear in mitochondrial quality control. It has been reported that phenotypes of non-alcoholic hepatitis, such as fat accumulation, ROS formation, inflammation and cell death, are increased in the liver of mice knocked out of Bnip3 involved in mitochondrial fission and mitophagy (Glick et al., 2012). In addition, overexpression of fis1 associated with mitochondrial fission in the liver of mouse reduced lipid accumulation, liver damage and lipotoxicity induced by Bmal1 knockout (Jacobi et al., 2015). The progression from fatty liver to nonalcoholic steatohepatitis showed that the expression of PGC-1α, a mitochondrial biogenesis regulator, was significantly reduced in liver tissue of patients (Handa et al., 2014). As nonalcoholic fatty liver disease progressed, the accumulation of LC3 and p62, which showed autophagic function, occurred with ER stress, which means a decrease in autophagy ability (Gonzalez-Rodriguez et al., 2014). The accumulation of these proteins was also accompanied by an increase in megamitochondria due to a decrease in mitophagy, which resulted in liver damage (Yamada et al., 2018). In addition, the acidification of lysosomes, which are closely related to autophagy function, was reduced in the NASH

mouse model (Wang et al., 2018). Therefore, identifying factors that regulate mitochondrial dynamics, biogenesis, and mitophagy simultaneously and identifying molecular mechanisms may contribute to the treatment of NAFLD.

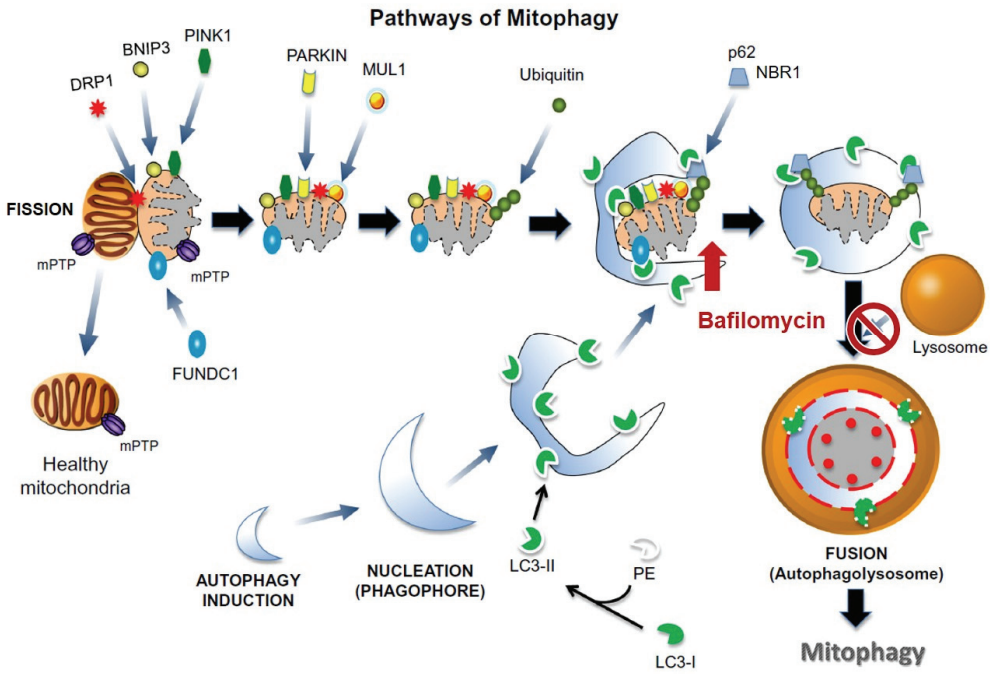

Figure 3. An overview of signaling of mitophagy pathways

Mitochondrial fission factors, Drp1 and Bnip3 are recruited into mitochondria, and ubiquitination of mitochondria occurs through the action of Fundc1 and PINK1. Then, the autophagosome is formed through the combination of LC3 and p62, and degradation occurs through fusion with the lysosome (Lee et al., 2017). Bafilomycin inhibits the fusion between autophagosome and lysosome.

3. Nuclear receptor, Retinoic acid receptor-related orphan receptor α (RORα)

3.1. Structure and mechanism of action

The retinoic acid receptor-related orphan receptor α (RORα) is an orphan nuclear receptor that is associated with the regulation of various genes in hepatic lipid metabolism and inflammation (Jetten, 2009). RORα has four isoforms, RORα1, RORα2, RORα3 and RORα4, and it is known that RORα1 and RORα4 exist in mouse. Differences in their N-terminus are indicated by alternative promoter usage or alternative splicing. RORα is present in tetris, kidney, adipose, and liver, especially in cerebellum and thalamus. RORs have the N-terminal (A/B) domain, the DNA-binding domain (DBD), the hinge domain and the C-terminal ligand-binding domain (LBD) (Jetten, 2009). RORα binds to a specific DNA sequence, called ROR response element (RORE), consisting of the monomeric RGGTCA motif or Rev-DR2 sites of direct repeats (Giguère et al., 1994; Raspe et al., 2002). Natural and synthetic ligands, such as cholesterol sulfates, SR1078, and JC1-40, reversibly bind to RORα and increase the transcriptional activity of target genes via the induction of the DNA binding of RORα and recruitment of coactivators such as p300 and PGC-1α (Kim et al.,

2012; Lau et al., 1999; Liu et al., 2007; Solt and Burris, 2012).

3.2. Physiological functions of RORα

RORα is related to circadian rhythm, and RORα has been identified in clock genes such as BMAL1, CLOCK, and CRY1 (Kumaki et al., 2008). RORα has abnormal circadian behavior in deficient mice, and RORα has also responded to hypoxia stress (Akashi and Takumi, 2005; Chauvet et al., 2004). Above all, RORα has many roles in the metabolic pathway. Studies on the metabolic role of RORα have been performed frequently in RORα-deficient staggerer mice ($RORα^{sg/sg}$). It has been shown that the expression of genes related to lipogenesis and fatty oxidation are altered by RORα deficiency (Lau et al., 2008). RORα increased the transcriptional activity of oxysterol 7 alpha-hydroxylase (Cyp7b1), one of the P450 enzymes, indicating that RORα is associated with an alternative pathway of cholesterol metabolism. In addition, RORα in liver cells, together with RORγ, regulated Cyp2c8 important for drug metabolism (Cheng et al., 2009). RORα also modulates the expression of fibroblast growth factor 21, one of the hepatic hormones, and has been shown to be associated with liver lipid metabolism and glucose tolerance (Wang et al., 2010).

3.3. Protective functions of RORα in NAFLD

In patients with NAFLD and animal NASH models, the hepatic expression levels of RORα are significantly decreased, suggesting that RORα may be associated with pathogenesis in NASH (Han et al., 2014; Ou et al., 2013). Recently, RORα was demonstrated that it has an inhibitory effect on lipid accumulation. RORα increased the activities of AMPK and ACC, which are involved in fatty acid metabolism, and decreased the activity of LXRα, thereby suppressing SREBP and FAS which increase lipogenic enzyme expression (Kim et al., 2012). In addition, in the NASH mouse model induced by the methionine-choline deficient (MCD) diet, RORα mitigated NASH by reducing oxidative stress in hepatocytes and Kupffer cells (Han et al., 2014). Studies have also shown that fatty liver is alleviated by overexpression of sulfotransferase 2B1b, which synthesizes the natural ligand of RORα, cholesterol sulate (Shi et al., 2014). In addition, as a natural ligand of RORα, nobiletin has been shown to alleviate HFD-induced fatty liver (He et al., 2016). Recent hepatocyte-specific RORα knockout mouse models have observed steatosis and insulin resistance through increased PPARγ activity (Kim et al., 2017). RORα has also been shown to reduce inflammation by participating in polarity changes in macrophages and to modulate NASH through a macrophage-specific knockout mouse model (Han et al., 2017). The protective function of RORα against NASH strongly suggests

that RORα plays roles in mitochondrial quality control under the pathological condition of oversupply of nutrients. In this study, the molecular mechanism of mitochondrial quality control in the progression of NASH from steatosis was demonstrated using hepatocyte-specific RORα knockout mouse model, and RORα was proposed as a therapeutic target for NASH.

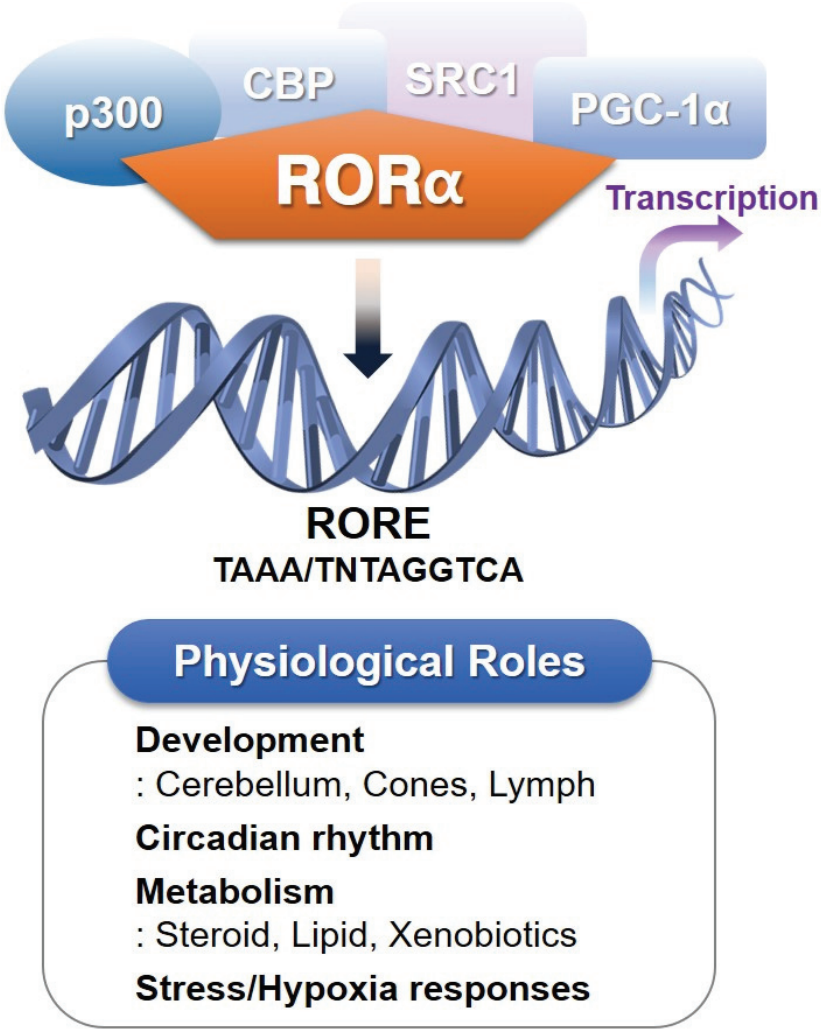

Figure 4. Nuclear receptor, RORα

The retinoic acid receptor-related orphan receptor α (RORα) is an orphan nuclear receptor that is associated with the regulation of various genes in hepatic lipid metabolism, inflammation, development, and circadian rhythm (Jetten, 2009). RORα binds to a specific DNA sequence, called ROR response element (RORE), consisting of the monomeric RGGTCA motif or Rev-DR2 sites of direct repeats to regulate target genes (Giguère et al., 1994; Raspe et al., 2002).

4. RORα knockout mouse model

4.1. Controversies on studies in RORα knockout mouse model

The physiological functions of RORα have been studied mainly using the RORα-deficient staggerer mice ($RORα^{sg/sg}$), which carry a C-terminal deleted form of RORα (Hamilton et al., 1996; Steinmayr et al., 1998). $RORα^{sg/sg}$ mice fed a high-fat diet (HFD) are resistant to the development of hepatic steatosis and exhibit decreased fasting blood glucose levels and increased insulin sensitivity (Kang et al., 2011; Lau et al., 2011; Lau et al., 2008).

In contrast, two research groups reported a protective role of RORα against hepatic steatosis by employing the liver-specific depletion of RORα or RORα/γ, recently. They showed that loss of negative regulation of the peroxisome proliferators-activated receptor-γ or overactivation of the sterol regulatory element-binding proteins exacerbated diet-induced hepatic steatosis in these animals (Kim et al., 2017; Zhang et al., 2017).

Here, I revealed a novel role of RORα in mitochondrial quality control and autophagy that inhibits further progression of hepatic steatosis to NASH.

4.2. Necessity of generation of hepatocyte-specific RORα knockout mouse model for the studies of NASH

RORα-deficient staggerer mouse model has limitations regarding liver studies, because the systemic expression of the staggerer gene leads to the development of pathological phenotypes, such as immunodeficiencies, osteoporosis, cerebellar degeneration, atherosclerosis, and muscular atrophy (Hamilton et al., 1996). Moreover, homozygous RORα -/- mice exhibit tremor and abnormal body balance and die between 24 and 28 days of life (Dussault et al., 1998). Thus, I generated mice with a hepatocyte-specific deletion of the ROR α gene using albumin-cre, to study the hepatic roles of RORα in the progression of NASH. Here, I demonstrated that RORα is a potent regulator of mitochondrial quality control in the liver in response to metabolic input. In particular, Bnip3 and PGC-1α were the transcriptional targets of RORα in the regulation of mitochondrial fission and biogenesis and RORα induced autophagy via inactivation of mTOR signaling.

II. PURPOSE OF THIS STUDY

Nonalcoholic fatty liver disease is a metabolic disorder caused by excessive dietary intake, drugs, and genetic causes, and is associated with diseases such as obesity, hyperlipidemia, and diabetes. Nonalcoholic steatohepatitis is an advanced disease accompanied by cell damage and inflammation in the state of lipid-accumulating fatty liver. Oxidative stress, lipid toxicity, and cell death, all of which are due to malfunction of the mitochondria (Fuchs and Sanyal, 2012; Koek et al., 2011; Schattenberg and Schuppan, 2011). Indeed, mitochondria in patients with nonalcoholic hepatitis have structural and functional abnormalities (Perez-Carreras et al., 2003; Sanyal et al., 2001). The function of the mitochondria is regulated through various actions such as fission, biogenesis, and mitochondria-specific autophagy (Palikaras and Tavernarakis, 2014). Identifying the mitochondrial function modulators in the pathogenesis of nonalcoholic steatohepatitis and identifying the molecular mechanisms may contribute to the treatment of the disease. However, there is no drug for the treatment of nonalcoholic steatohepatitis, and drugs in clinical trials are focused on improving morbidity associated with nonalcoholic steatohepatitis rather than directly eliminating the pathogenesis of mitochondrial dysfunction. In addition, side effects such as causing hyperlipidemia have been reported

(Neuschwander-Tetri et al., 2015).

The nuclear receptor, RORα, is a transcriptional factor associated with lipid metabolism, circadian rhythm, development of cerebellum, and hypoxia response (Jetten, 2009). In the last report, RORα was reported that it activates AMPK and inhibits LXRα, thereby inhibiting lipid accumulation and alleviating hepatic steatosis (Kim et al., 2012). In addition, RORα has been reported to reduce the incidence of nonalcoholic fatty liver disease by increasing the expression of SOD2 and Gpx1, thereby preventing oxidative stress and relieving inflammation (Han et al., 2014). Increased fatty oxidation through AMPK activation and reduced oxidative stress are directly or indirectly related to mitochondrial quality. Therefore, I hypothesized that RORα may be a factor in mitochondrial quality control.

The aim of this study was to investigate the effect of hepatic RORα on the incidence of nonalcoholic fatty liver disease by using hepatocyte-specific RORα knockout mice. Second, to identify the target genes that can be regulated by RORα in the pathogenesis of nonalcoholic fatty liver disease. Third, to investigate the molecular mechanism by RORα in mitochondrial quality. Specifically, I have identified the role of RORα to regulate mitochondrial fission and autophagy.

III. MATERIALS AND METHODS

Animal studies

The RORα$^{f/f}$ mutant embryo, which has loxP sites flanking exon 4 of the RORα gene, was obtained from the Institut Clinique de la Souris (Illkirch, France) and the mutant mouse was generated by in vitro fertilization (Korea Research Institute of Bioscience and Biotechnology). To produce the liver-specific RORα KO line (AlbCre-RORα$^{f/f}$), RORα$^{f/f}$ animals were crossbred with AlbCre animals, which express Cre recombinase in hepatocytes under the control of the albumin promoter (Jackson Laboratories). Several backcrosses of the two mouse lines produced the liver-specific RORα KO mice on the C57BL/6 background. Offspring were genotyped to confirm the inclusion of loxP sites within RORα alleles and the presence of Cre recombinase via PCR using specific primers. All animals were maintained with 12 h light (7 am) and dark (7 pm) cycles.

Six-week-old male RORα$^{f/f}$ or RORα-LKO mice were fed an HFD (D12492) or low-fat diet (D12450J) (Research Diets, New Brunswick, NJ) for 12 weeks. HFD-fed RORα-LKO mice gained more weight compared with control mice (Data not shown). After feeding, liver tissues were excised and cross sections of the left lobe of the liver were analyzed for protein and mRNA, or fixed in 10% neutral buffered formalin (Sigma-Aldrich) for immunohistochemistry. The activities of ALT and AST in the serum were measured using a Fuji DRI-CHEM 3500s serum biochemistry analyzer (Fujifilm, Japan), and the amount of hepatic TG was measured using an EnzyChromTM Triglyceride Assay Kit (BioAssay Systems). For histological examinations, 3 μm sections of paraffin-embedded tissue were stained with hematoxylin and eosin (H&E). Frozen liver tissue sections were stained with Oil red O staining. All

experiments were performed in a blinded and randomized fashion. The experimental protocols were approved by the Seoul National University Institutional Animal Care and Use Committee (permission number SNU-140424-2-5) and all experiments were conducted according to the committee's guidelines.

Determination of OXPHOS protein expression and complex I activity

OXPHOS proteins in ETC complexes were analyzed by western blotting using a commercially available anti-total OXPHOS primary antibody cocktail (458099, Invitrogen, 1:20000). Proteins were extracted from liver tissues and quantified by bicinchoninic acid assay (Pierce). After quantification, I added sample buffer and let the samples stand for 30 min at 37 °C, for the detection of mitochondrially encoded cytochrome c oxidase I (MTCO1) proteins. An anti-Hsp60 antibody (ab45134, Abcam, 1:10000) was used as a control and the intensity of western blots was quantified by ImageJ. Complex I activity was measured using the Complex I Activity Assay Kit (AAMT001-1KIT, Novagen). Proteins were extracted from liver tissues by adding detergent, and each diluted sample (100 μg protein/200 μl) was added into a well coated with a monoclonal antibody against the NADH dehydrogenase complex. Complex I activity was determined based on the rate of NADH oxidation, which is linked to the reduction of a dye, leading to increased absorbance at 450 nm (according to the manufacturer's protocol).

Electron microscopy

Liver tissues were excised and small blocks from the left lobe were fixed and primary hepatocytes were collected in 2.5% glutaraldehyde in 0.1 M phosphate buffer (pH 7.0). The blocks were postfixed with osmium tetroxide, followed by En bloc staining with 0.5% uranyl acetate. After samples were dehydrated with 30%, 50%, 70%, 80%, 90%, and 100% ethanol, they were embedded in Spurr's resin and polymerized. Ultrathin sections were cut using an EM UC7 ultramicrotome (Leica, Germany), and examined by JEM1010 transmission electron microscope (JEOL, Japan).

Assessment of oxygen consumption rate

Primary hepatocytes were isolated from 8 - 10-week-old male C57BL/6 mice via the perfusion of livers with collagenase type IV (Sigma-Aldrich), as described previously. After perfusion, cells were suspended in Dulbecco's modified Eagle's medium (DMEM) (Hyclone) containing 10% fetal bovine serum (FBS). The oxygen consumption rate (OCR) was analyzed using the Seahorse XFp Extracellular Flux Analyzer. Mouse primary hepatocytes isolated from control and RORα-LKO mice were plated in assay plates at 10^4 cells/well with minimal DMEM (XF base medium) supplemented with 10 mM pyruvate, as described previously. In the case of assessment of the OCR of primary hepatocytes infected with either Ad-GFP or Ad-GFP-RORα, hepatocytes were plated in DMEM with 10% FBS 4 h prior to transduction. After 18 h, media were exchanged to unbuffered minimal DMEM supplemented with 10 mM pyruvate. To determine the basal and maximal respiration, carbonyl

cyanide-4-(trifluoromethoxy)phenylhydrazone (FCCP, an inducer of maximal respiration; 0.25 μM) and antimycin A/rotenone (2 μM) were added to hepatocytes. The basal OCR was calculated by the OCR baseline levels before FCCP injection minus the average of three OCR levels after antimycin A/rotenone injection (non-mitochondrial respiration). Maximal OCR was produced by subtracting non-mitochondrial respiration from the OCR levels after FCCP injection. The production and infusion of Ad-GFP and Ad-GFP-RORα1 were as previously described (Kim et al., 2012).

Confocal microscopy

For the time course of experiments, hepatocytes were plated in DMEM with 10% FBS 4 h prior to refreshment of media or transduction. After 18 h, hepatocytes were cultured in Earle's balanced salt solution with 5.5 mM glucose for 2 h. Next, cells were exposed to DMEM with 25 mM glucose and 0.3 mM palmitic acid conjugated with bovine serum albumin for the indicated time course. For real-time confocal microscopy, mitochondria were tagged by Ad-COX8a-GFP for visualization, as described previously. For GFP-LC3 puncta formation assay, cells were treated by adenovirus carrying GFP-LC3 and bafilomycin. For mitophagy and lipophagy assay, cells were stained by mitotracker red CMXRos 150 nM, lysotracker green DND-26 100 nM, nile red, or/and LipidTOX dye for 15 min. Subsequently, live images were acquired at 37 °C using a confocal microscope with a Nikon Plan Apochromat 20x/0.75 objective (Nikon Eclipse Ti; Nikon, Japan) or a confocal microscope (LSM 700; Carl Zeiss Microscopy, Jena, Germany). Ad-COX8a-GFP was kindly provided by

Dr. Lee C-H (Harvard University, MA).

Analysis of mitochondrial mass using flow cytometry

Primary hepatocytes were isolated and incubated with low glucose DMEM media containing 100 nM mitotracker green FM (Invitrogen) for 30 min. Green fluorescence was detected by flow cytometry.

Western blotting, ChIP, and quantitative real-time PCR (qRT-PCR)

Western blotting was performed as described previously using specific antibodies against α-SMA (ab7817, Abcam, 1:5000), TGFβ1 (sc-130348, Santa Cruz Biotechnology, 1:1500), Bnip3 (ab109362, Abcam, 1:7000), phospho-DRP1 (Ser616) (#4494, Cell Signaling Technology, 1:2000), Drp1 (#8570, Cell Signaling Technology, 1:2000), Fis1 (ab71498, Abcam, 1:2000), LC3 (L8918, Sigma, 1:5000), NBR1 (#9891, Cell Signaling Technology, 1:2000), phospho-mTOR (#2971, Cell Signaling Technology, 1:2000), mTOR (#2972, Cell Signaling Technology, 1:2000), phospho-Ulk1 (Ser555) (#5869, Cell Signaling Technology, 1:2000), phospho-Ulk1 (Ser638) (#14205, Cell Signaling Technology, 1:2000), Ulk (#8054, Cell Signaling Technology, 1:2000), Ctsd (sc-377299, Santa Cruz Biotechnolog, 1:2000), RORα (sc-6062, Santa Cruz Biotechnolog, 1:2000), and actin (sc-1616, Santa Cruz Biotechnology, 1:2000). The ChIP assay was performed using anti-RORα (sc-6062, Santa Cruz Biotechnology), anti-p300 (sc-585, Santa Cruz Biotechnology), and anti-histone 3 (acetyl K27) (ab4729, Abcam) antibodies or a control IgG antibody (Santa Cruz Biotechnology), and specific primers (Han et al., 2014). Relative mRNA expression was determined by qRT-PCR using the

ABI StepOnePlusTM Real-Time PCR system (Applied Biosystems, Foster City, CA) using specific primers. The mRNA expression of genes was calculated relative to controls using the $2^{-\Delta\Delta CT}$ method (Han et al., 2014).

Reporter gene analysis

The RORE/Bnip3-Luc and RORE(I)/PGC-1α-Luc were constructed by inserting three copies of putative ROREs into a pGL2-promoter vector (Promega) using specific oligomers. An eukaryotic expression vector encoding RORα1 ΔDBD was constructed by a PCR-mediated deletion method. Chang liver cells (CCL-13TM, ATCC, Rockville, MD) were transfected with a plasmid mixture containing reporter plasmid, eukaryotic expression vector, and pCMV-β-galactosidase using the Polyfect (Qiagen) according to the manufacturer's protocol. Cells were lysed using luciferase lysis buffer (Promega, Madison, WI) and luciferase activity was measured using LB9508 luminometer (Berthold, Bad Wildbad, Germany) and normalized to β-galactosidase activity.

RNA-seq and ChIP-seq analyses

The RNA used in sequencing analysis was obtained from the liver tissues of HFD-fed RORα-LKO and $RORα^{f/f}$ mice. For control and test RNAs, the construction of a library was performed using a SENSE mRNA-Seq Library Prep Kit (Lexogen, Inc., Austria), according to the manufacturer's instructions. High-throughput sequencing was performed as paired-end 100 sequencing using HiSeq 2500 (Illumina, Inc., USA). RNA-Seq reads were mapped using the TopHat software tool, to obtain the alignment file. The alignment file was used

for assembling transcripts, estimating their abundance, and detecting the differential expression of genes or isoforms using cufflinks. Gene classification was based on searches of the BioCarta (http://www.biocarta.com/), GenMAPP (http://www.genmapp.org/), DAVID (http://david.abcc.ncifcrf.gov/), and Medline databases (http://www.ncbi.nlm.nih.gov/). The GO analysis was performed in DAVID Bioinformatics Resources 6.7. RORα ChIP-seq (GSE59486) and liver input control (GSE26345) were downloaded from gene expression omnibus (GEO) (http://www.ncbi.nlm.nih.gov/geo) (Fang et al., 2014, Feng et al., 2011). A public ChIP-seq is conducted in C57BL/6 mouse liver. Low-quality small RNA reads and adapter sequences were removed using FASTX-Toolkit (http://hannonlab.cshl.edu/fastx_toolkit/). Analysis was performed as previously described (Feng et al., 2011). High-quality reads were aligned with the mouse reference genome (mm9) using Bowtie v1.1.2 with options '-n 2 -l 34 --best --strata -m 1' (Langmead et al., 2009). Only uniquely aligned reads to the genome were chosen for further analysis. Peak calling was performed using HOMER and a published liver input control (Heinz et al., 2010). Peaks were filtered according to two criteria: (1) score ≥ 10 and (2) peaks between -100 kb from transcription start site (TSS) and TSE. ChIP-seq peaks were visualized in IGV (Robinson et al., 2011).

Database-based gene expression analysis

Database-based gene expression analysis was conducted using public datasets obtained from GEO site at the NCBI gene expression (http://www.ncbi.nlm.nih.gov/geo/). The data from GSE33814, GSE48452 and

GSE89632 processed as median-normalized signal intensity value. These public datasets were obtained from liver tissues of human patients. Normal (n=13) and steatohepatitis (n=12) for GSE33814 28; healthy obese (n=27) and NASH (n=18) for GSE48452; for healthy controls (n=24) and NASH patients (n=19) for GSE89632.

Statistical analysis

All analyses were performed using the GraphPad Prism software. Statistical analyses between two groups were conducted using the nonparametric Mann - Whitney U test (two-tailed) or unpaired Student's t-test (two-tailed). Two-way ANOVA followed by the Bonferroni posttest was used to analyze the statistical significance of complex I activity, OCRs, and of ex vivo studies of nutrient switch. Data are presented as the mean ± SEM. Statistical significance was set at $P < 0.05$.

Accession number

Raw data for HFD-fed control and RORα-LKO mouse RNA-seq are available in GSE90844.

Table 1: Primer sequences used for Quantitative real time PCR

Gene	Accession number	Nucleotide sequence		Species
RORα	NM_013646.2	Sense	5′-TTTCAGGAGAAGTCAGCAGAG-3′	Mouse
	NM_001289916.1	Antisense	5′-TCTGCTGGTCCGATCAATCAA-3′	
RORβ	NM_001043354.2	Sense	5′-ATGGCAGACCCACACCTACG-3′	Mouse
	NM_146095.4	Antisense	5′-TATCCGCTTGGCGAACTCC-3′	
	NM_001289921.1			
RORɣ	NM_011281.3	Sense	5′-CGAGATGCTGTCAAGTTTGGC-3′	Mouse
	NM_001293734.1	Antisense	5′-TGTAAGTGTGTCTGCTCCGCG-3′	
LXRα	NM_001177730.1	Sense	5′-AGGAGTGTCGACTTCGCAAA-3′	Mouse
	NM_013839.4	Antisense	5′-CTCTTCTTGCCGCTTCAGTTT-3′	
Fasn	NM_007988.3	Sense	5′-CATGACCTCGTGATGAACGTGT-3′	Mouse
		Antisense	5′-CGGGTGAGGACGTTTACAAAG-3′	
SCD1	NM_009127.4	Sense	5′-AGATCTCCAGTTCTTACACGACCAC-3′	Mouse
		Antisense	5′-GACGGATGTCTTCTTCCAGGTG-3	
Acly	NM_001199296.1	Sense	5′-GATGAAGTGGCACCTGCAAAG-3′	Mouse
	NM_134037.3	Antisense	5′-GGTATGTCGGCTGAAGAGGGT-3′	
Acaca	NM_133360.2	Sense	5′-GCGGGAGGAGTTCCTAATTC-3′	Mouse
		Antisense	5′-GGTTGGCATTGTGGATTTTC-3′	
CD36	NM_001159558.1	Sense	5′-TCCTCTGACATTTGCAGGTCTATC-3′	Mouse
	NM_001159557.1	Antisense	5′-AAAGGCATTGGCTGGAAGAA-3′	
	NM_001159556.1			
	NM_001159555.1			
	NM_007643.4			
TNFα	NM_013693.3	Sense	5′-AATGGCCTCCCTCTCATCAGTT-3	Mouse
		Antisense	5′-CCACTTGGTGGTTTGCTACGA-3′	
NLRP3	NM_145827.3	Sense	5′-AGCCTTCCAGGATCCTCTTC-3′	Mouse
		Antisense	5′-CTTGGGCAGCAGTTTCTTTC-3′	
IL-1β	NM_008361.4	Sense	5′-AGAGCCCATCCTCTGTGACTCA-3	Mouse
		Antisense	5′-TGCTTGGGATCCACACTCTCCA-3	
Col1a1	NM_007742.4	Sense	5′-GACATCCCTGAAGTCAGCTGC-3′	Mouse
		Antisense	5′-TCCCTTGGGTCCCTCGAC-3′	
α-SMA	NM_007392.3	Sense	5′-GGCACCACTGAACCCTAAGG-3′	Mouse
		Antisense	5′-TCTCCAGAGTCCAGCACAAT-3′	
TGFβ	NM_011577.2	Sense	5′-CGACATGGAGCTGGTGA-3′	Mouse
		Antisense	5′-TCCCGAATGTCTGACGTA-3′	
MMP-2	NM_008610.3	Sense	5′-TTTGCTCGGGCCTTAAAAGTAT-3′	Mouse
		Antisense	5′-CCATCAAATGGGTATCCATCTC-3′	

TIMP1	NM_001294280.2	Sense	5′-CTTGGTTCCCTGGCGTACTC-3′	
	NM_011593.2	Antisense	5′-ACCTGATCCGTCCACAAACAG-3′	Mouse
	NM_001044384.1			
Bnip3	NM_009760.4	Sense	5′-CTCCCAGACACCACAAGATAC-3′	
		Antisense	5′-CTTCCTCAGACAGAGTGCTG-3′	Mouse
Drp1	NM_152816.3	Sense	5′-CGTGACAAATGAAATGGTGC-3′	
	NM_001025947.2	Antisense	5′-CATTAGCCCACAGGCATCAG-3′	
	NM_001276340.1			Mouse
	NM_001276341.1			
Fis1	NM_025562.3	Sense	5′-AGGCTCTAAAGTATGTGCGAGG-3′	
	NM_001163243.1	Antisense	5′-GGCCTTATCAATCAGGCGTTC-3′	Mouse
Pink1	NM_026880.2	Sense	5′-GCTTGCCAATCCCTTCTATG-3′	
		Antisense	5′-CTCTCGCTGGAGCAGTGAC-3′	Mouse
Mfn1	NM_024200.4	Sense	5′-CCTACTGCTCCTTCTAACCCA-3′	
		Antisense	5′-AGGGACGCCAATCCTGTGA-3′	Mouse
Mfn2	NM_001285920.1	Sense	5′-AGAACTGGACCCGGTTACCA-3′	
	NM_133201.3	Antisense	5′-CACTTCGCTGATACCCCTGA-3′	
	NM_001285921.1			Mouse
	NM_001285922.1			
	NM_001285923.1			
OPA1	NM_001199177.1	Sense	5′-CTGAGGCCCTTCTCTTGTTAGG-3′	
		Antisense	5′-CTGACACCTTCCTGTAATGCTTG-3′	Mouse
PGC-1α	NM_008904.2	Sense	5′-CCCTGCCATTGTTAAGACC-3′	
		Antisense	5′-TGCTGCTGTTCCTGTTTTC-3′	Mouse
TFAM	NM_009360.4	Sense	5′-GGAATGTGGAGCGTGCTAAAA-3′	
		Antisense	5′-ACAAGACTGATAGACGAGGGG-3′	Mouse
Idha	NM_029573.2	Sense	5′-CCTCCTGCTTAGTGCTGTGA-3′	
		Antisense	5′-CGTTGCCTCCCAGATCTTT-3′	Mouse
Acadm	NM_007382.5	Sense	5′-GATCGCAATGGGTGCTTTTGATAGAA-3′	
		Antisense	5′-AGCTGATTGGCAATGTCTCCAGCAAA-3′	Mouse
ND1	NC_005089.1	Sense	5′-ACGCAAAATCTTAGGGTACA-3′	
	NC_006914.1	Antisense	5′-GAGTGATAGGGTAGGTGCAA-3′	Mouse
COX1	NC_005089.1	Sense	5′-ATTCGAGCAGAATTAGGTCA-3′	
	NC_006914.1	Antisense	5′-CTCCGATTATTAGTGGGACA-3′	Mouse
Ndufv1	NM_025523.1	Sense	5′-TTCCTCTGGATTCACCCTCA-3′	
		Antisense	5′-CATGAGGAGCGCGAGTATTT-3′	Mouse
Sdha	NM_023281.1	Sense	5′-GAAAGGCGGGCAGGCTCATC-3′	
		Antisense	5′-CACCACGGCACTCCCCATTTT-3′	Mouse
Uqcr	NM_025650.2	Sense	5′-TGCCGAGGCCTCAGACACAG-3′	
		Antisense	5′-TCCAAGGCATAAGAATAAGGTTT-3′	Mouse

Cox5a	NM_007747.2	Sense	5′-TTGATGCCTGGGAATTGCGTAAAG-3′	Mouse
		Antisense	5′-AACAACCTCCAAGATGCGAACAG-3′	
Atp5g1	NM_007506.6	Sense	5′-AGTTGGTGTGGCTGGATCA-3′	Mouse
	NM_001161419.1	Antisense	5′-GCTGCTTGAGAGATGGGTTC-3′	
CytC	NM_007808.4	Sense	5′-GGAGGCAAGCATAAGACTGG-3′	Mouse
		Antisense	5′-TCCATCAGGGTATCCTCTCC-3′	
18s rRNA	NR_003278.3	Sense	5′-GTAACCCGTTGAACCCCATT-3′	Mouse
		Antisense	5′-CCATCCAATCGGTAGTAGCG-3′	
Atg2a	NM_194348.3	Sense	5′-CCACCTCTGCAAATCGGCA-3′	Mouse
		Antisense	5′-CCAGTTGTCCTGATACCTCCA-3′	
Atg3	NM_026402.3	Sense	5′-ACACGGTGAAGGGAAAGGC-3′	Mouse
		Antisense	5′-TGGTGGACTAAGTGATCTCCAG-3′	
Atg4a	NM_174875.4	Sense	5′-GCTGGTATGGATTCTGGGGAA-3′	Mouse
		Antisense	5′-TGGGTTGTTCTTTTTGTCTCTCC-3′	
Gabarapl2	NM_026693.5	Sense	5′-TCGGGCTCTCAGATTGTTGAC-3′	Mouse
		Antisense	5′-ATGGCCTTCTCGGAGGGAA-3′	
Vmp1	NM_001356531.2	Sense	5′-CTGGCAGTTCAAAAACTAGTAC-3′	Mouse
	NM_029478.5	Antisense	5′-CCGGGGACAGCACCAATGAAAG-3′	
Atg101	NM_026566.2	Sense	5′-ATGAACTGTCGATCAGAAGTGC-3′	Mouse
		Antisense	5′-CCTATGGAGTACGTGCCCT-3′	
Becn1	NM_001359820.1	Sense	5′-GGAAAAGAACCGCAAGGTGGTG-3′	Mouse
	NM_001359819.1	Antisense	5′-AAACTGTCCGCTGTGCCAGATG-3′	
	NM_019584.4			
Fundc1	NM_028058.4	Sense	5′-CCCCCTCCCCAAGACTATGAA-3′	Mouse
	NM_001313745.1	Antisense	5′-CCACCCATTACAATCTGAGTAGC-3′	
Gabarapl1	NM_020590.4	Sense	5′-GGACCACCCCTTCGAGTATC-3′	Mouse
		Antisense	5′-CCTCTTATCCAGATCAGGGACC-3′	
LC3B	NM_026160.5	Sense	5′-CCCACCAAGATCCCAGTGAT-3′	Mouse
		Antisense	5′-CCAGGAACTTGGTCTTGTCCA-3′	
ATP6v0e1	NM_025272.2	Sense	5′-GCATACCACGGCCTTACTGT-3′	Mouse
		Antisense	5′-GAGGATTGAGCTGTGCCAGA-3′	
ATP6v1h	NM_001310442.1	Sense	5′-ACTCCCCGAGGCTATCCAG-3′	Mouse
	NM_133826.5	Antisense	5′-CACGAACTTCAGCAGCCTTG-3′	
Ctsa	NM_001038492.2	Sense	5′-CAGCCCCTTCCAACTACCTC-3′	Mouse
	NM_008906.4	Antisense	5′-CCGTTGTAGAGCAGGATCTGG-3′	
Ctsb	NM_007798.3	Sense	5′-CTTAGGAGTGCACGGGAGAG-3′	Mouse
		Antisense	5′-CTTGTCATGGGCACTGGTCA-3′	
Ctsd	NM_009983.3	Sense	5′-TACTCCATGCAGTCATCGCC-3′	Mouse
		Antisense	5′-GACGACTGTGAAACACTGCG-3′	

Ctsf	NM_019861.2	Sense	5′-TGGCTCCACTCTTCAAGGAC-3′	Mouse
		Antisense	5′-ATCCCATACTGAGCTGTGCC-3′	
Clcn7	NM_001317404.1	Sense	5′-CACGGCCAGGGAAGTAATGAG-3′	Mouse
	NM_011930.4	Antisense	5′-CGCAGGATCAAGCCTTGGAG-3′	
Lamp1	NM_001317353.1	Sense	5′-GCCCACAAACCCCACTGTAT-3′	Mouse
	NM_010684.3	Antisense	5′-TTTGGGCTGATGTTGAACGC-3′	
Lamp2	NM_001290485.2	Sense	5′-GATGTGCCTCTCTCCGGTTA-3′	Mouse
	NM_010685.4	Antisense	5′-ATTGGACTGAACGGCTCCTA-3′	
	NM_001017959.2			
Mcoln1	NM_053177.1	Sense	5′-TCATTGCACTCATCACCGGC-3′	Mouse
		Antisense	5′-CCAGATGTGGGGCTATCCTG-3′	
Vps11	NM_001357393.1	Sense	5′-AAGGAGCCGCTGGGTAATGAT-3′	Mouse
	NM_027889.2	Antisense	5′-TTGTAGGCCTGGAACCCTGTA-3′	
Vps18	NM_172269.3	Sense	5′-GCCCGCACCGTGTACATTAT-3′	Mouse
		Antisense	5′-TGCGAAGTTCCTCATCCTCC-3′	

Table 2: Primer sequences for Chip assay

Nucleotide sequence			Species
Reads-enriched region in Bnip3	Sense	5′-GAAACTGGCGTGATGAAATCTT-3′	Mouse
	Antisense	5′-GATCTCACTTTGCAGCCAAC-3′	
Reads-enriched region in PGC-1α I	Sense	5′-CGGAGCTGCTAACTAACAATGG-3′	Mouse
	Antisense	5′-GATGTGTATCACTGCACCACAC-3′	
II	Sense	5′-GTGTGGTGAAGAGTGAGGAT-3′	Mouse
	Antisense	5′-AGGATTGCTATGAGCCTCTG-3′	
III	Sense	5′-GGCCCTGCCTGATCTTTAG-3′	Mouse
	Antisense	5′-GAGCACACAAACAAGAAGTTAGG-3′	

Table 3: Primer sequences for Cloning

		Nucleotide sequence
RORE/ Bnip3	Sense	5′-CCCAACTGGGACGCCCAACTGGGACGCCCAACTGGGACGCG-3′
	Antisense	5′-CTAGCGCGTCCCAGTTGGGCGTCCCAGTTGGGCGTCCCAGTTGGGAGCT-3′
RORE(I)/ PGC-1α	Sense	5′-CGGGAGGGTCAAGTGGGAGGGTCAAGTGGGAGGGTCAAGTG-3′
	Antisense	5′-CTAGCACTTGACCCTCCCACTTGACCCTCCCACTTGACCCTCCCGAGCT-3′

Table 4: Primer sequences for Genotyping

		Nucleotide sequence	Species
$RORa^{f/f}$ allele (P1 and P2)	Sense	5′-TTGTGTATACCACCACAAGTGCACC-3′	Mouse
	Antisense	5′-AGTACAGGACACTTCGGTGTCTACC-3′	
Alb^{Cre}allele (Cre)	Sense	5′-TACAGACTGTGAGCAGATGTTC-3′	Mouse
	Antisense	5′-TTCTTGCGAACCTCATCACTCGTTG-3′	

IV. RESULTS

1. Liver-specific KO of the RORα gene enhances susceptibility to HFD-induced steatohepatitis

To study the hepatic role of RORα during the progression of NAFLD, I generated a hepatocyte-specific RORα-null mouse, RORα-LKO (Figure 5A, C, D). The absence of RORα gene expression was demonstrated in the liver of RORα-LKO mice, whereas the hepatic expression of RORβ or RORɣ remained at control levels (Figure 5B). I fed an HFD to RORα-LKO mice for 12 weeks, to monitor the effects of deletion of the RORα gene on symptoms of NASH. Hepatic steatosis was severe in RORα-LKO mice compared with flox/flox (f/f) mice. The livers of RORα-LKO mice weighed more than did those of f/f mice, and the accumulation of lipid droplets was evident in the hepatocytes of the former (Figure 6). The indicators of liver injury, i.e., serum alanine aminotransferase (ALT), aspartate aminotransferase (AST), and the marker of lipid peroxidation 4-hydroxynonenal (4-HNE) were increased largely in the livers of RORα-LKO mice (Figure 7). Consistently, hepatic expression of a proinflammatory cytokine, tumor necrosis factor alpha (TNFα), were increased in RORα-LKO mice (Figure 8A). Also, the expression level of F4/80, a marker of infiltrated macrophages, was increased in the livers of RORα-LKO mice (Figure 8B). In addition, collagen deposition was increased in the liver tissues of RORα -LKO mice and the expression of alpha-smooth muscle actin (α-SMA) and

transforming growth factor β1 (TGFβ1), pro-fibrotic factors, were significantly increased in the livers of RORα-LKO mice (Figure 9). The mRNA levels of genes involved in lipogenesis such as liver X receptor alpha and fatty acid synthase, inflammation such as TNFα and NACHT, LRR and PYD domains-containing protein 3 (NLRP3), and fibrosis such as collagen Type I (Col1a1) and α-SMA were significantly increased in the livers of RORα-LKO mice (Figure 10). Together, these data showed that the hepatic expression of RORα is closely associated with the development of NASH.

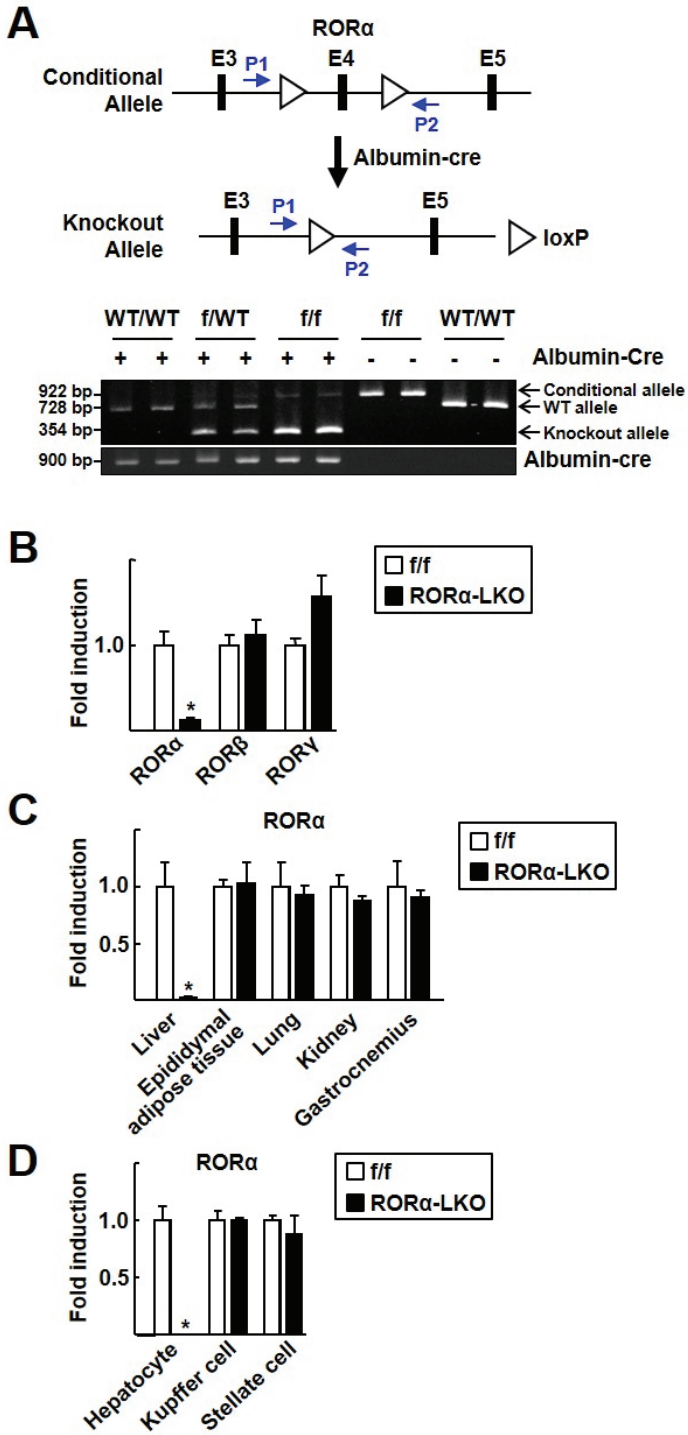
A
RORα
Conditional Allele
E3
P1
E4
E5
P2
Albumin-cre
Knockout Allele
E3
P1
E5
loxP
P2
WT/WT
f/WT
f/f
f/f
WT/WT
+ + + + + + - - - -
Albumin-Cre
922 bp
728 bp
354 bp
900 bp
Conditional allele
WT allele
Knockout allele
Albumin-cre
B
f/f
RORα-LKO
Fold induction
1.0
*
RORα
RORβ
RORγ
C
RORα
f/f
RORα-LKO
Fold induction
1.0
0.5
*
Liver
Epididymal adipose tissue
Lung
Kidney
Gastrocnemius
D
RORα
f/f
RORα-LKO
Fold induction
1.0
0.5
*
Hepatocyte
Kupffer cell
Stellate cell

Figure 5. Generation and characterization of the hepatocyte-specific RORα knockout mice.

(A) Schematic representation of the conditional RORα floxed allele and the strategy of generation of the liver-specific RORα-deficient allele through Albumin-Cre recombination. E; Exon (upper). Genotyping analysis of the $RORα^{f/f}$ and AlbCre-$RORα^{f/f}$ (RORα-LKO) mice. The primer sequences (P1/P2 and Cre) used for the genotyping were shown in Table (lower).

(B) The mRNA expression levels of the RORα, RORβ, and RORɣ in liver tissues were measured by qRT-PCR. Values represent mean ± SEM. $*P < 0.05$ vs $RORα^{f/f}$ (n=4).

(C) The relative mRNA expression levels of RORα in various tissues. Values represent mean ± SEM. $*P < 0.05$ vs $RORα^{f/f}$ (n=4).

(D) The relative mRNA expression levels of RORα in various cells such as hepatocytes, kupffer cells and stellate cells. Values represent mean ± SEM. $*P < 0.05$ vs $RORα^{f/f}$ (n=4).

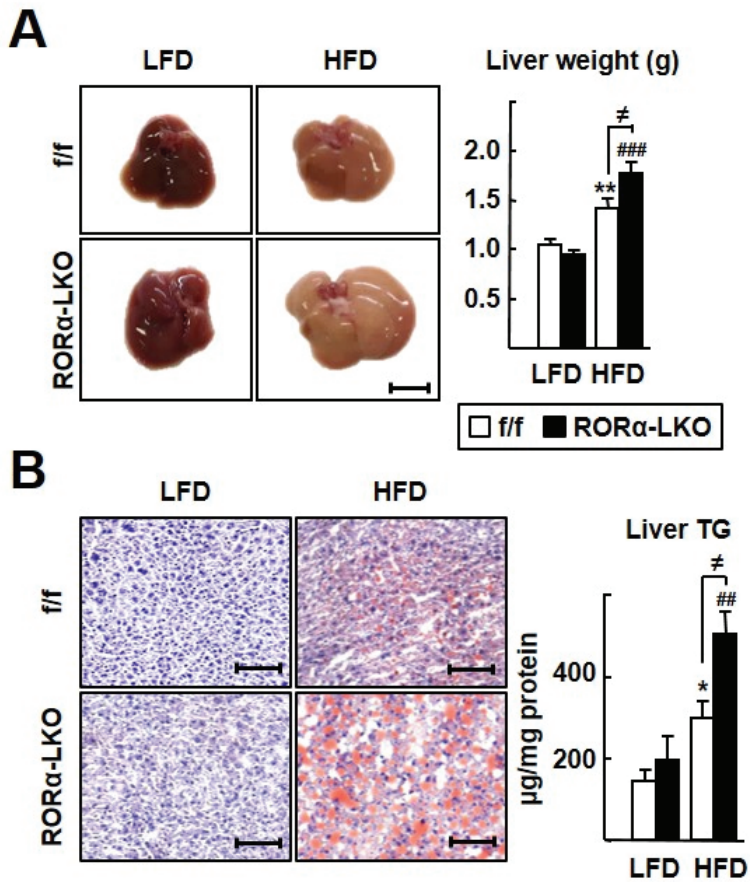

Figure 6. Liver-specific KO of RORα increases to HFD-induced lipid accumulation

(A) Six week-old RORα-LKO and RORα$^{f/f}$ mice were fed with either LFD or HFD for 12 weeks. Representative images of livers and the liver weights of experimental mice at the end of experiments. Scale bar: 1 cm. Values represent mean ± SEM (n=7-9). **P < 0.01 vs LFD-fed RORα$^{f/f}$, ###P < 0.001 vs LFD-fed RORα-LKO, ≠P < 0.05 vs HFD-fed RORα$^{f/f}$.

(B) Oil red O staining of liver sections and hepatic TG levels. Scale bar: 100 μm. Representative images are shown. Values represent mean ± SEM (n=7-9). *P < 0.05 vs LFD-fed RORα$^{f/f}$, ##P < 0.01 vs LFD-fed RORα-LKO, ≠P < 0.05 vs HFD-fed RORα$^{f/f}$.

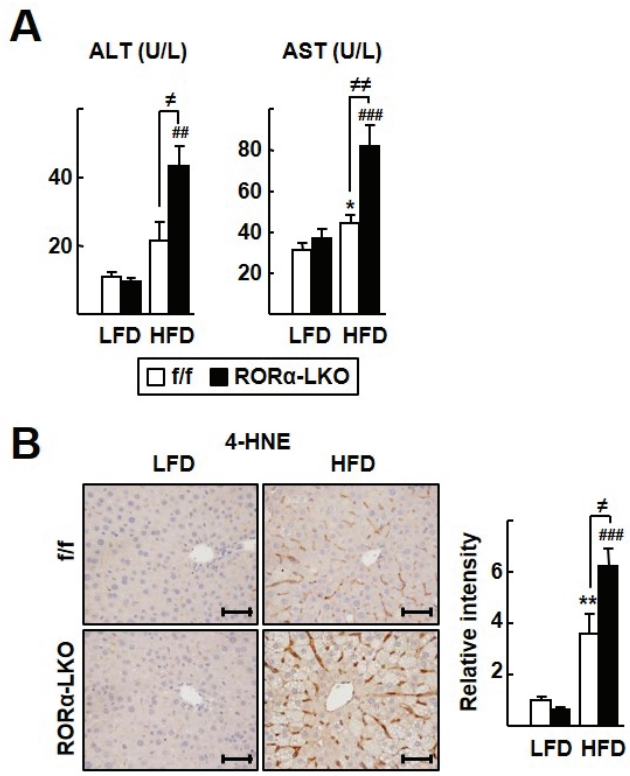

Figure 7. Liver-specific KO of RORα enhances HFD-induced cell injury and lipid peroxidation

(A) Serum ALT and AST activities were measured by standard clinical chemistry assays at the end of experiments. Data presented as mean ± SEM (n=7-9). ALT; ##P < 0.01 vs LFD-fed RORα-LKO, ≠P < 0.05 vs HFD-fed RORα$^{f/f}$, AST; *P < 0.05 vs LFD-fed RORα$^{f/f}$, ###P < 0.001 vs LFD-fed RORα -LKO, ≠≠P < 0.01 vs HFD-fed RORα$^{f/f}$.

(B) Histological staining of 4-HNE (brown). Scale bar: 50 μm. Representative Images of liver sections from the RORα$^{f/f}$ and RORα-LKO mice were presented. Relative intensities were quantified using ImageJ. Values represent mean ± SEM (n=6-8). **P < 0.01 vs LFD-fed RORα$^{f/f}$, ###P < 0.001 vs LFD-fed RORα-LKO, ≠P < 0.05 vs HFD-fed RORα$^{f/f}$.

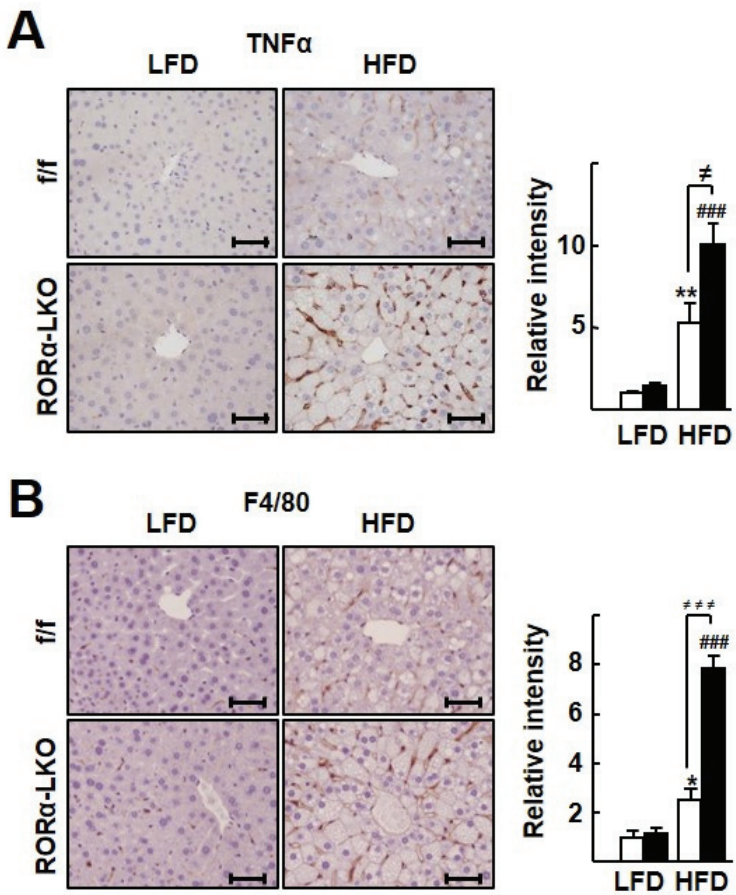

Figure 8. Liver-specific KO of RORα exacerbates the inflammation

(A) Histological staining of TNFα (brown). Scale bar: 50 μm. Representative Images of liver sections from the RORα$^{f/f}$ and RORα-LKO mice were presented. Relative intensities were quantified using ImageJ. Values represent mean ± SEM (n=6-8). *P < 0.05 vs LFD-fed RORα$^{f/f}$, ###P < 0.001 vs LFD-fed RORα-LKO, ≠P < 0.05 vs HFD-fed RORα$^{f/f}$.

(B) Histological staining of F4/80. Scale bar: 50 μm. Representative Images of liver sections from the RORα$^{f/f}$ and RORα-LKO mice were presented. Relative intensities were quantified using ImageJ. Values represent mean ± SEM (n=6-8). *P < 0.05 vs LFD-fed RORα$^{f/f}$, ###P < 0.001 vs LFD-fed RORα-LKO, ≠≠≠P < 0.001 vs HFD-fed RORα$^{f/f}$.

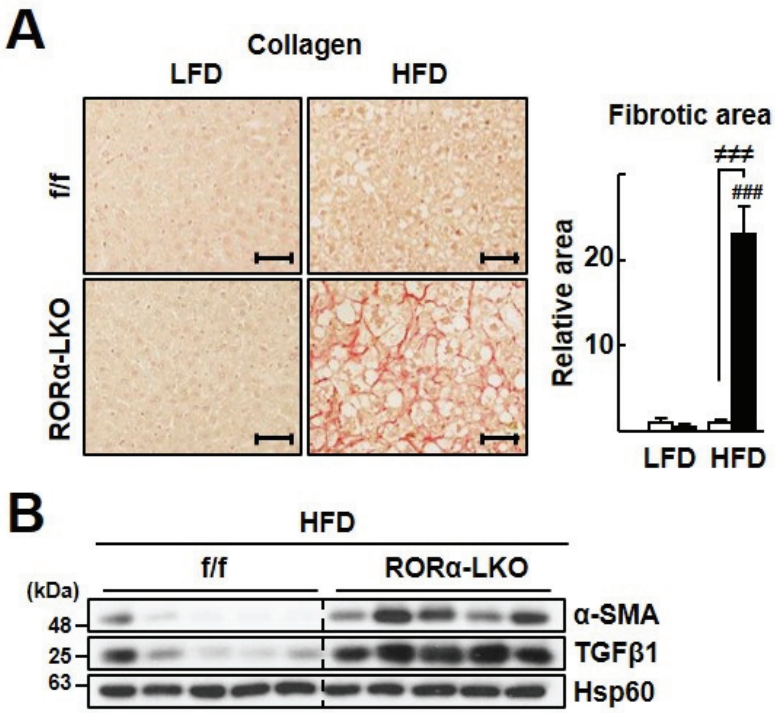

Figure 9. Liver-specific KO of RORα enhances HFD-induced hepatic fibrosis

(A) Sirius red staining in the liver sections for detection of collagen type I deposition (red, left). Scale bar: 50 μm. Fibrotic area in the liver sections was analyzed using ImageJ (right). Values represent mean ± SEM (n=6-8). ###P < 0.001 vs LFD-fed RORα-LKO, ≠≠≠P < 0.001 vs HFD-fed RORα$^{f/f}$.

(B) The protein levels of α-SMA and TGFβ1 were analyzed by western blotting in the liver tissues (n=5).

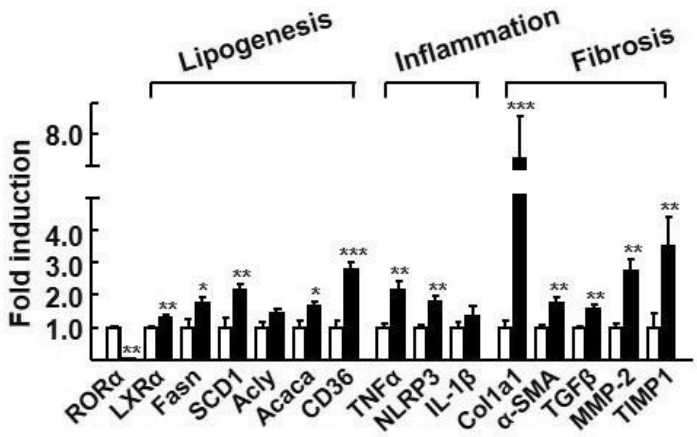

Figure 10. Liver-specific KO of RORα enhances susceptibility to HFD-induced steatohepatitis

The mRNA levels of factors related to lipogenesis, inflammation, and fibrosis were measured by qRT-PCR in the liver tissues. LXRα, Liver X receptor alpha; Fasn, Fatty acid synthase; SCD1, Stearoyl-CoA desaturase 1; Acly, ATP citrate lyase; Acaca, Acetyl-CoA carboxylase; TNFα, tumor necrosis factor alpha; NLRP3, NACHT, LRR and PYD domains-containing protein 3; IL-1β, Interleukin 1 beta; Col1a1, collagen Type I; α-SMA, alpha-smooth muscle actin; TGFβ, transforming growth factor β; MMP-2, matrix metalloproteinase-2, and TIMP1, TIMP metallopeptidase inhibitor 1. Values represent mean ± SEM (n=7-9). *P < 0.05, **P < 0.01, and ***P < 0.001 vs HFD-fed RORα$^{f/f}$.

2. Mitochondrial function is a target of hepatic RORα

Next, I carried out a transcriptomics study to identify the target genes of RORα associated with the development of NASH. Results from an RNA-seq analysis combined with the data from a public ChIP-seq analysis (GSE59486) revealed that a total of 2,639 genes were specifically altered by RORα (Figure 11A). A gene ontology (GO) analysis of the altered genes revealed that "oxidation-reduction" was the top-ranked GO biological process that was targeted by RORα. Interestingly, the GO term "electron transport chain" was the top GO biological process among the 134 genes in the cluster of oxidation-reduction (Figure 11B). Moreover, I found that the GO cellular component included mitochondrial components with statistical significance (Figure 15C). Surprisingly, the relative expression of most of the genes in the GO terms of "electron transport chain", "carboxylic catabolic process", and "ATP biosynthetic process" were significantly decreased in the livers of HFD-fed ROR α-LKO mice, suggesting that mitochondrial function may be a target of RORα -mediated transcriptional regulation (Figure 11D).

Therefore, I examined whether mitochondrial function was defective in the livers of RORα-LKO mice. First, I found that the expression of mitochondrial OXPHOS proteins, such as NADH dehydrogenase [ubiquinone] 1 beta subcomplex subunit 8 (NDUFB8), succinate dehydrogenase [ubiquinone]

iron-sulfur subunit (SDHB), cytochrome b-c1 complex subunit 2 (UQCRC2), mitochondrially encoded cytochrome c oxidase I (MTCO1), and ATP synthase, H+ transporting, mitochondrial F1 complex, alpha 1 (ATP5A), was decreased in the livers of HFD-fed RORα-LKO mice (Figure 12). Similarly, the activity of the mitochondrial complex I was decreased in the liver tissues of RORα-LKO mice (Figure 13). Moreover, I observed that mitochondria in the hepatocytes of RORα-LKO animals were deformed and showed an enlarged or swollen phenotype after HFD feeding (Figure 14). Together, these data showed that mitochondrial function may be a target of hepatic RORα.

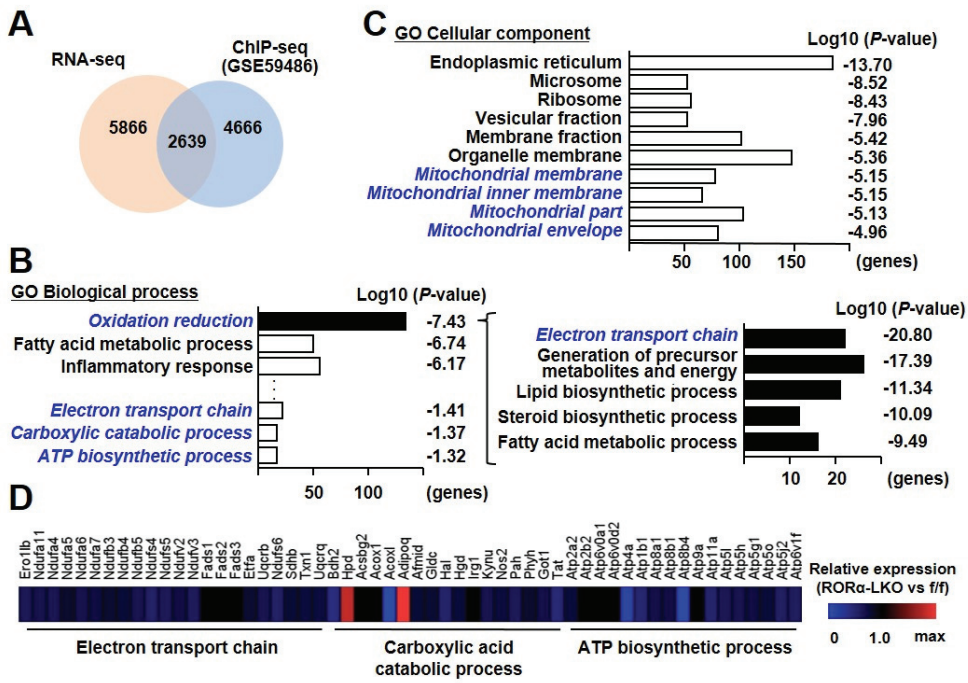
A
RNA-seq
ChIP-seq
(GSE59486)
5866
2639
4666
C
GO Cellular component
Log10 (P-value)
Endoplasmic reticulum
Microsome
Ribosome
Vesicular fraction
Membrane fraction
Organelle membrane
Mitochondrial membrane
Mitochondrial inner membrane
Mitochondrial part
Mitochondrial envelope
-13.70
-8.52
-8.43
-7.96
-5.42
-5.36
-5.15
-5.15
-5.13
-4.96
50
100
150
(genes)
B
GO Biological process
Log10 (P-value)
Oxidation reduction
Fatty acid metabolic process
Inflammatory response
Electron transport chain
Carboxylic catabolic process
ATP biosynthetic process
-7.43
-6.74
-6.17
-1.41
-1.37
-1.32
50
100
(genes)
Log10 (P-value)
Electron transport chain
Generation of precursor metabolites and energy
Lipid biosynthetic process
Steroid biosynthetic process
Fatty acid metabolic process
-20.80
-17.39
-11.34
-10.09
-9.49
10
20
(genes)
D
Ero1lb
Ndufa11
Ndufa4
Ndufa5
Ndufa6
Ndufa7
Ndufb3
Ndufb4
Ndufb5
Ndufs4
Ndufs5
Ndufv2
Ndufv3
Fads1
Fads2
Fads3
Etfa
Uqcrb
Ndufs6
Sdhb
Txn1
Uqcrq
Bdh2
Hpd
Acsbg2
Acox1
Acoxl
Adipoq
Afmid
Gldc
Hal
Hgd
Irg1
Kynu
Nos2
Pah
Phyh
Got1
Tat
Atp2a2
Atp2b2
Atp6v0a1
Atp6v0d2
Atp4a
Atp1b1
Atp8a1
Atp8b1
Atp8b4
Atp9a
Atp11a
Atp5l
Atp5h
Atp5g1
Atp5g
Atp5j2
Atp6v1f
Relative expression
(RORα-LKO vs f/f)
0
1.0
max
Electron transport chain
Carboxylic acid
catabolic process
ATP biosynthetic process

Figure 11. Gene expression profiling for liver tissues from the RORα-LKO mice

(A) Venn diagrams showing the overlapping target genes those delineated by the RNA-seq analysis in this study and the publically available ChIP-seq dataset (Fang et al, 2014). RNA-seq data was obtained from liver tissues of RORα-LKO and RORα$^{f/f}$ mice and the fold change of each gene was calculated by dividing the normalized read count of HFD-fed RORα-LKO by that of RORα$^{f/f}$. (cut-off: 0.8-fold, 1.5-fold).

(B) GO biological process analysis for the overlapped genes (left). Genes clustered in the top ranked GO biological process term, oxidation reduction, were further analyzed for GO biological process analysis. Top 5 GO based on P-value are shown (right).

(C) GO cellular component analysis for the overlapped genes. Bar graph showing the top 10 enriched cellular component based on P-value. The number of genes in each ontology category is shown.

(D) Heat map representation of differentially regulated genes associated with electron transport, carboxylic acid catabolic process, and ATP biosynthetic process. Gene symbols are indicated.

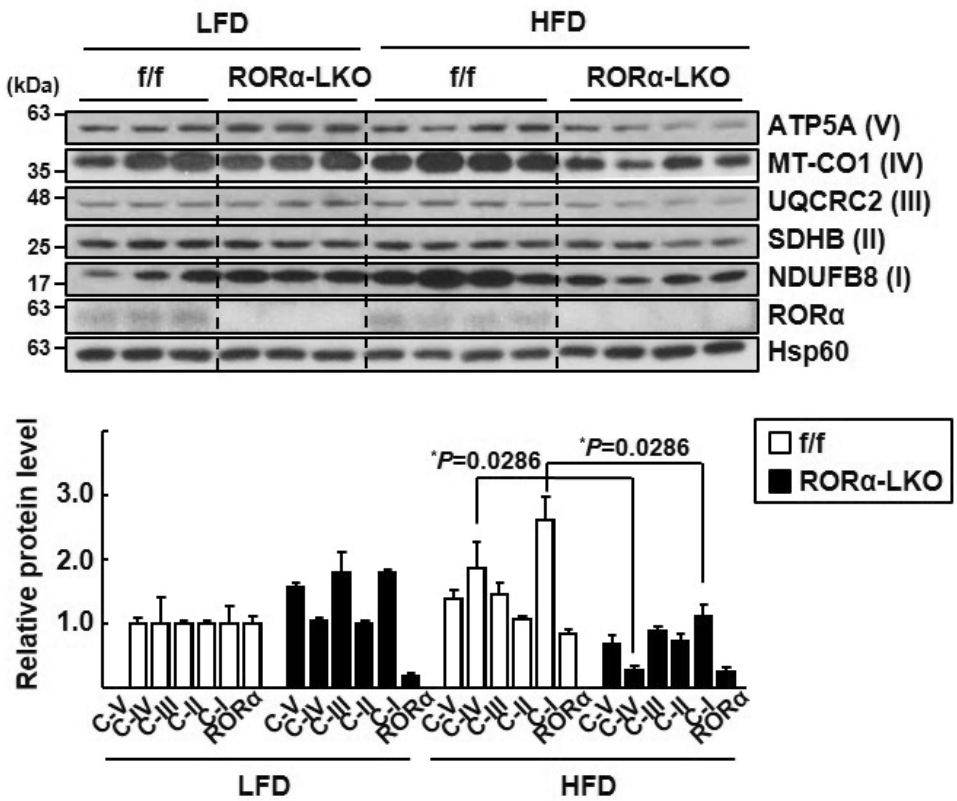

Figure 12. The expression of mitochondrial complex components in the liver tissues of RORα-LKO mice

Hepatic levels of OXPHOS proteins in ETC complexes were analyzed by western blotting using a commercially available anti-total OXPHOS primary antibody cocktail. NDUFB8, NADH dehydrogenase [ubiquinone] 1 beta subcomplex subunit 8; SDHB, Succinate dehydrogenase [ubiquinone] iron-sulfur subunit; UQCRC2, Cytochrome b-c1 complex subunit 2; MTCO1, mitochondrially encoded cytochrome c oxidase I; and ATP5A, ATP synthase, H+ transporting, mitochondrial F1 complex, alpha 1. Roman numbers represent the corresponding ETC complex. Band intensities of each protein were quantified using ImageJ and normalized to that of Hsp60 band. Data presented as mean ± SEM. $*P < 0.05$ vs HFD-fed $RORα^{f/f}$ (n=4).

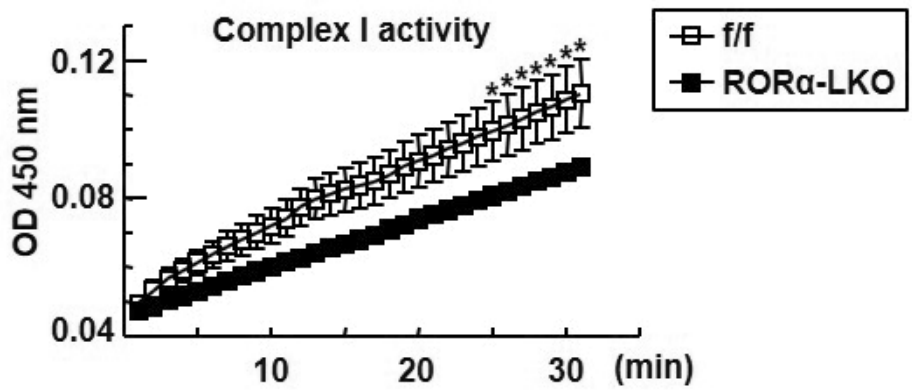

Figure 13. Complex I activity in the liver tissues of RORα-LKO mice

Activities of complex I in the liver tissues from HFD-fed mice were measured by spectrophotometry based on the rates of NADH oxidation. Data presented as mean ± SEM. *P < 0.05 vs HFD-fed RORα$^{f/f}$ (n=3-4).

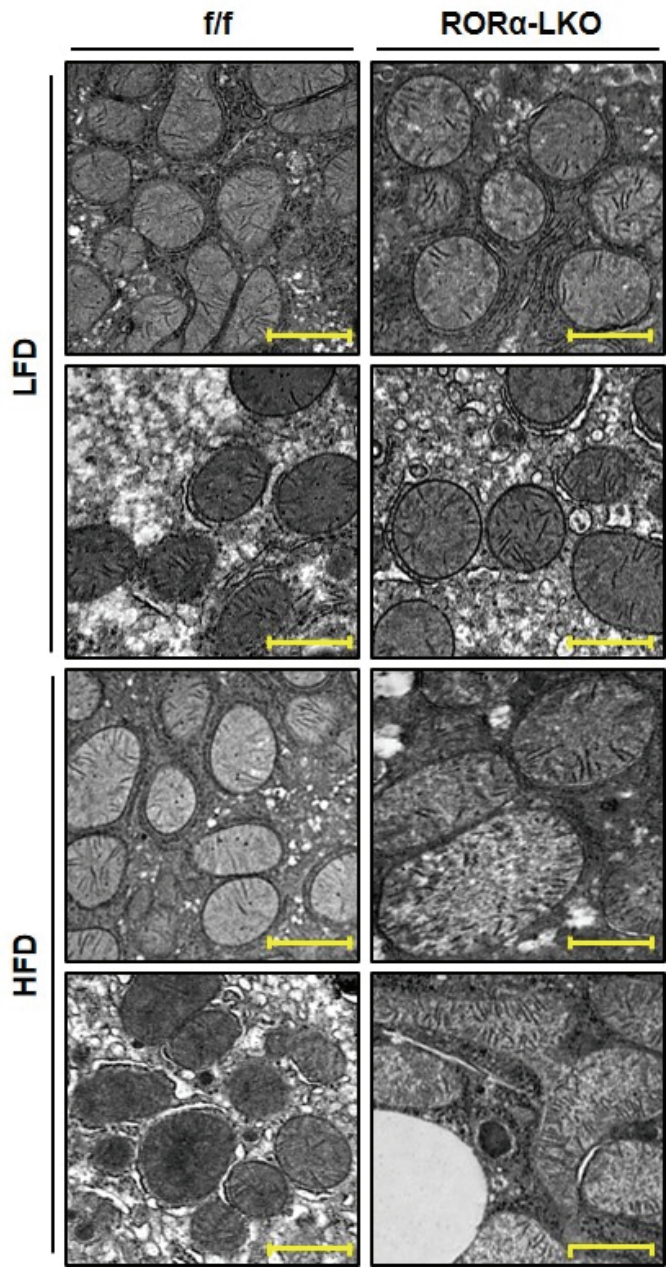

Figure 14. Structural defects of mitochondria in the liver tissues of RORα-LKO mice

Representative EM images of the liver sections from RORα$^{f/f}$ and RORα-LKO mice. Scale bar: 1 μm.

3. RORa is a novel modulator of mitochondrial fission in response to nutrient status

Based on the observation of enlarged mitochondria in the livers of HFD-fed RORα-LKO mice, I hypothesized that the deletion of RORα causes defects in the process of mitochondrial fission, especially under conditions of nutrient overload. First, I measured the oxygen consumption rate (OCR) in hepatocytes isolated from RORα-LKO mice. Although the basal OCR was not much different between RORα-LKO and f/f control mice, the maximal OCR was significantly lower in RORα-LKO hepatocytes (Figure 15). To investigate mitochondrial dynamics further, I employed ad-COX8a-GFP to label mitochondria. The culture of primary hepatocytes from control mice in medium with low glucose (5.5 mM), which is a condition of energy demand, led to a hyperfused and elongated mitochondrial network. After the culture was challenged by high glucose (25 mM) with palmitic acid (300 μM), mitochondria were rapidly fragmented (Figure 16). However, the morphology and dynamics of mitochondria in RORα-LKO hepatocytes were largely different from those of control animals, in that mitochondria were swollen and remained not much different after the nutrient challenge (Figure 17). Along the time lapse after the high-nutrient challenge, the protein levels of Bnip3 and phospho-Drp1 (pDrp1), which are fission proteins, were decreased in RORα-LKO hepatocytes, whereas

those of Fis1 was not (Figure 18). The decreases in Bnip3 and Drp1 levels were also observed in the liver tissues of HFD-fed RORα-LKO mice (Figure 22). However, total mitochondrial number was not affected by knock-down of RORα (Figure 19). Together, these data showed that mitochondrial fission in response to nutrient stimuli was abolished in RORα-LKO hepatocytes and suggest that the downregulation of Bnip3 and phospho-Drp1 might cause defects in mitochondrial quality control in RORα-LKO hepatocytes.

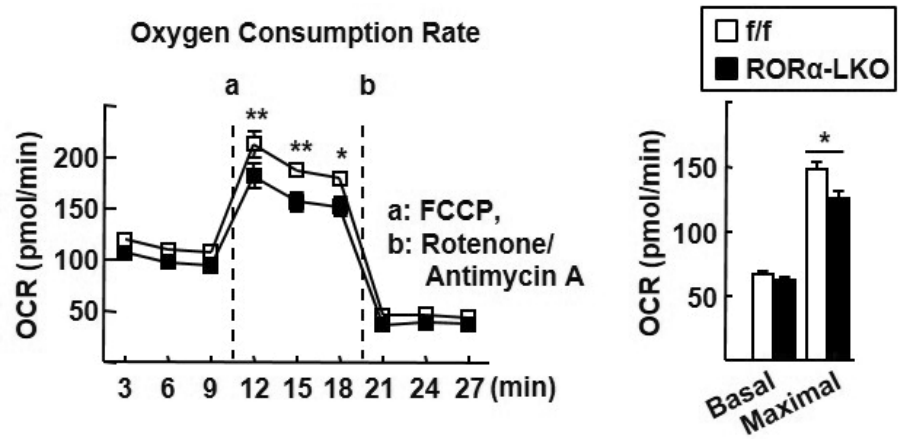

Figure 15. OCR is decreased in the hepatocytes of RORα-LKO mice

The basal OCR and maximal respiration of control and RORα-LKO primary hepatocytes. a, b refer to the time course of adding FCCP, a inducer of maximal respiration, and antimycin A/rotenone, respectively (left). Data presented as mean ± SEM (n=3). $*P < 0.05$ and $**P < 0.01$ vs RORα-LKO. The basal OCR, and maximal respiration were calculated based on data in left panel (right). Data presented as mean ± SEM. $*P < 0.05$ vs $ROR\alpha^{f/f}$.

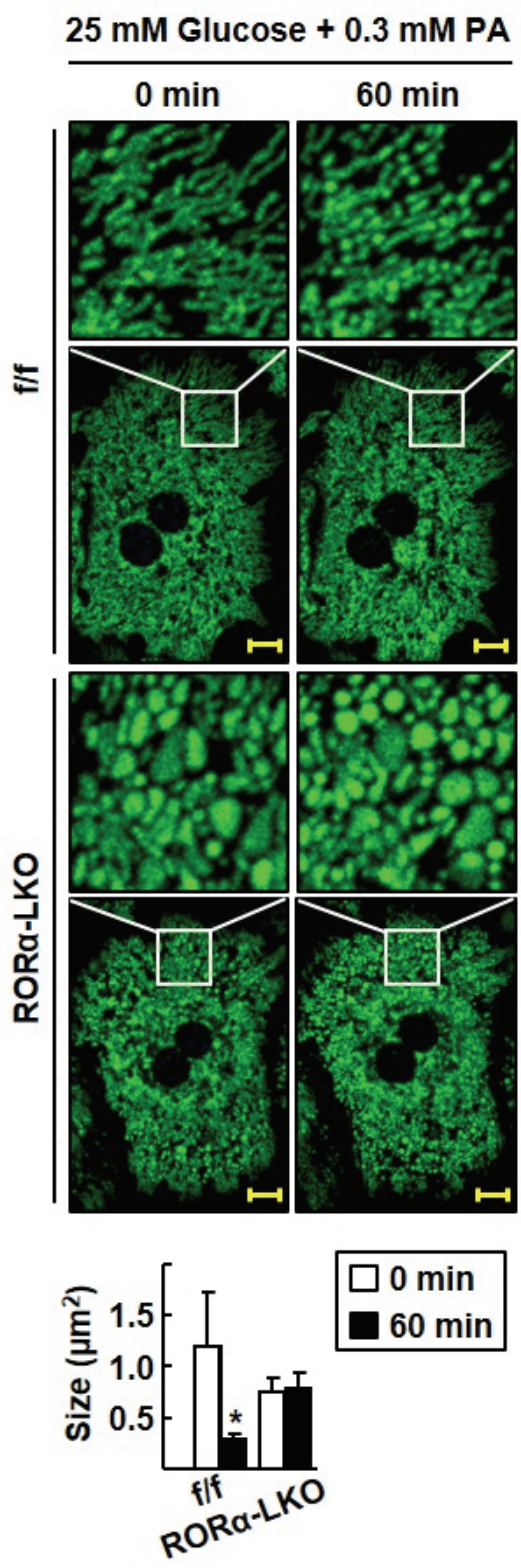
25 mM Glucose + 0.3 mM PA
0 min
60 min
f/f
RORα-LKO
0 min
60 min
Size (μm²)
1.5
1.0
0.5
*
f/f
RORα-LKO

Figure 16. Mitochondrial fission is impaired in the hepatocytes of RORα-LKO mice

Hepatocytes were infused by ad-COX8a-GFP to tag mitochondria for visualization. Hepatocytes were cultured in low nutrient condition (5.5 mM glucose) for 2 h, and then exchanged to the media containing 25 mM glucose and 0.3 mM palmitic acid. Photos were taken by real-time confocal microscopy. Representative time-lapse images of the mitochondrial morphology are shown (upper). Scale bar: 10 μm. The average mitochondrial size was quantified using ImageJ (lower). Data presented as mean ± SEM. *P < 0.05 vs 0 min ($RORα^{f/f}$).

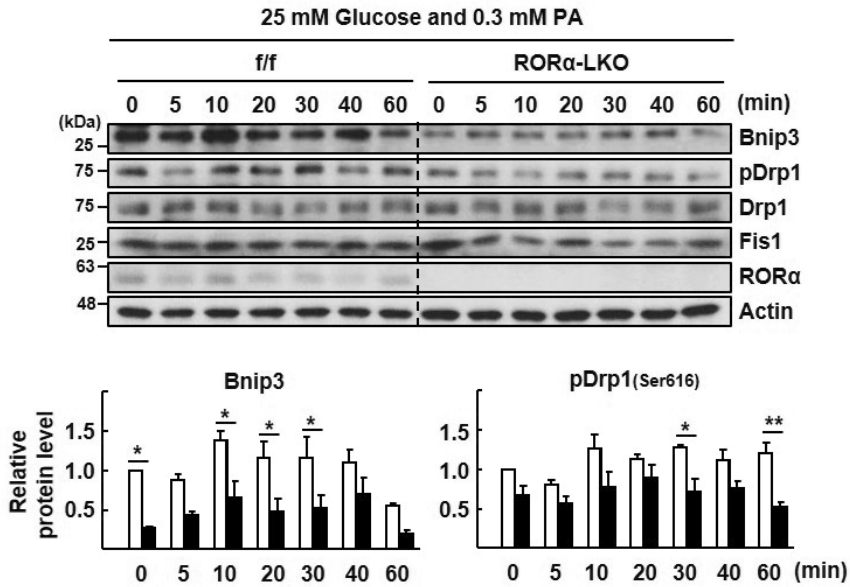

Figure 17. The regulatory factors of mitochondrial fission is reduced in the hepatocytes of RORα-LKO mice

Cell lysates were obtained at the indicated time after media change and the levels of proteins associated with mitochondria dynamics were analyzed by western blotting (upper). Band intensities of Bnip3 and pDrp1 were quantified using ImageJ and normalized to that of actin (lower). Data presented as mean ± SEM. *P < 0.05 and **P < 0.01 vs RORα-LKO (n=3).

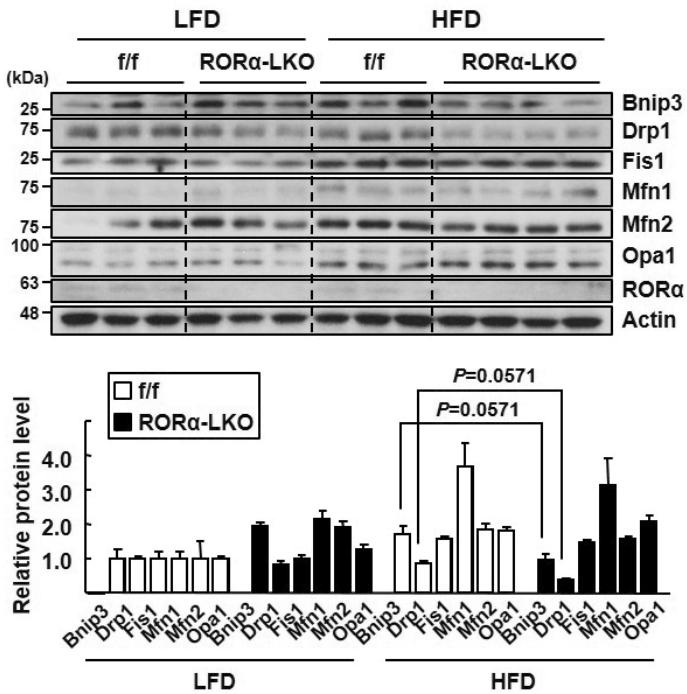

Figure 18. The expression levels of Bnip3 and Drp1 were decreased in the HFD-fed RORα-LKO with marginal significances

The levels of indicated proteins were analyzed by western blotting (upper). Band intensities of each protein were quantified using ImageJ and normalized to that of actin (lower). Data presented as mean ± SEM (n=3-4).

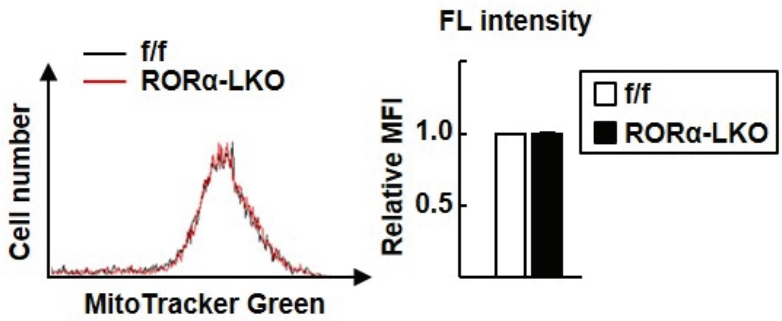

Figure 19. Analysis of mitochondrial mass using flow cytometry

Primary hepatocytes were isolated from control and RORα-LKO mice and were incubated with 100nM MitoTracker Green FM (Invitrogen) for 30 min. Green fluorescence was detected by flow cytometry (left) and relative mean fluorescence intensity (MFI) of stained cells was presented. Data presented as mean ± SEM (n=3).

4. Overexpression of RORα enhances mitochondrial dynamics via the induction of Bnip3 and pDrp1

Finally, I confirmed the function of RORα in mitochondria quality control via the transient overexpression of RORα. Viral infusion of Ad-GFP-RORα1 into primary hepatocytes dramatically enhanced OCR at both the basal and maximal levels (Figure 20). The expression levels of Bnip3 and pDrp1 after nutrient overload were significantly higher in RORα1-overexpressing hepatocytes (Figure 21). Consistently, the mRNA expression of Bnip3, but not that of the PTEN-induced putative kinase 1, Mfn1, and Opa1, increased in the presence of overexpression of RORα1, indicating that Bnip3 is a potential target of RORα. In addition, the overexpression of RORα1 resulted in increases in the mRNA expression of genes associated with mitochondrial biogenesis, including PGC-1α, and oxidative phosphorylation (Figure 22). Indeed, data from the ChIP-seq analysis showed that RORα-binding signals were present on the regulatory regions of Bnip3 and PGC-1α (Figure 23A). Additional ChIP assays confirmed that RORα bound to the reads-enriched regions in the Bnip3 and PGC-1α genes. Signals of transcription activation, such as the recruitment of p300 and the acetylation of H3K27, were clearly observed in the presence of RORα in some of these regions (Figure 23B). Analysis of the reporter genes encoding the putative ROREs present in the regulatory regions of Bnip3 and PGC-1α showed that

RORα induced transcriptional activities of the RORE/Bnip3-Luc and the RORE(I)/PGC-1α-Luc by 9-fold and 2-fold, respectively. However, the RORα1 Δ DBD, which lacked DNA binding domain, did not induce the reporters (Figure 23C). These results indicate direct regulation of Bnip3 and PGC-1α by RORα.

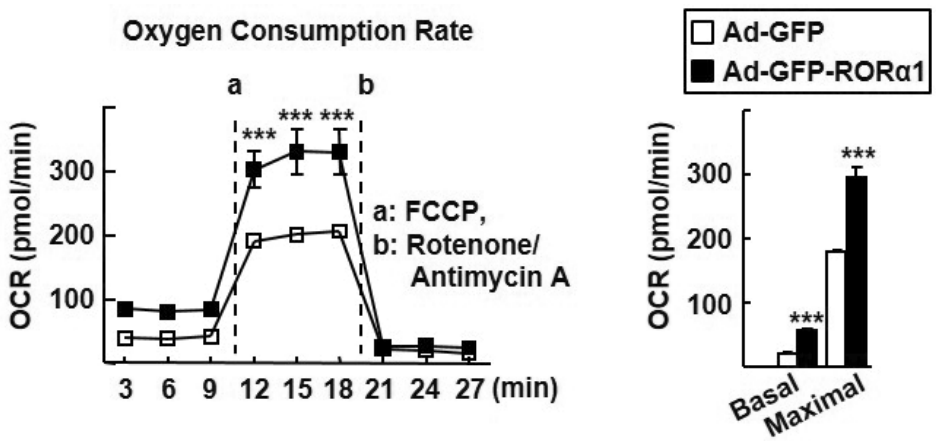

Figure 20. Overexpression of RORα enhances the OCR

The basal OCR and maximal respiration of primary hepatocytes infused by either Ad-GFP or Ad-GFP-RORα1. a, b refer to the time course of adding FCCP, and antimycin A/rotenone, respectively (left). Data presented as mean ± SEM. ***P < 0.001 vs Ad-GFP infused hepatocytes (n=3). The basal OCR, and maximal respiration (right). Data presented as mean ± SEM. ***P < 0.001 vs Ad-GFP infused hepatocytes.

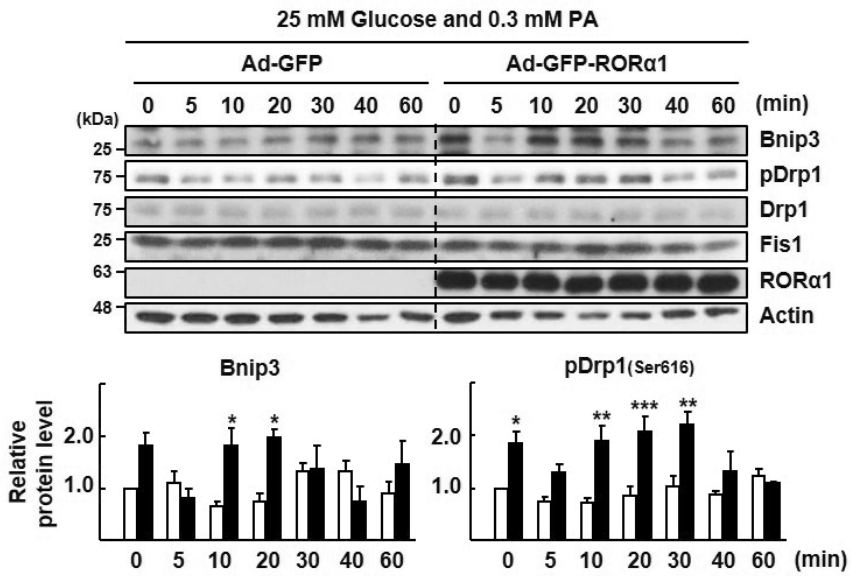

Figure 21. Overexpression of RORα increases mitochondrial dynamic response

Cell lysates were obtained at the indicated time after media change and the level of proteins associated with mitochondria dynamics were analyzed by western blotting (left). Band intensities of Bnip3 and pDrp1 were quantified using ImageJ and normalized to that of actin (right). Data presented as mean ± SEM. *P < 0.05, **P < 0.01, and ***P < 0.001 vs Ad-GFP infused hepatocytes (n=3).

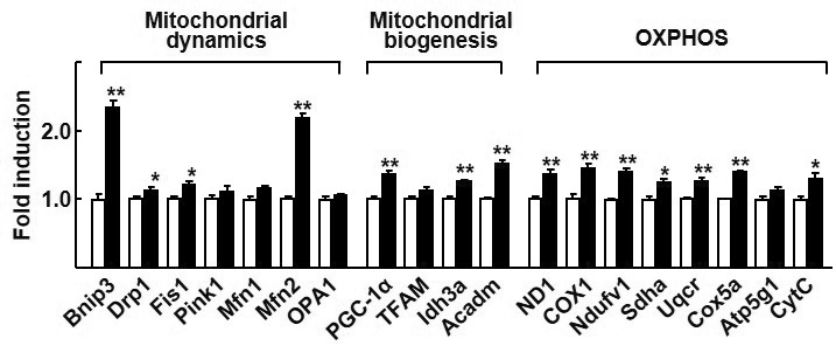

Figure 22. Overexpression of RORα enhances the expression of genes related mitochondrial function

After mouse primary hepatocytes were infected by either Ad-GFP or Ad-GFP-RORα1 for 18 h, the mRNA levels of factors related to mitochondrial dynamics, mitochondrial biogenesis, and OXPHOS were measured by qRT-PCR. The values represented as mean ± SEM. *P < 0.05 and **P < 0.01 vs Ad-GFP infused hepatocytes (n=6).

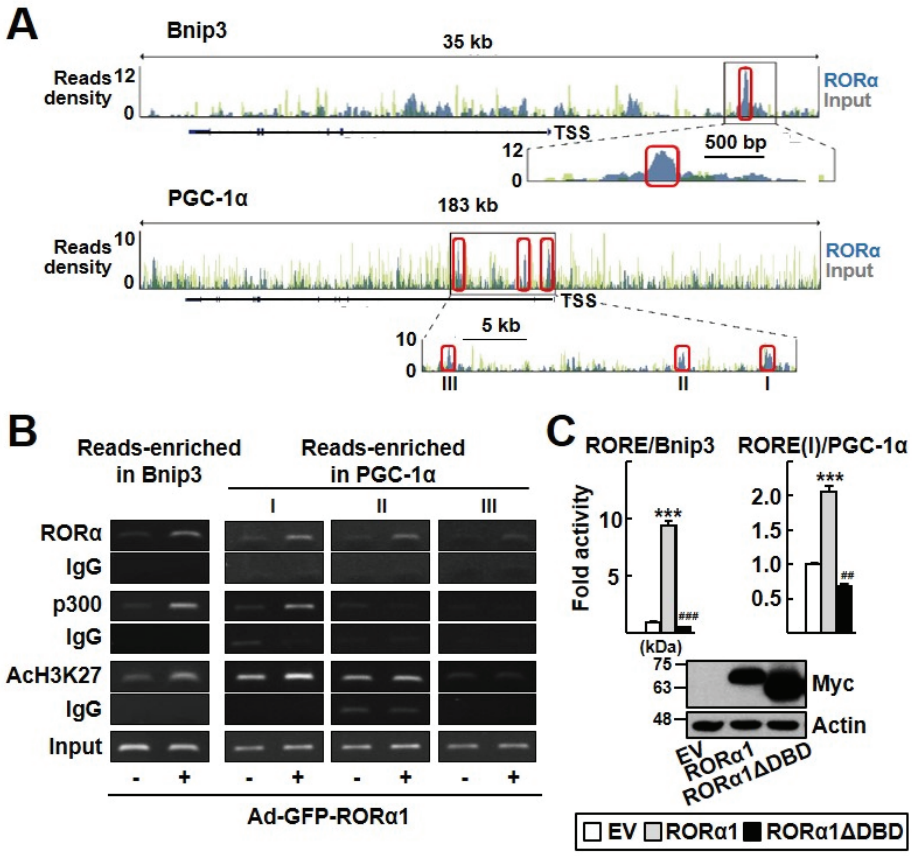
A
Bnip3
35 kb
Reads density
12
0
RORα
Input
TSS
500 bp
PGC-1α
183 kb
10
5 kb
III
II
I
B
Reads-enriched in Bnip3
Reads-enriched in PGC-1α
RORα
IgG
p300
AcH3K27
Input
Ad-GFP-RORα1
C
RORE/Bnip3
RORE(I)/PGC-1α
Fold activity
(kDa)
75
63
48
Myc
Actin
EV
RORα1
RORα1ΔDBD

Figure 23. Direct regulation of Bnip3 and PGC-1α by RORα

(A) The ChIP-seq reads of RORα and liver input control in the genome loci of Bnip3 and PGC-1α are shown in ChIP-seq tracks. Boxes indicate the regions that RORα signals are significantly enriched (Bnip3, chr7 146111103-146111273; PGC-1α I, chr5 51943784-51943954; PGC-1α II, chr5 51937131-51937301; PGC-1α III, chr5 51919125-51919295). A line below the ChIP-seq track represents transcript of the gene. TSS, transcription start site.

(B) Primary hepatocytes were infused with either Ad-GFP or Ad-GFP-RORα1 for 18 h. DNA fragments were immunoprecipitated with the anti-RORα, anti-p300, or anti-histone antibodies and then amplified by PCR with specific primers.

(C) Chang liver cells were transfected with the RORE/Bnip3-Luc or RORE(I)/PGC-1α-Luc with empty vector or the expression vector encoding Myc-RORα1 or Myc-RORα1 ΔDBD for 24 h (upper). The protein expression of Myc-RORα1 and Myc-RORα1 ΔDBD is shown (lower). The values represented as mean ± SEM. ##P < 0.01 and ***, ###P < 0.001 vs empty vector transfected cells (n=3).

5. Expression levels of hepatic Bnip3 and PGC-1α are low and correlate positively with those of RORα in patients with steatohepatitis

To assess the clinical relevance of our findings, I analyzed the expression levels of RORα, Bnip3, and PGC-1α in the livers of patients with steatohepatitis, including NASH, using publicly available databases (GSE33814 and GSE48452). As shown in previous reports, the expression level of RORα was diminished in patients with steatohepatitis. Interestingly, the levels of Bnip3 and PGC-1α were also decreased in the livers of patients with steatohepatitis compared with those of healthy obese patients (Figure 24A). The observation that the expression levels of Bnip3 and PGC-1α correlated positively with those of RORα suggests a potential application of our findings to diagnostic and therapeutic interventions for NASH (Figure 24B).

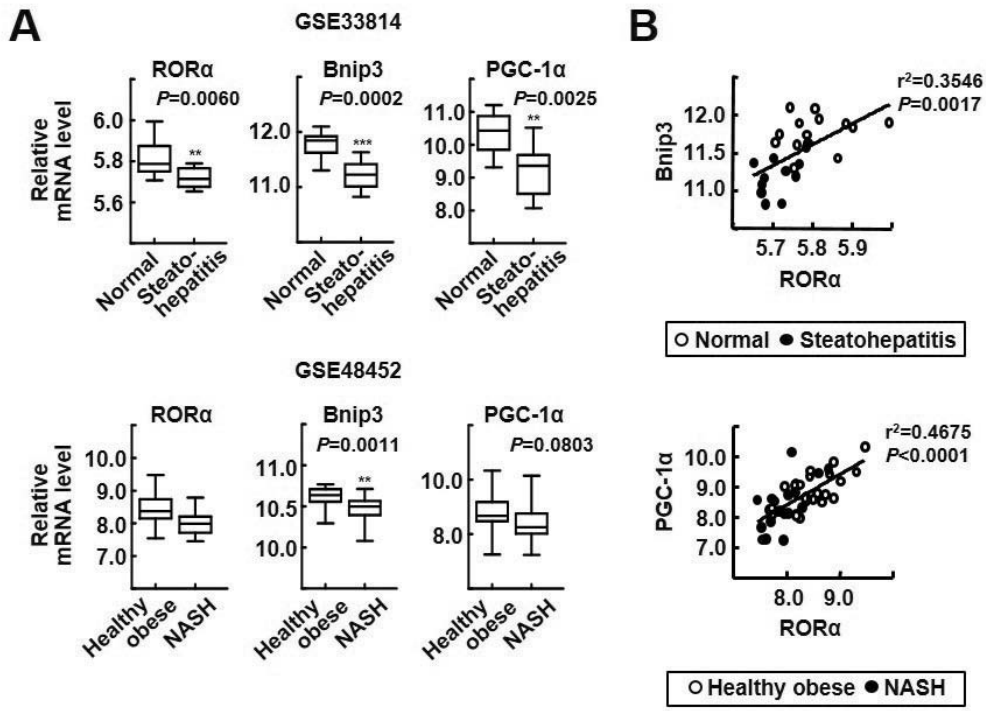

Figure 24. Expression levels of RORα, Bnip3, and PGC-1α in the livers of patients with steatohepatitis

(A, B) Database-based gene expression analysis was conducted using public datasets obtained from GEO site at the NCBI gene expression (http://www.ncbi.nlm.nih.gov/geo/). The data processed as median-normalized signal intensity value. Significances were analyzed by Mann-whitney U test and the positive correlation coefficient (r^2) was calculated by Pearson correlation test. **P < 0.01, and ***P < 0.001 vs normal or healthy obese (n=13 (normal) and n=12 (steatohepatitis) for GSE33814; n=27 (healthy obese) and n=18 (NASH) for GSE48452.

6. Autophagy is impaired in the liver of RORα knockout mice

It has been reported that liver autophagic activity is decreased in a mouse model of nonalcoholic fatty liver disease. Therefore, I examined whether autophagy was changed in the liver of RORα-LKO mice. Electron microscopic analysis showed that the formation of autophagosome induced by high-fat diet was reduced in liver of RORα-LKO mice (Figure 25). The accumulation of p62, one of the cargo proteins, was markedly increased in the liver of RORα-LKO mice, confirming the accumulation of LC3-Ⅱ and NBR1 protein (Figure 26). These results indicate that autophagic activity is decreased in the liver of RORα -LKO.

To determine which pathway is associated with regulation of autophagy by RORα, I combined genes in Autophagy as GO ontology with altered genes in RNA-seq analysis using liver tissue of RORα-LKO mice fed high-fat diet. As a result, mitophagy, lysosome and mTOR signaling pathway were found to form a network of high confidence level (Figure 27). This suggests that the reduction of autophagic activity by RORα deletion is associated with the mTOR signaling pathway, and specifically that RORα can regulate mitophagy and lysosomal function.

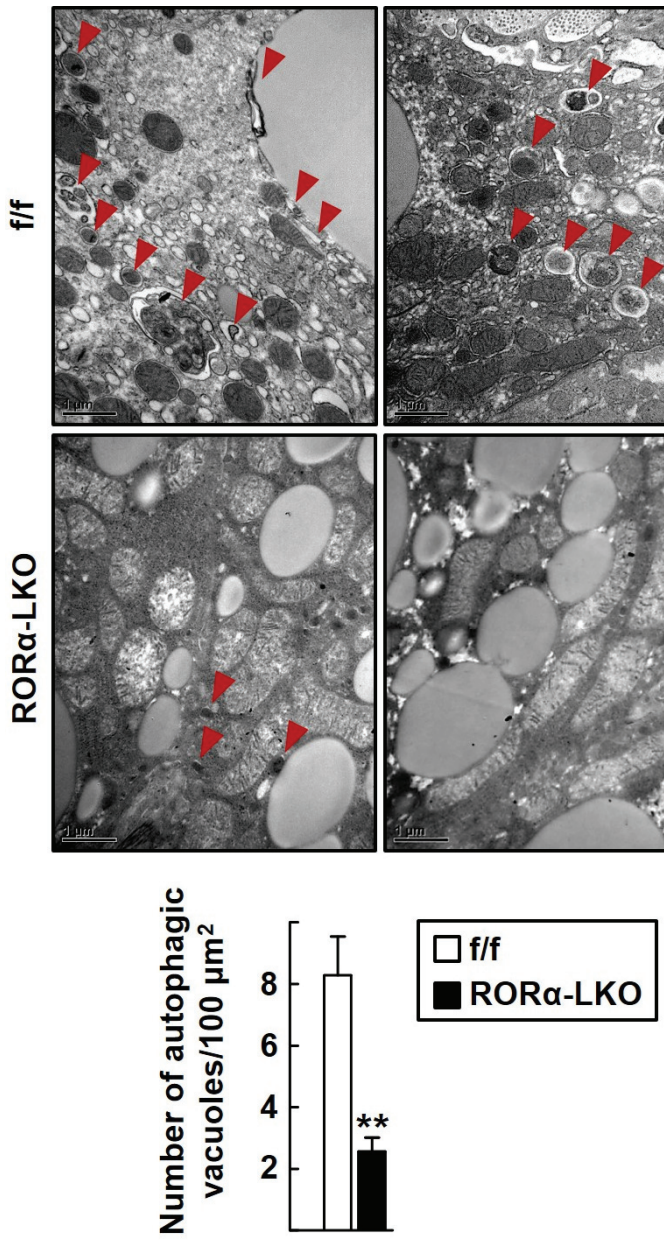

Figure 25. Autophagosome formation in the liver tissues of RORα-LKO mice

Representative EM images of the liver sections from HFD-fed RORα$^{f/f}$ and RORα-LKO mice. Red arrows indicate the autophagosomes. Data presented as mean ± SEM (n=4-6 mice). **P < 0.01 vs RORα$^{f/f}$.

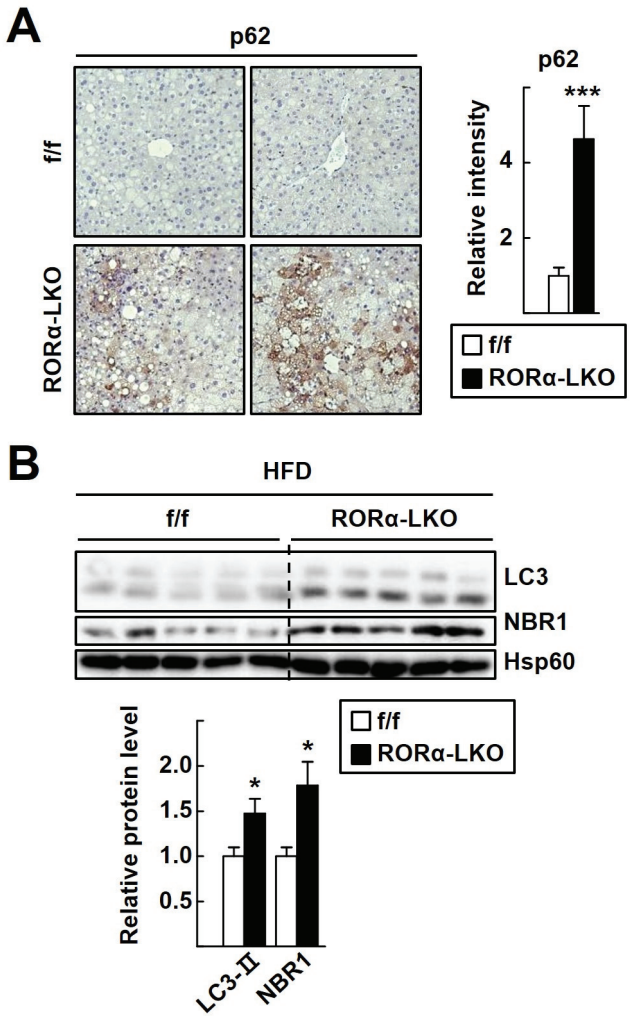

Figure 26. Impaired autophagic activity in the liver of RORα-LKO mice

(A) Histological staining of p62 (brown). Representative Images of liver sections from the RORα$^{f/f}$ and RORα-LKO mice were presented. Relative intensities were quantified using ImageJ. Values represent mean ± SEM (n=6-8). ***P < 0.001 vs HFD-fed RORα$^{f/f}$.

(B) The levels of indicated proteins were analyzed by western blotting (upper). Band intensities of each protein were quantified using ImageJ and normalized to that of Hsp60 (lower). Data presented as mean ± SEM (n=5). *P < 0.05 vs HFD-fed RORα$^{f/f}$

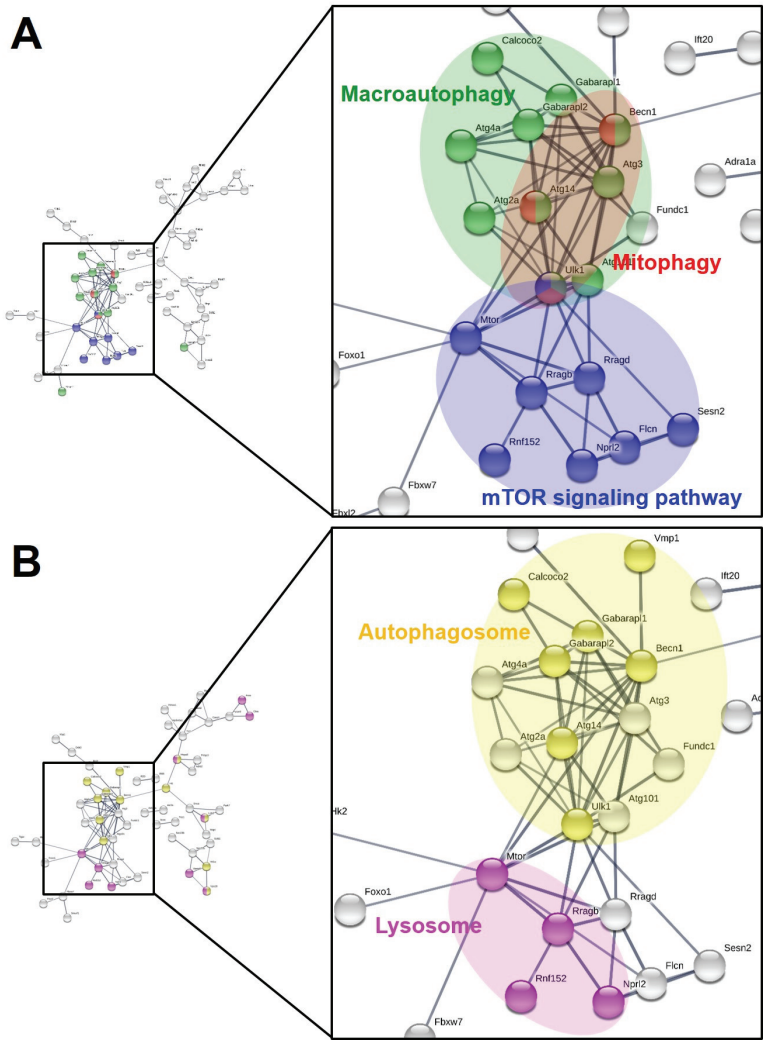

Figure 27. STRING protein network

Analysis of functional protein association networks by STRING database. Genes in GO Autophagy ontology were combined with altered genes in RNA-seq analysis using liver tissue of RORα-LKO mice fed high-fat diet.

7. RORα deletion in the hepatocytes results in decrease of autophagic flux

Primary hepatocytes were isolated from RORα-LKO mice to confirm autophagic flux. Confocal microscopy showed that the formation of GFP-LC3 puncta through bafilomycin treatment was significantly reduced by RORα deletion (Figure 28A). When metabolic stress was induced by treatment with palmitic acid, accumulation of LC3-Ⅱ by bafilomycin treatment was reduced in RORα-LKO-derived hepatocytes (Figure 28B). These results suggest that the decrease of autophagy in RORα-LKO mouse liver tissue was also decreased in primary hepatocyte. As a tool to confirm the autophagic flux, I confirmed the change by RORα deletion using Ad-GFP-mCherry-LC3. As a result, the formation of autophagosome and autolysosome in liver cells of RORα-LKO mice was remarkably reduced (Figure 29).

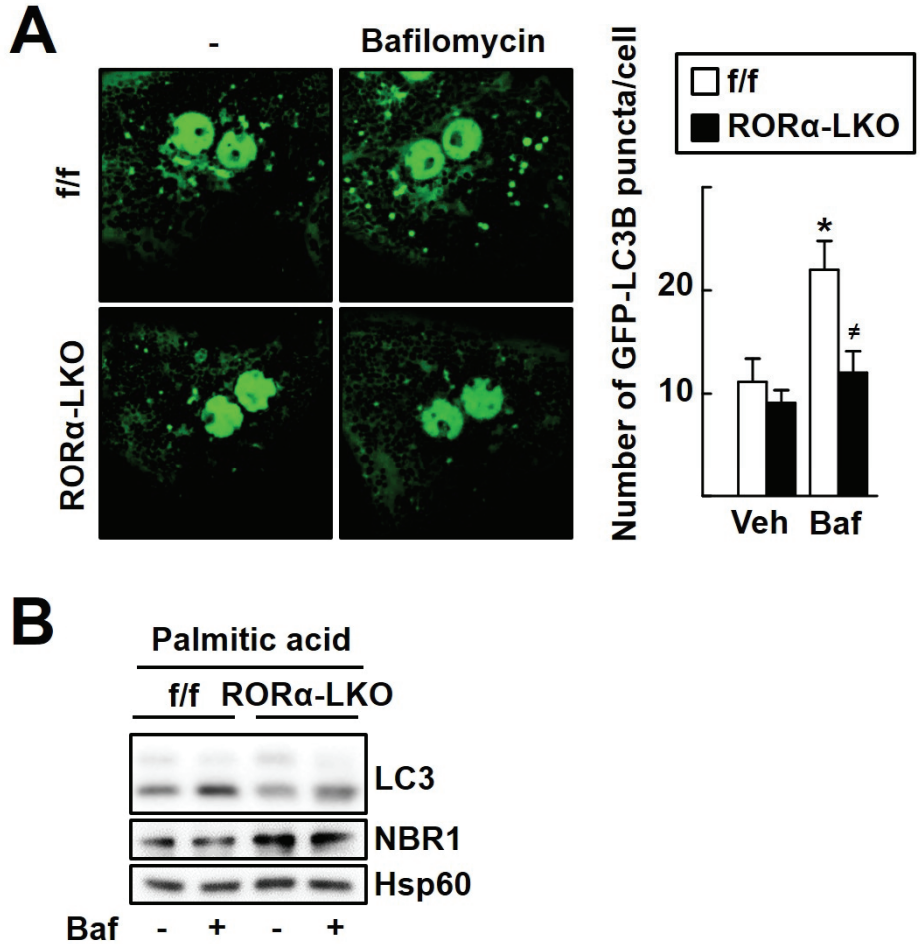

Figure 28. RORα deletion in the hepatocytes results in decrease of autophagic flux

(A) Mouse primary hepatocytes were infected by Ad-GFP-LC3 to observe the number of autophagic puncta. Data presented as mean ± SEM (n=25-40 cells). *P < 0.05, vs veh-treated hepatocytes of RORα$^{f/f}$ and ≠P < 0.05 vs bafilomycin-treated RORα$^{f/f}$.

(B) After treatment of palmitic acid, the expression levels of LC3 proteins in the presence or absence of bafilomycin A1, which blocks the fusion between autophagosomes and lysosomes were measured in hepatocytes of RORα$^{f/f}$ and RORα-LKO mice.

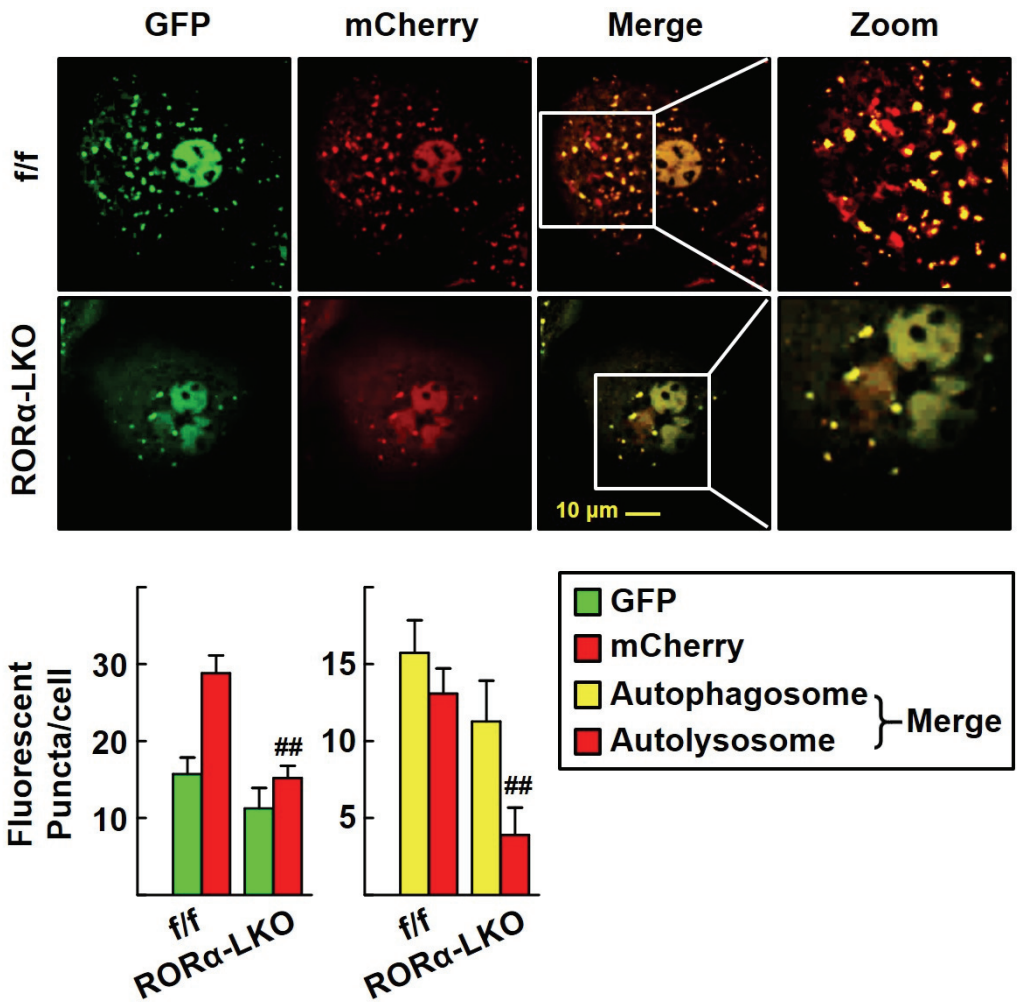

Figure 29. Autolysosome formation was decreased in hepatocytes of RORα -LKO

Mouse primary hepatocytes were infected by Ad-GFP-mCherry-LC3 to observe the number of autophagic puncta to observe the formation of autolysosomes. Data presented as mean ± SEM (n=20-29 cells). ##P < 0.01, vs hepatocytes of $RORα^{f/f}$.

8. Increase of mitophagy induced by metabolic stress is impaired in hepatocyte-specific RORa knockout mice

I expected that RORα could regulate mitophagy through the STRING protein network. I also examined electron microscopy of the liver tissues of ROR α-LKO mice induced by nonalcoholic fatty liver disease. As a result, the formation of hepatic mitophagosomes in RORa-LKO mice was markedly reduced (Figure 30).

Next, The primary cultured hepatocytes were isolated and mitophagy induced by fatty acid treatment was confirmed by Ad-GFP-LC3 infection and mitotracker staining. In the hepatocytes of RORα-LKO mice, not only the formation of LC3 puncta was reduced, but the formation of mitophagosome was also reduced (Figure 31). The lysosomal function is closely related to autophagic activity. When stained with Lysotracker and mitotracker dye, the degradation of mitochondria was significantly reduced in liver cells of RORα knockout mice (Figure 32). These results suggest that RORα promotes not only mitochondrial division but also mitophagy, thereby alleviating the incidence of nonalcoholic fatty liver disease.

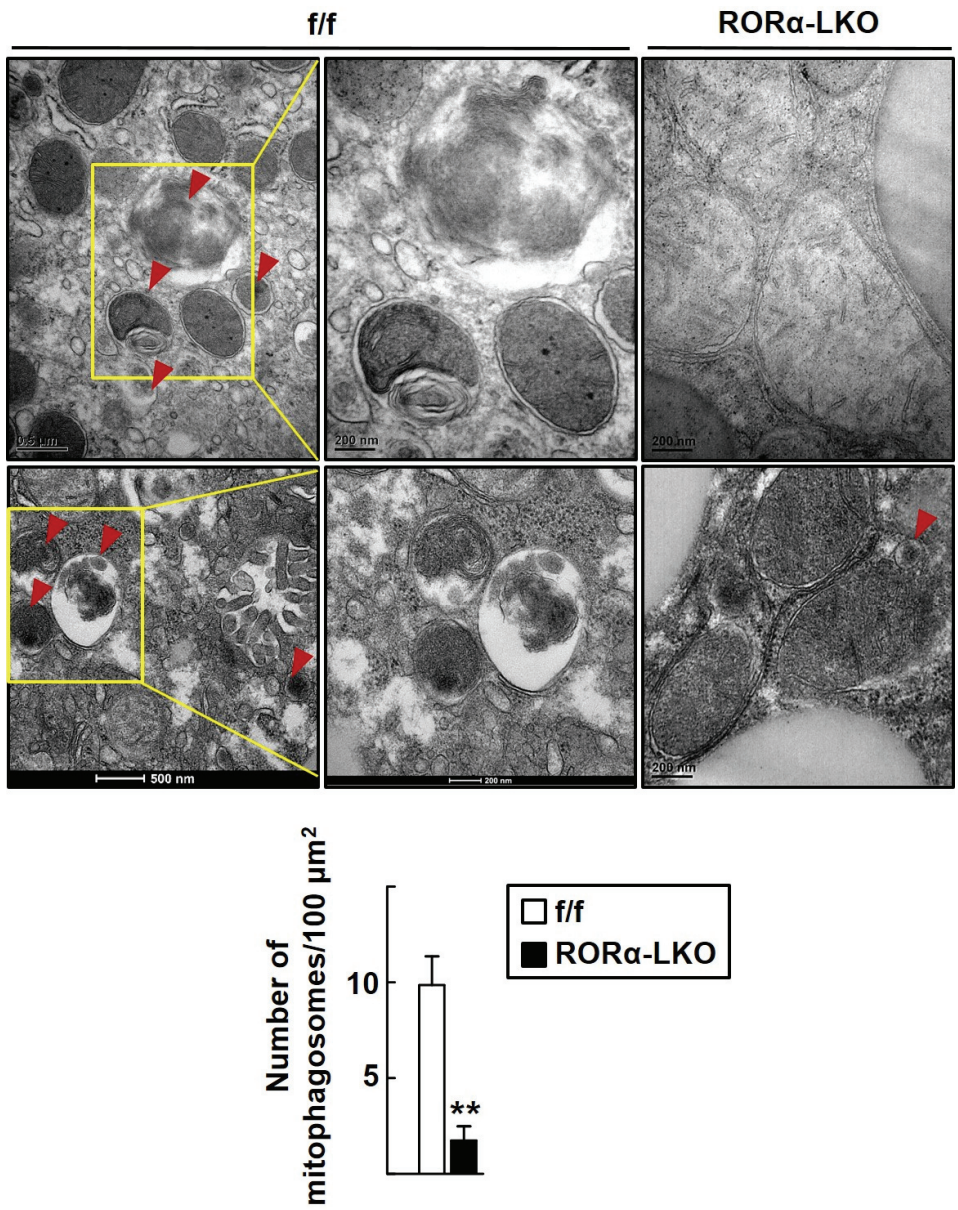

Figure 30. Decreased mitophagosome formation in the liver tissues of RORα-LKO mice

Representative EM images of the liver sections from HFD-fed RORα$^{f/f}$ and RORα-LKO mice. Red arrows indicate the mitophagosomes. Data presented as mean ± SEM (n=4-6 mice). **P < 0.01 vs RORα$^{f/f}$.

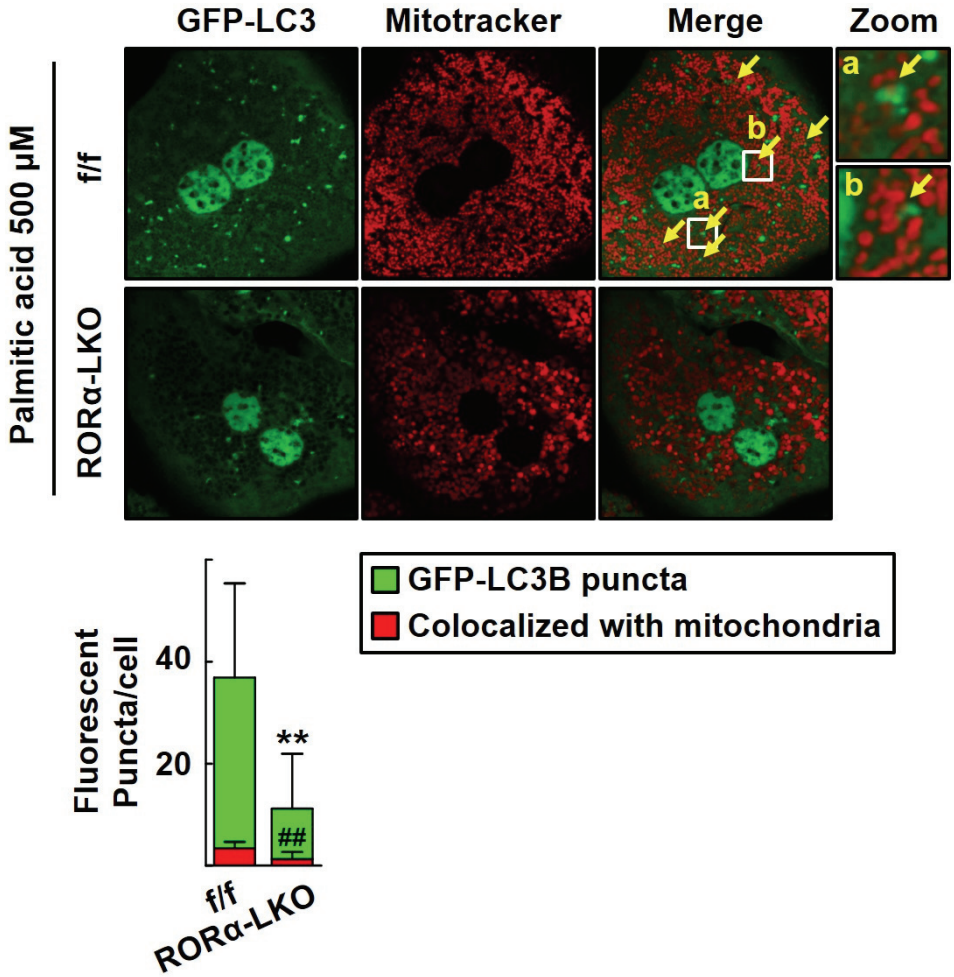

Figure 31. RORα knockout results in the decrease of mitophagosome

Mouse primary hepatocytes were infected by Ad-GFP-LC3 to observe the number of autophagic puncta. Cells were treated by palmitic acid 500 μM and stained by mitotracker red CMXRos dye. Data presented as mean ± SEM (n=10-11 cells). **, ##P < 0.01 vs hepatocytes of RORα$^{f/f}$.

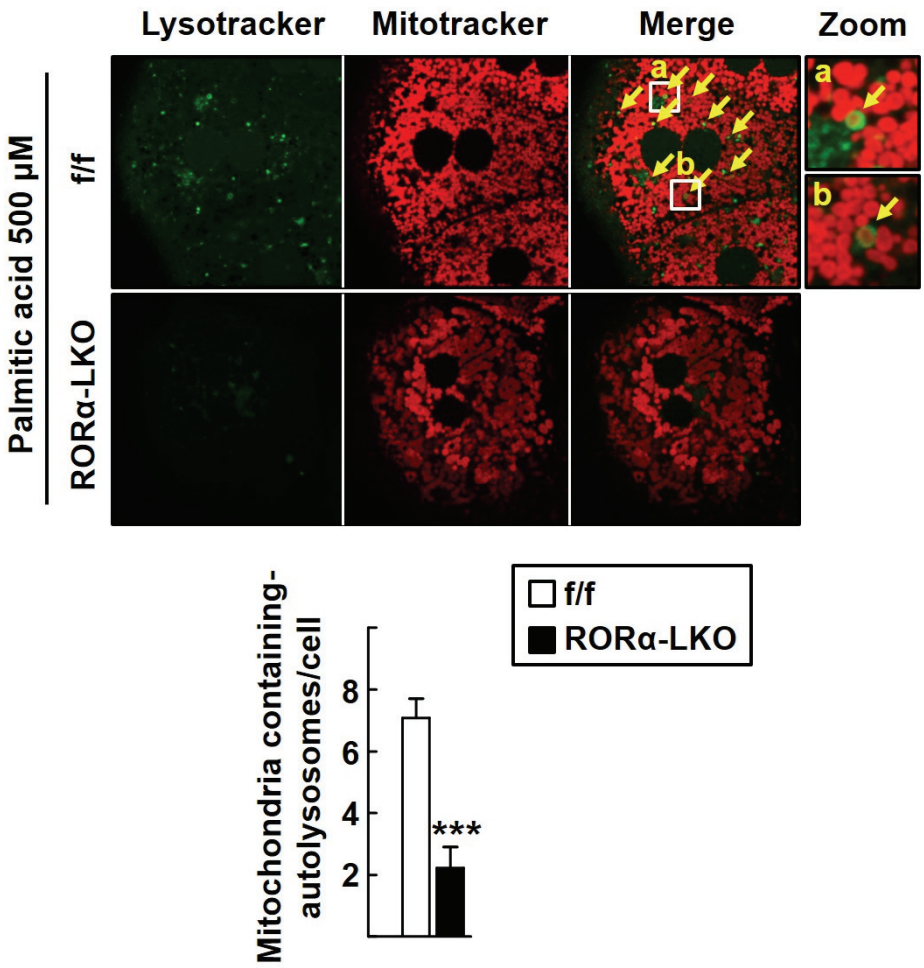

Figure 32. Mitochondria-containing autolysosomes were reduced in RORα-LKO

After treatment of palmitic acid 500 μM, mouse primary hepatocytes were stained by mitotracker red CMXRos dye and lysotracker green DND-26 to observe mitochondria and lysosomes. Data presented as mean ± SEM (n=13 cells). ***P < 0.001 vs hepatocytes of RORα$^{f/f}$.

9. The formation of lipophagosome and lysosomal degradation of lipid are reduced in RORα knockout mice

Along with the degradation of damaged mitochondria, lipid degradation through autophagy has also been reported to help alleviate nonalcoholic steatohepatitis. Thus, I tried to determine whether the lipid-specific autophagic effect in RORα-LKO mice was altered.

As a result, in the liver of RORα-LKO mice, combination of the lipid droplet and the autophagic membrane known as the formation of lipophagosome, were remarkably reduced with excessive lipid accumulation (Figure 33). The increase in lipid accumulation by RORα knockout was attributed by the decrease in lipophagy. After primary hepatocyte was isolated and treated with palmitic acid to induce lipid accumulation, LC3 puncta and lipid droplets were observed. As a result, puncta was significantly reduced by RORα knockout, and the binding between the stained lipid and the LC3 membrane was reduced (Figure 34). In order to confirm the lysosome degradation of lipid, lipid droplet was seen in the form of lipolysosome wrapped in lysosome when stained with lysotracker dye. This phenomenon was significantly reduced by RORα deletion (Figure 35). These results suggest that RORα promotes the formation of lipophagosome and lysosomal degradation of lipid, thereby contributing to decrease of lipid accumulation.

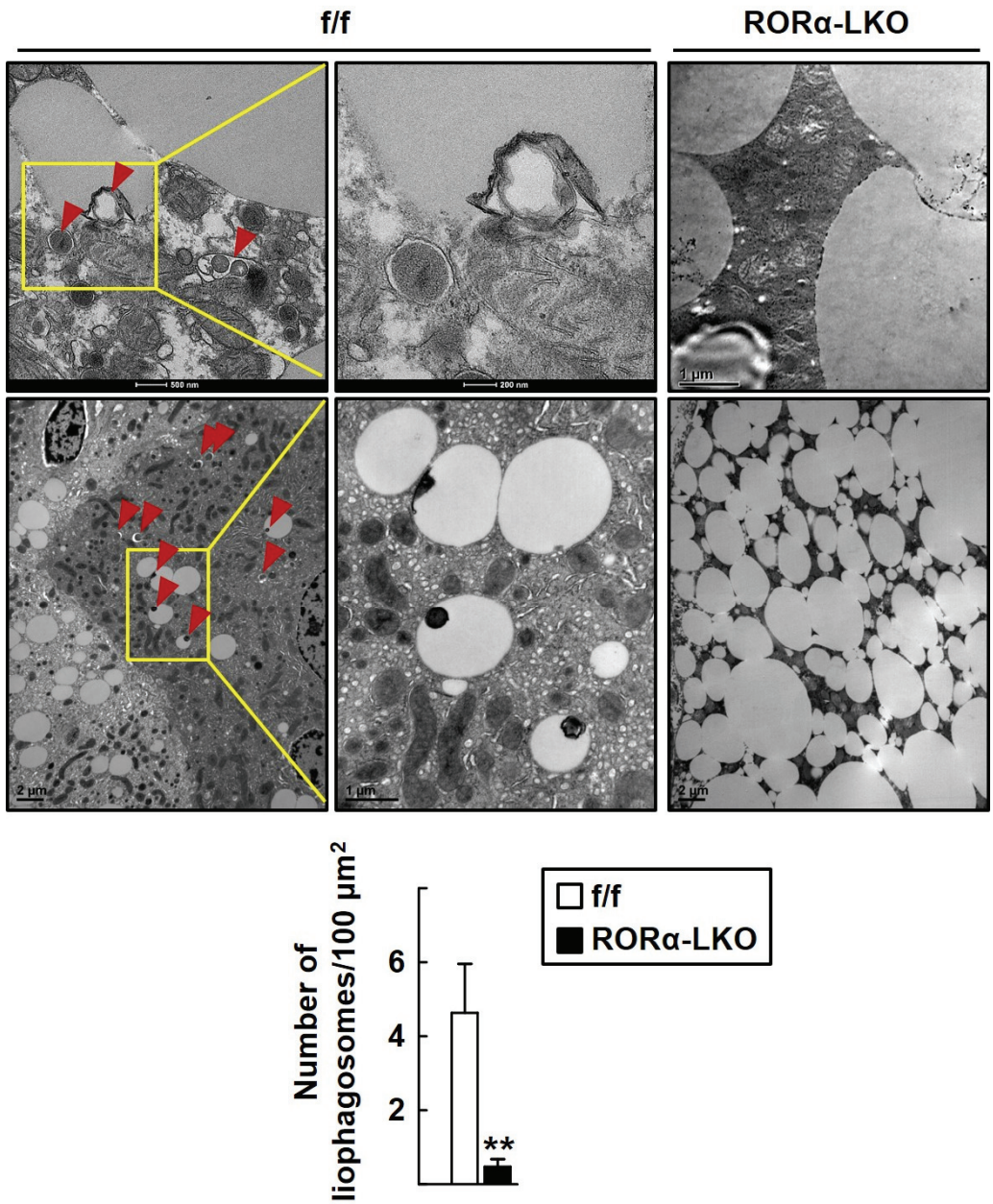

Figure 33. Decreased lipophagosome formation in the liver tissues of ROR α-LKO mice

Representative EM images of the liver sections from HFD-fed RORα$^{f/f}$ and RORα-LKO mice. Red arrows indicate the lipophagosomes. Data presented as mean ± SEM (n=4-6 mice). **P < 0.01 vs RORα$^{f/f}$.

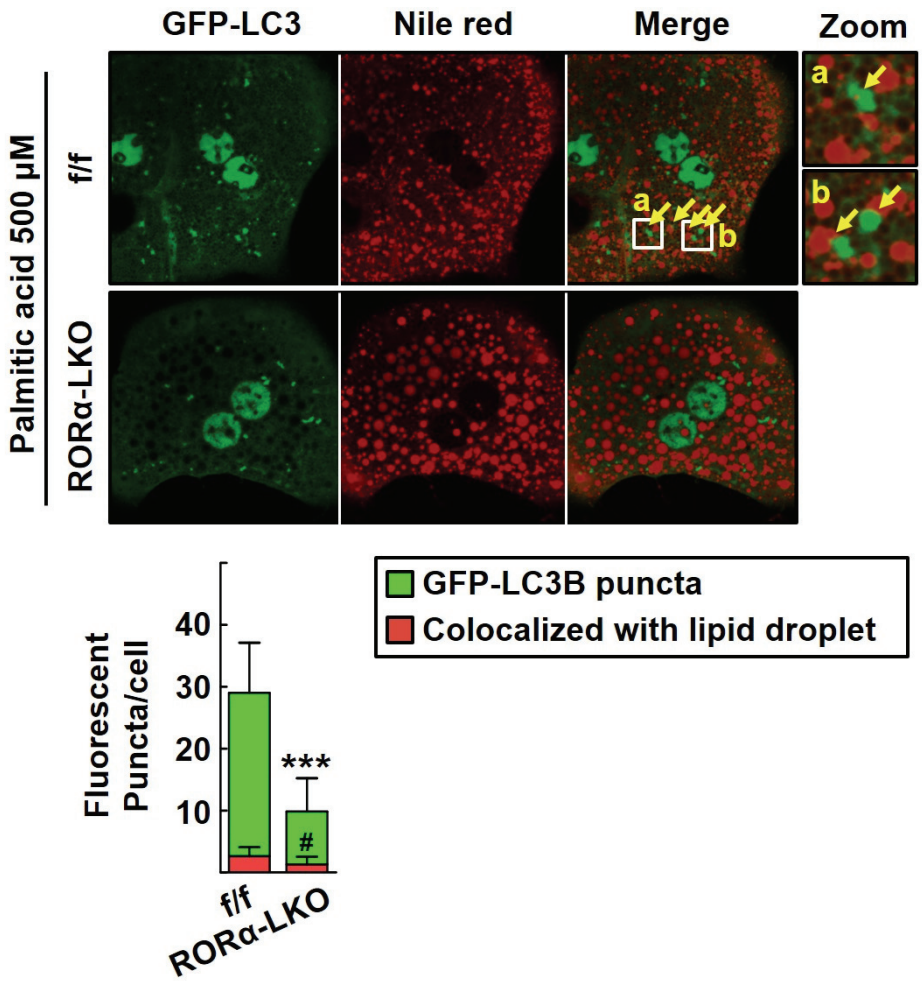

Figure 34. RORα deletion results in the decrease of lipophagosome in the hepatocytes

Mouse primary hepatocytes were infected by Ad-GFP-LC3 to observe the number of autophagic puncta. After treatment of palmitic acid 500 μM cells were stained by nile red dye. Data presented as mean ± SEM (n=11-13 cells). ***P < 0.001, and #P < 0.05 vs hepatocytes of RORα$^{f/f}$.

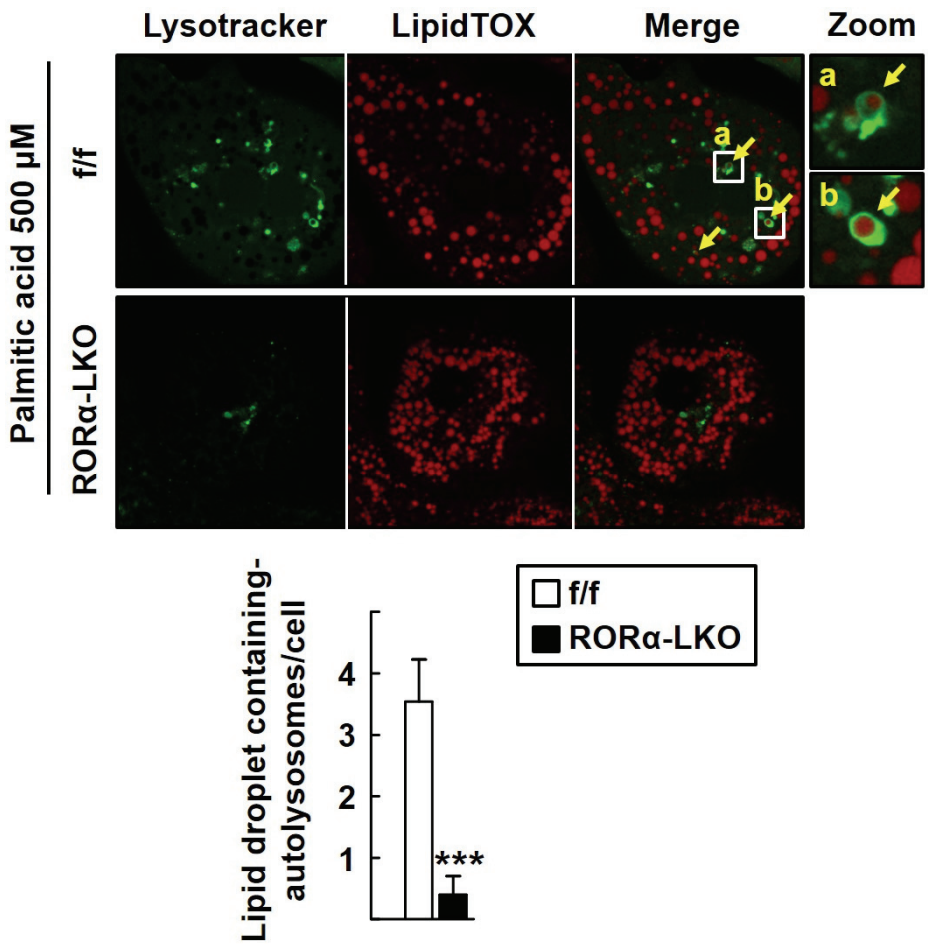

Figure 35. Lipid-containing autolysosomes were decreased in the hepatocytes of RORα-LKO

Mouse primary hepatocytes were treated by palmitic acid to induce lipid accumulation. After 6 h, cells were stained by LipidTOX dye and Lysotracker green DND-26 to observe lipid droplets and lysosomes. Data presented as mean ± SEM (n=10-13 cells). ***P < 0.001 vs hepatocytes of RORα$^{f/f}$.

10. Overexpression of RORα enhances autophagic activity via inactivation of mTOR and induction of target genes

Finally, RORα overexpression experiments were performed to confirm the reduction of autophagic activity observed by RORα knockout. When overexpressed by RORα in primary hepatocytes, the formation of autophagic vacuole was increased in electron microscopic analysis (Figure 36). In addtion, when bafilomycin was induced to accumulate LC3-Ⅱ, autophagic flux was increased by RORα overexpression in hepatocytes (Figure 37). Previous results from the STRING protein network analysis suggested that reduction of autophagy by RORα knockout might be related to the mTOR signaling pathway (Figure 27). Therefore, when examined the protein of the molecule involved in mTOR signaling through RORα overexpression was analyzed, it was confirmed that the phosphorylation of mTOR decreased and inactivation was induced (Figure 38A). In contrast to the inactivation of mTOR by RORα overexpression, the phosphorylation of mTOR was significantly increased by RORα knockout in the liver (Figure 38B). In addition, overexpression of RORα in primary hepatocytes increased expression of genes related to autophagy and lysosome function. Especially, the expression of Atg2a and Ctsd was remarkably increased (Figure 39A, B).

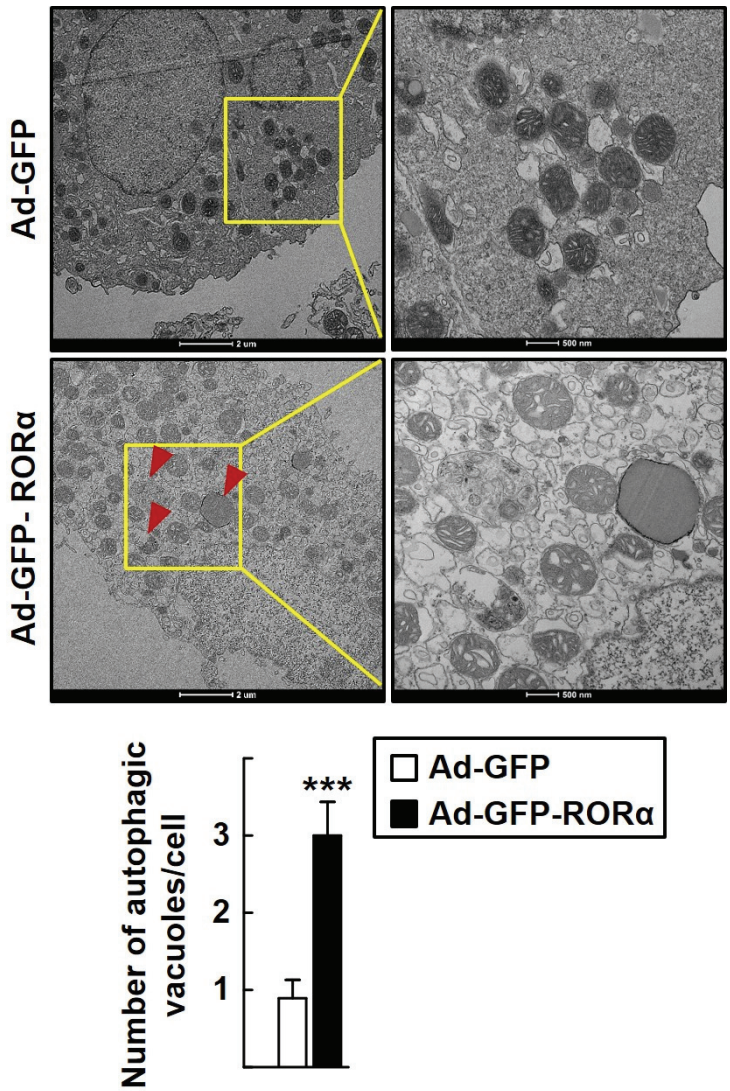

Figure 36. Increased autophagosomes in the hepatocytes of RORα overexpression

Representative EM images of the hepatocytes infected by Ad-GFP or Ad-GFP-RORα. Red arrows indicate the autophagosomes. Data presented as mean ± SEM (n=16-19 cells). ***P < 0.001 vs hepatocytes infected by Ad-GFP.

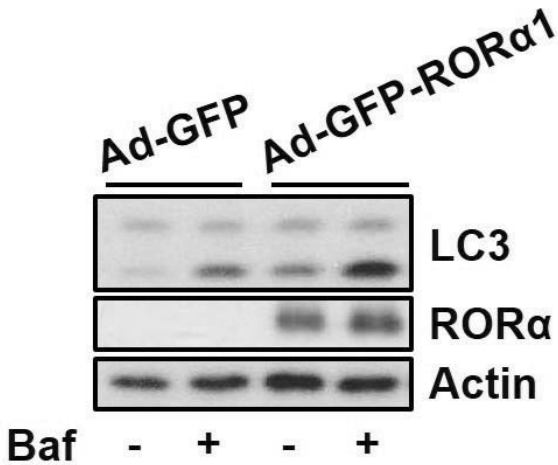

Figure 37. Autophagic flux is increased by RORα overexpression in hepatocytes

After mouse primary hepatocytes were infected by either Ad-GFP or Ad-GFP-RORα1 for 18 h, the expression of LC3 proteins in the presence or absence of bafilomycin A1 30 nM for 1 h was measured.

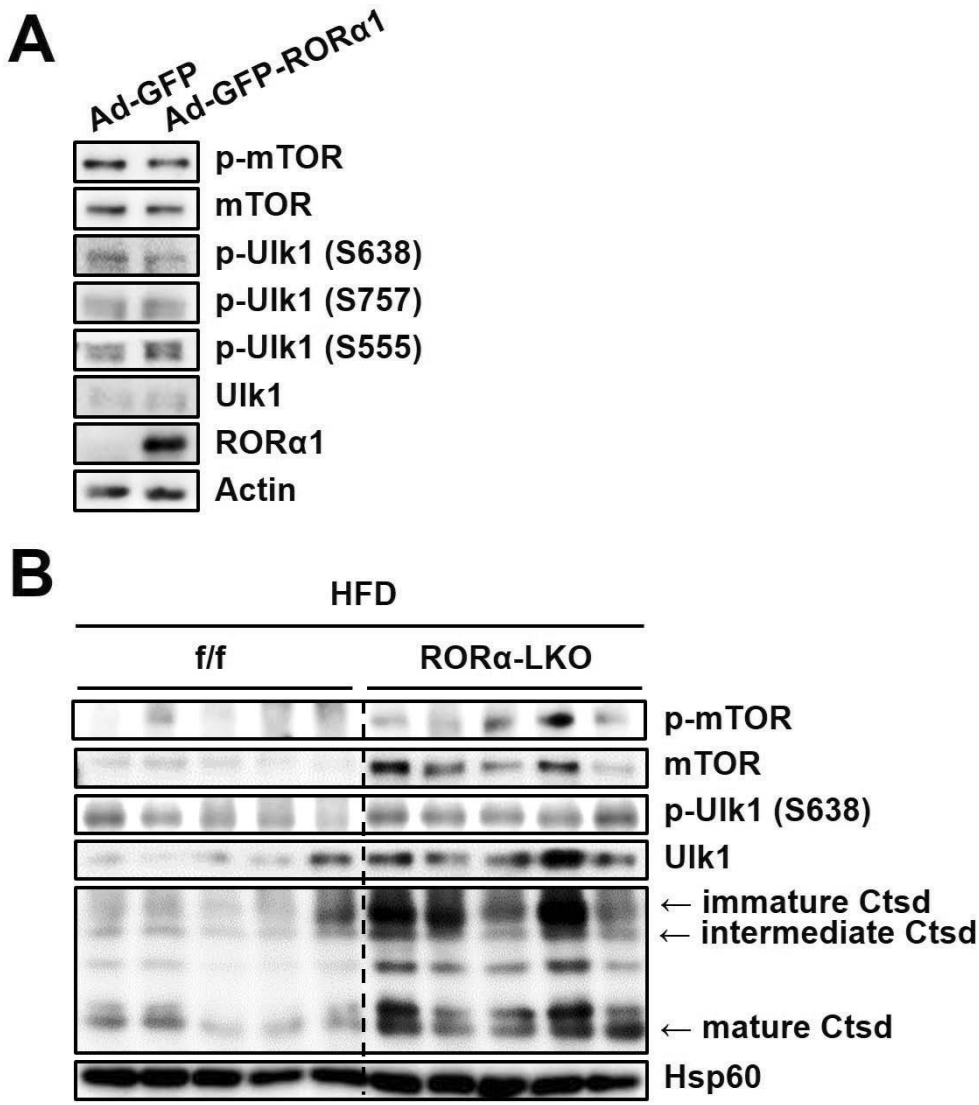

Figure 38. Activation of mTOR signaling is significantly increased by RORa knockout

(A) The protein levels of factors in mTOR pathway in mouse primary hepatocytes infused by either Ad-GFP or Ad-GFP-RORα.

(B) Hepatic protein levels of factors in mTOR pathway and Ctsd were analyzed by western blotting in HFD-fed RORα$^{f/f}$ and RORα-LKO mice (n=5).

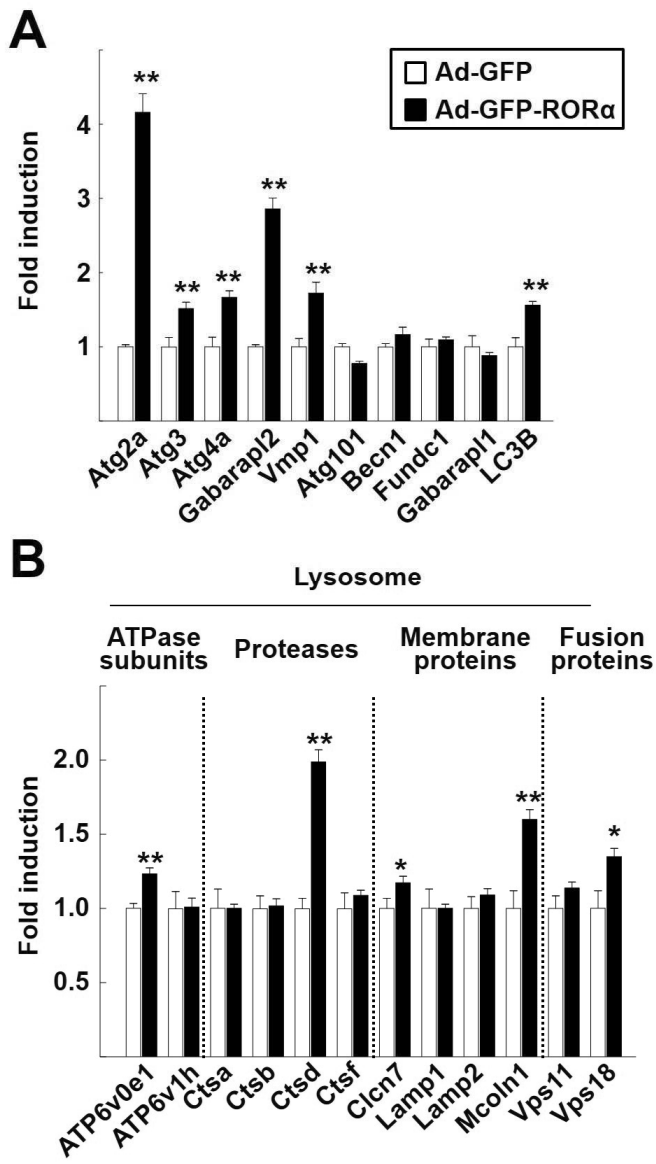

Figure 39. Overexpression of RORα enhances the expression of genes related autophagy and lysosome function

(A, B) After mouse primary hepatocytes were infected by either Ad-GFP or Ad-GFP-RORα for 18 h, the mRNA levels of factors related to autophagy and lysosome function were measured by qRT-PCR. The values represented as mean ± SEM. *P < 0.05 and **P < 0.01 vs Ad-GFP infused hepatocytes.

11. Expression levels of hepatic autophagy-related genes are low in patients with steatohepatitis

In order to confirm the above results and clinical relevance, I analyzed the expression of autophagy-related factors in liver tissue of patients with steatohepatitis through publicly available database. Interestingly, I observed that expression of Atg2a, LC3B, Calcoco2, and Gabarapl2 was reduced in the liver of patients with steatohepatitis (Figure 40).

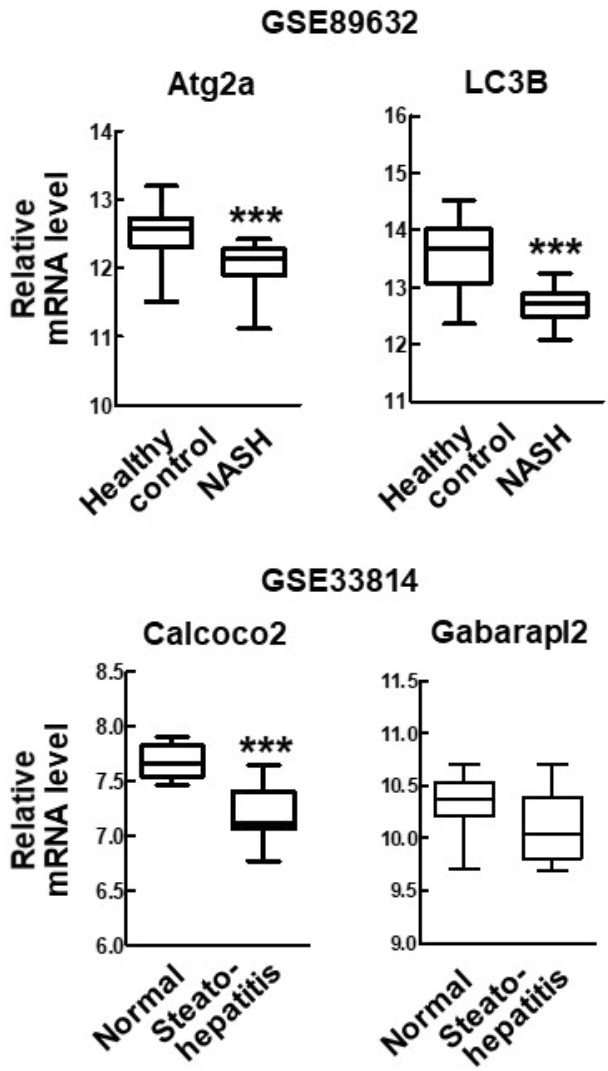

Figure 40. Expression levels of Atg2a, LC3B, Calcoco2, and Gabarapl2 in the livers of patients with steatohepatitis

Database-based gene expression analysis was conducted using public datasets obtained from GEO site at the NCBI gene expression (http://www.ncbi.nlm.nih.gov/geo/). The data processed as median-normalized signal intensity value. Significances were analyzed by Mann-whitney U test. ***P < 0.001 vs healthy control or normal.

V. DISCUSSION

1. The liver-specific deletion of RORα results in the development of severe NASH in mouse model

Here, I report that the loss of the function of hepatic RORα resulted in the development of severe NASH in mice, which supports a protective role of RORα against the progression of NAFLD. The function of RORα in hepatic lipid metabolism has been controversial for some decades. RORα$^{sg/sg}$ mice fed an HFD are resistant to diet-induced hepatic steatosis and insulin resistance (Kang et al., 2011; Lau et al., 2008). In contrast, RORα was reported to activate AMPK, while it represses the transcription function of LXRα, thereby protecting from hepatic lipid accumulation (Kim et al., 2012). Moreover, RORα upregulated antioxidative and anti-inflammatory genes, which ameliorated the symptoms of NASH in the methionine and choline deficient diet mouse model (Han et al., 2014). Although the reasons for this discrepancy are not fully understood, the secondary effects generated by the sg/sg phenotype may contribute, at least in part, to this discordance in hepatic lipid metabolism. For example, the secretion of hormones that are important for energy balance, such as leptin, norepinephrine, adrenocorticotropic hormone, and corticosterone, was abnormal in RORα$^{sg/sg}$ mice (Bertin et al., 1990; Frederic et al., 2006; Lau et al., 2008). These mice were lean despite their hyperphagia, probably because of an enhancement of the energy metabolism in brown adipose tissue (Bertin et al., 1990). This

imbalanced whole-body metabolism may cover or surpass the primary phenotype of RORα depletion in the liver; thus, the liver-specific RORα mice may provide a better animal model for studying the hepatic function of RORα.

2. Mitochondrial quality control that inhibits the progression of NASH is a novel role of RORα

Mitochondrial dysfunction is the primary pathogenesis of nonalcoholic steatohepatitis. This is because a molecular mediator caused by mitochondrial dysfunction is associated with cell injury and inflammation, which plays a crucial role in the progression of NASH. Thus, identifying a molecular mechanism associated with mitochondrial dysfunction and identifying regulatory factors may be an effective strategy for treating NASH. In this study, I have shown that RORα can be a therapeutic target for alleviating the NASH by controlling mitochondrial fission and autophagy (Figure 41).

Analysis of liver tissues of RORα-LKO mice revealed severe lipid accumulation, inflammation and fibrosis, which were accompanied by mitochondrial dysfunction (Figure 6-10, 12-14). Mitochondrial dysfunction in RORα-LKO mice is not simply a result of the onset of nonalcoholic fatty liver disease. There was no morphological difference of mitochondria in the liver of control mice and knockout mice fed low fat diets, but there was a difference between control and RORα-LKO in oxygen consumption when hepatocytes were isolated (Figure 15). In addition, when palmitic acid treatment induced mitochondrial fission and mitophagy, it was confirmed that the reactivity due to stimulation disappeared by knockout. In addition, when starvation was performed

on hepatocytes, the shape of mitochondria was already irregular by RORα knockout (Figure 16). It is thought that the defects on mitochondrial fission and autophagy due to RORα knockout are gradually accumulating and impairing the disease since the onset of nonalcoholic steatohepatitis is due to persistent and complex pathological factor inflows.

The observation that RORα increased the expression of markers for mitochondrial biogenesis, such as PGC-1α, Idh3a, and Acadm, suggests that RORα may enhance mitochondrial biogenesis (Figure 22). The expression of mitochondrial OXPHOS proteins was decreased in the livers of HFD-fed RORα -LKO mice (Figure 12). However, total mitochondrial number was not affected by knock-down of RORα in basal condition (Figure 19). One of the possible causes of this discrepancy may be that quantity of mitochondria is regulated by the balance of two opposing processes, i.e., mitochondrial biogenesis and elimination of mitochondria. Thus, no effect on the mitochondrial number by RORα could be due to the RORα-induced biogenesis and simultaneous elimination of mitochondria by RORα-induced Bnip3, one of the key factors involved in the mitophagic process (Hanna et al., 2012).

3. RORα mediates the mitochondrial quality control, which is linked to the regulation of ER maintenance and lysosomal function

The results of our RNA-seq and ChIP-seq analyses showed that the ER ranked at the top of the GO cellular components for RORα-regulated genes (Figure 15). In addition, RORα induced the mRNA levels of Mfn2, which is enriched at the ER-mitochondria interface and promotes intercommunication (Figure 22) (de Brito and Scorrano, 2008). These observations suggest that RORα mediates the mitochondrial quality control, which is linked to the regulation of ER maintenance.

The relationship between mitochondria and ER is closely related to lysosomal function via Ca^{2+} signaling. Ca^{2+} signaling of lysosomes is known to regulate several cellular precesses such as autophagy, membrane fusion and cell death (Todkar et al., 2017). Thus, the association of mitochondria with lysosomes through Ca^{2+} signaling can be expected, and mitochondrial activity is actually needed to maintain lysosomal structure and function. Specifically, it is known that when mitochondrial function is reduced, enlarged endo-lysosomal structures accumulate, and activity and acidification of lysosome are impaired (Baixauli et al., 2015; Demers-Lamarche et al., 2016). These lesions are found in

the deletion of TFAM, OPA1, and PINK1 associated with mitochondrial biogenesis, fusion, and mitophagy, demonstrating a correlation between mitochondrial function and lysosome activity. The results of this study showed that the fluorescence of lysosomes stained with lysotracker in hepatocytes of RORα knockout mice was decreased and the lysosomal degradation of mitochondria and lipids was decreased (Figure 32, 35). In addition, the expression of genes associated with lysosome activity such as ATP6v0e1, Ctsd, Mcoln1, and Vps18 was increased by RORα (Figure 39). Based on these results, it can be seen that the increase of mitochondrial function by RORα also affected lysosome activity.

4. RORα-mediated regulation of Bnip3 links mitochondrial fission to mitophagy

I found that Bnip3 is one of the major downstream effectors of RORα-controlled mitochondrial quality maintenance (Figure 22, 23). Bnip3 is a well-known mitochondrial fission factor that promotes the translocation of Drp1 to mitochondria and simultaneously decreases Opa1-induced mitochondrial fusion (Dhingra and Kirshenbaum, 2014). Consistently, the depletion of Bnip3 in mice resulted in the loss of mitochondrial membrane potential and structural integrity, probably because of impairment of mitochondrial fission and subsequent mitophagy (Glick et al., 2012). Interestingly, the loss of Bnip3 led to typical features of steatohepatitis, such as reduced AMPK activity and fatty acid β-oxidation and increased lipid synthesis, which were observed in the livers of RORα-LKO mice (Glick et al., 2012). In human patients with NASH, the hepatic levels of Bnip3 were decreased compared with those of healthy obese individuals and correlated positively with the expression levels of RORα (Figure 24). Together, these observations strongly support our proposed mechanism of Bnip3-mediated RORα action. Bnip3 is also involved in the mitophagic process by interacting with the microtubule-associated protein 1 light chain 3 (LC3) (Hanna et al., 2012). Mitophagy is a cellular process triggered by severe mitochondrial defects that eventually promotes the survival of cells under stress

conditions (Palikaras and Tavernarakis, 2014). It was reported that the mitophagic flux is impaired in the livers of both NAFLD patients and murine models of NAFLD, which could be caused by an elevation of endoplasmic reticulum (ER) stress (Gonzalez-Rodriguez et al., 2014). The results of this study show that mitophagy is regulated by RORα-mediated gene regulation of Bnip3, LC3b, and Atg2a as well as mTOR inactivation. In fact, the Chip-seq results suggest that RORα can directly regulate Bnip3, LC3b, and Atg2a (Data not shown).

The Bnip3 and phosphorylation of Drp1 was increased by RORα, but the expression of Fis1, the fission factor, was not changed by RORα knockout or overexpresion (Figure 17, 21). Since Fis1 translocates to mitochondria through coordination of Drp1 and Mff, it is necessary to investigate whether localization has changed by RORα (Zhang et al., 2016).

5. Relationship of RORα-mediated mitochondrial quality control with other nuclear receptors

Nuclear receptors, PPARs, and ERRα, and their coactivator PGC-1α have been implicated in nuclear - mitochondrial communication, as they regulate the expression of genes that are important for mitochondrial biogenesis, cellular respiration, and fatty acid oxidation (Scarpulla, 2008). Recent reports demonstrated that PPARα and PPARɣ agonists modulated mitochondrial fusion-fission dynamics (Zolezzi et al., 2013). Also, PGC-1α directly regulated the mitochondrial fusion genes Mfn1 and Mfn2 by coactivating ERRα (Martin et al., 2014; Soriano et al., 2006). PGC-1α-ERRα-ULK1 pathway regulates the mitochondrial fission and mitophagy and has been to increase the expression of ERRα reported to be adjusted mitochondrial quality in metabolic diseases (Engelsdorf et al., 2018). It has also been reported that mTOR modulates the activity of ERRα through ubiquitin-mediated degradation and that this crosstalk has a clinical impact on nonalcoholic fatty liver disease (Chaveroux et al., 2013). Here, I found that RORα-mediated mitochondrial quality check was closely connected to PGC-1α and mTOR signaling. PGC-1α was demonstrated as being a transcriptional downstream target of RORα (Figure 23). All of these nuclear receptors employ PGC-1α as a coactivator in their transcription function (Liu et al., 2007; Schreiber et al., 2004; Vega et al., 2000). Recently, PPARα was shown

to be a transactional target of RORα in the periostin-dependent pathway, which mediates obesity-induced hepatic steatosis (Lu et al., 2014). Together, these observations suggest that RORα is an integrator of the nuclear - mitochondrial communication and mitochondrial dynamics by coordinating ERRα and PPARα via the modulation of PGC-1α and mTOR signaling.

6. Inactivation of mTOR by RORα

Previously, it was known that RORα activates AMPK in liver and attenuates steatosis. RORα increased the level of pLKB1 and demonstrated that it was independent of Ca^{2+}/calmodulin-dependent protein kinase kinase β. In addition, RORα decreased ATP levels, indicating that ATP consumption was increased or ATP production was reduced. In this study, mitochondrial dysfunction was induced by RORα knockout, which was demonstrated by the decrease of complex 1 activity and NASH was developed in RORα knockout mouse (Figure 17). Oxygen consumption as a measure of mitochondrial function in primary hepatocyte as decreased by RORα knockout and increased by RORα overexpression (Figure 15, 20). Therefore, ATP reduction by RORα can be expected to be due to increased consumption of ATP, rather than decreased production of ATP in mitochondria, indicating that AMPK is activated. In addition, the NAD^+/NADH ratio was increased by RORα. The synthesis of NAD^+ starts from the tryptophan and is known to enhance the mitochondrial function by increasing sirtuin activity (Katsyuba et al., 2018). An increase in NAD^+ by RORα may reduce the consumption of NAD^+ or increase production, thereby contributing to an increase in mitochondrial function and increase the activity of AMPK. Increased AMPK activity of RORα may cause inactivation of mTOR. RORα reduced the phosphorylation of mTOR by increasing AMPK

activity in smooth muscle cells and caused the deactivation of downstream targets (Kim et al., 2014). Therefore, RORα in hepatocytes can also be expected to inactivate mTOR and increase autophagy through increased AMPK activity.

Inactivation of mTOR by RORα may not only increase autophagy but also contribute to increased lysosome activity. Inactivation of mTOR increases the biogenesis of the lysosome, changes the lysosomal membrane potential, and increases the fusion of autophagosome and lysosome (Puertollano, 2014). The expression of mTOR on the surface of lysosome was increased in TFEB-knocked hepatocytes, and it was confirmed that this is a phenomenon of lysosome dysfunction through mTOR activation (Chao et al., 2018). Therefore, further studies may be needed to investigate the functional changes of lysosomes by RORα-mediated mTOR inhibition in hepatocytes.

7. Various roles of RORα on lipid metabolism including lipophagy, fatty acid oxidation and suppression of lipogenesis

In this study, RORα increased lipophagy and alleviated the progression of NASH. Electron microscopy revealed that the lipophagosomes in the liver of RORα knockout mice were reduced (Figure 33). The lipophagosomes observed by LC3 puncta were reduced in hepatocytes of RORα knockout mice (Figure 34). Lysosomal degradation of lipid was also reduced in RORα knockout (Figure 35). Specifically, the expression of Atg2a was markedly increased by RORα overexpression (Figure 39). Atg2a is present in the autophagic membrane and is involved in the autophagic flux as well as in the lipid droplet, suggesting that autophagy can be linked to lipid metabolism (Velikkakath et al., 2012). In fact, when silencing Atg2, autophagic flux was blocked and aggregation of lipid droplets occurred (Velikkakath et al., 2012). Therefore, it can be expected that RORα not only increases autophagy through Atg2a but also participates in lipid metabolism. In fact, fatty acids liberated through lipophagy enter the mitochondria and in mitochondria ATP production occurs through fatty acid oxidation. RORα is known to activate AMPK and increase the expression of genes related to hepatic fatty oxidation, such as CPT-1, ACS, MCAD, ACO1,

and the like. In addition, RORα reduces the lipogenesis by inhibiting the transcriptional activity of LXRα through physical binding with LXRα (Kim et al., 2012). In fact, the expression of FAS, a downstream target of LXRα, was increased in liver tissues of RORα knockout mice fed HFD (Data not shown). In a recent report, RORα has been reported to regulate hepatic lipid homeostasis by inhibiting signaling of PPARγ through recruitment of HDAC3 (Kim et al., 2017). However, PPARγ is known to have a beneficial effect on neurological disease by increasing mitochondrial function and mediating antioxidant and inflammatory responses (Corona and Duchen, 2016). Therefore, it is unclear to explain the increase of NASH by RORα knockout only by dysregulation of PPARγ signaling. In conclusion, I suggest that regulation of mitochondrial function and lipophagy by RORα may be a molecular mechanism to explain progress of NASH.

8. The roles of RORa in the pathophysiology of diseases caused by mitochondrial dysfunction

As mitochondrial dysfunction is associated with various human diseases, including Alzheimer's disease, multiple sclerosis (MS), and retinal diseases, the roles of RORα in the pathophysiology of these diseases should be addressed. Acquaah-Mensah et al (2015) reported that RORα expression was abnormal in the hippocampus of patients with Alzheimer's disease, and that RORα was highly connected in a network of differentially expressed genes, which included genes involved in mitochondrial dynamics such as Fis1 and Opa1 (Acquaah-Mensah et al., 2015). The pathobiology of MS, which is an autoimmune disorder of the central nervous system, is accompanied by mitochondrial dysfunction; the expression of nuclear-encoded mitochondrial genes and the activities of mitochondrial complexes were decreased in the MS motor cortex in patients with this disease. Interestingly, polymorphism of intronic variations in the RORα gene was associated with susceptibility to MS (Eftekharian et al., 2016). Similarly, a significant link between single-nucleotide polymorphisms present in intron 1 of the RORα gene and a mitochondrial dysfunction-related disease, aged-related macular degeneration, was demonstrated using a systems biology-based approach (Silveira et al., 2010). Although there is no clear evidence currently, I suspect that RORα-mediated

mitochondrial function might be associated with the development of these diseases. In addition, mitochondrial function in pancreas, gut, heart, and skeletal muscle, including liver, may also be involved in metabolic diseases. Therefore, the role of RORα in regulating mitochondrial function in each tissue can be a therapeutic target for systemic metabolic syndrome.

9. Clinical potential of RORa to protect against NASH

Non-alcoholic fatty liver disease is a worldwide prevalent disease, but it is a disease with no approved medication. To treat nonalcoholic steatohepatitis, the first aim is to inhibit lipid accumulation. For this purpose, PPARs modulator, OCA targeting FXRα, and FGF-12 analogues that inhibit de novo lipogenesis can be used. Second, vitamin E and ASK1 inhibitor can be used to suppress oxidative stress, inflammation, and apoptosis (Sumida and Yoneda, 2018). However, these drugs have low efficacy and side effect problems. Particularly, obeticholic acid, a farnesoid X receptor agonist have been effective in decreasing the liver damage level but have serious adverse effects in raising the level of LDL in the blood and increasing the risk of cardiovascular disease (Neuschwander-Tetri et al., 2015). In addition, studies that FXRα reduces autophagy in the liver suggest that it is unlikely to avoid side effects from these results (Lee et al., 2014; Seok et al., 2014). Therefore, it is necessary to overcome these limitations and to develop therapeutic drugs to eliminate the underlying pathogenesis.

In the past reports, thiourea derivatives, JC compounds have been shown to act as agonists of RORα, inhibiting lipid accumulation and attenuating the fatty liver. In addition, the antioxidant effect alleviated the pathology of nonalcoholic steatohepatitis (Han et al., 2014; Kim et al., 2012). I found a

potential that JC1-40, an agonistic ligand of RORα, improved mitochondrial function (Data not shown). Further studies of pharmacological interventions targeting RORα-mediated mitochondria quality control may provide therapeutic strategies against NASH as well as other diseases associated with defects in mitochondrial function.

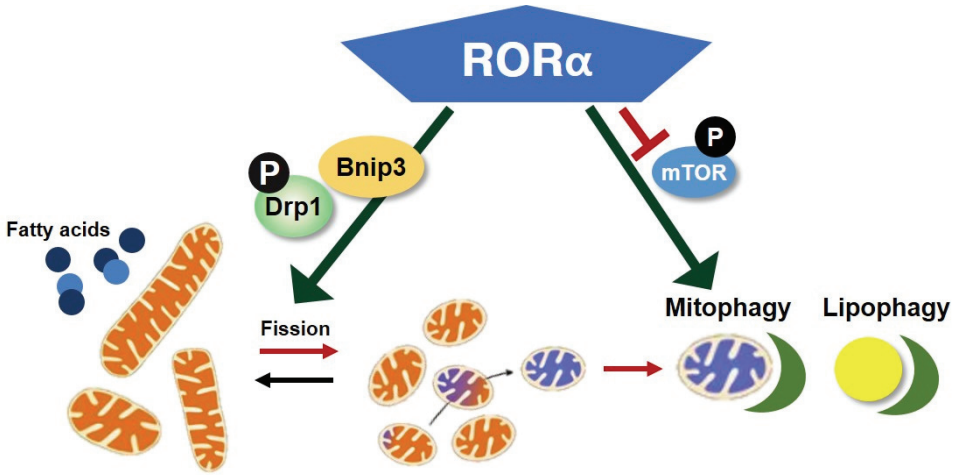

Figure 41. Summary: RORα-regulated mitochondrial fission and autophagy

RORα induced mitochodnrial fission by Bnip3 and p-Drp1 and increased autphagic activity by inactivation of mTOR signaling.

REFERENCES

Acquaah-Mensah, G.K., Agu, N., Khan, T., and Gardner, A. (2015). A Regulatory Role for the Insulin- and BDNF-Linked RORA in the Hippocampus: Implications for Alzheimer's Disease. J Alzheimers Dis 44, 827-838.

Akashi, M., and Takumi, T. (2005). The orphan nuclear receptor RORalpha regulates circadian transcription of the mammalian core-clock Bmal1. Nature structural & molecular biology 12, 441-448.

Baixauli, F., Acin-Perez, R., Villarroya-Beltri, C., Mazzeo, C., Nunez-Andrade, N., Gabande-Rodriguez, E., Ledesma, M.D., Blazquez, A., Martin, M.A., Falcon-Perez, J.M., et al. (2015). Mitochondrial Respiration Controls Lysosomal Function during Inflammatory T Cell Responses. Cell Metab 22, 485-498.

Bertin, R., Guastavino, J.M., and Portet, R. (1990). Effects of cold acclimation on the energetic metabolism of the Staggerer mutant mouse. Physiology & Behavior 47, 377-380.

Byrne, C.D., and Targher, G. (2015). NAFLD: a multisystem disease. J Hepatol 62, S47-64.

Chauvet, C., Bois-Joyeux, B., Berra, E., Pouyssegur, J., and Danan, J.L. (2004). The gene encoding human retinoic acid-receptor-related orphan receptor alpha is a target for hypoxia-inducible factor 1. The Biochemical journal 384, 79-85.

Chaveroux, C., Eichner, L.J., Dufour, C.R., Shatnawi, A., Khoutorsky, A., Bourque, G., Sonenberg, N., and Giguere, V. (2013). Molecular and genetic crosstalks between mTOR and ERRalpha are key determinants of rapamycin-induced nonalcoholic fatty liver. Cell Metab 17, 586-598.

Cheng, Z.Y., Guo, S.D., Copps, K., Dong, X.C., Kollipara, R., Rodgers, J.T., Depinho, R.A., Puigserver, P., and White, M.F. (2009). Foxo1 integrates

insulin signaling with mitochondrial function in the liver. Nat Med 15, 1307-U1105.

Cohen, J.C., Horton, J.D., and Hobbs, H.H. (2011). Human fatty liver disease: old questions and new insights. Science 332, 1519-1523.

Corona, J.C., and Duchen, M.R. (2016). PPARgamma as a therapeutic target to rescue mitochondrial function in neurological disease. Free radical biology & medicine 100, 153-163.

de Brito, O.M., and Scorrano, L. (2008). Mitofusin 2 tethers endoplasmic reticulum to mitochondria. Nature 456, 605-U647.

Demers-Lamarche, J., Guillebaud, G., Tlili, M., Todkar, K., Belanger, N., Grondin, M., Nguyen, A.P., Michel, J., and Germain, M. (2016). Loss of Mitochondrial Function Impairs Lysosomes. J Biol Chem 291, 10263-10276.

Dhingra, R., and Kirshenbaum, L.A. (2014). Regulation of Mitochondrial Dynamics and Cell Fate. Circ J 78, 803-810.

Drew, L., (2017). Fighting the fatty liver. Nature 550, S102-S103.

Dussault, I., Fawcett, D., Matthyssen, A., Bader, J.A., and Giguere, V. (1998). Orphan nuclear receptor ROR alpha-deficient mice display the cerebellar defects of staggerer. Mech Develop 70, 147-153.

Eftekharian, M.M., Noroozi, R., Sayad, A., Sarrafzadeh, S., Toghi, M., Azimi, T., Komaki, A., Mazdeh, M., Inoko, H., Taheri, M., et al. (2016). RAR-related orphan receptor A (RORA): A new susceptibility gene for multiple sclerosis. J Neurol Sci 369, 259-262.

Engelsdorf, T., Gigli-Bisceglia, N., Veerabagu, M., McKenna, J.F., Vaahtera, L., Augstein, F., Van der Does, D., Zipfel, C., and Hamann, T. (2018). The plant cell wall integrity maintenance and immune signaling systems cooperate to control stress responses in Arabidopsis thaliana. Science Signaling 11, eaao3070.

Fang, B., Everett, L.J., Jager, J., Briggs, E., Armour, S.M., Feng, D., Roy, A., Gerhart-Hines, Z., Sun, Z., Lazar, M.A. (2014). Circadian enhancers coordinate multiple phases of rhythmic gene transcription in vivo. Cell 159,

1140-1152.

Feng, D., Liu, T., Sun, Z., Bugge, A., Mullican, S.E., Alenghat, T., Liu, X.S., Lazar, M.A. (2011). A circadian rhythm orchestrated by histone deacetylase 3 controls hepatic lipid metabolism. Science 331, 1315-1319.

Finley, L.W.S., and Haigis, M.C. (2009). The coordination of nuclear and mitochondrial communication during aging and calorie restriction. Ageing Res Rev 8, 173-188.

Frederic, F., Chianale, C., Oliver, C., and Mariani, J. (2006). Enhanced endocrine response to novel environment stress and lack of corticosterone circadian rhythm in Staggerer (Rora sg/sg) mutant mice. J Neurosci Res 83, 1525-1532.

Fuchs, M., and Sanyal, A.J. (2012). Lipotoxicity in NASH. J Hepatol 56, 291-293.

Giguère, V., Tini, M., Flock, G., Ong, E., Evans, R.M., and Otulakowski, G. (1994). Isoform-specific amino-terminal domains dictate DNA-binding properties of ROR alpha, a novel family of orphan hormone nuclear receptors. Genes & Development 8, 538-553.

Glick, D., Zhang, W.S., Beaton, M., Marsboom, G., Gruber, M., Simon, M.C., Hart, J., Dorn, G.W., Brady, M.J., and Macleod, K.F. (2012). BNip3 Regulates Mitochondrial Function and Lipid Metabolism in the Liver. Mol Cell Biol 32, 2570-2584.

Gonzalez-Rodriguez, A., Mayoral, R., Agra, N., Valdecantos, M.P., Pardo, V., Miquilena-Colina, M.E., Vargas-Castrillon, J., Lo Iacono, O., Corazzari, M., Fimia, G.M., et al. (2014). Impaired autophagic flux is associated with increased endoplasmic reticulum stress during the development of NAFLD. Cell death & disease 5, e1179.

Hamilton, B.A., Frankel, W.N., Kerrebrock, A.W., Hawkins, T.L., FitzHugh, W., Kusumi, K., Russell, L.B., Mueller, K.L., vanBerkel, V., Birren, B.W., et al. (1996). Disruption of the nuclear hormone receptor ROR alpha in staggerer mice. Nature 379, 736-739.

Hamishehkar, H., Ranjdoost, F., Asgharian, P., Mahmoodpoor, A., Sanaie, S.

(2016). Vitamins, Are They Safe? Adv Pharm Bull 6, 467-477.

Han, J., and Wang, Y. (2018). mTORC1 signaling in hepatic lipid metabolism. Protein & cell 9, 145-151.

Han, Y.H., Kim, H.J., Kim, E.J., Kim, K.S., Hong, S., Park, H.G., and Lee, M.O. (2014). RORalpha decreases oxidative stress through the induction of SOD2 and GPx1 expression and thereby protects against nonalcoholic steatohepatitis in mice. Antioxid Redox Signal 21, 2083-2094.

Han, Y.H., Kim, H.J., Na, H., Nam, M.W., Kim, J.Y., Kim, J.S., Koo, S.H., and Lee, M.O. (2017). RORalpha Induces KLF4-Mediated M2 Polarization in the Liver Macrophages that Protect against Nonalcoholic Steatohepatitis. Cell reports 20, 124-135.

Handa, P., Maliken, B.D., Nelson, J.E., Morgan-Stevenson, V., Messner, D.J., Dhillon, B.K., Klintworth, H.M., Beauchamp, M., Yeh, M.M., Elfers, C.T., et al. (2014). Reduced adiponectin signaling due to weight gain results in nonalcoholic steatohepatitis through impaired mitochondrial biogenesis. Hepatology 60, 133-145.

Hanna, R.A., Quinsay, M.N., Orogo, A.M., Giang, K., Rikka, S., and Gustafsson, A.B. (2012). Microtubule-associated Protein 1 Light Chain 3 (LC3) Interacts with Bnip3 Protein to Selectively Remove Endoplasmic Reticulum and Mitochondria via Autophagy. J Biol Chem 287, 19094-19104.

He, B., Nohara, K., Park, N., Park, Y.S., Guillory, B., Zhao, Z., Garcia, J.M., Koike, N., Lee, C.C., Takahashi, J.S., et al. (2016). The Small Molecule Nobiletin Targets the Molecular Oscillator to Enhance Circadian Rhythms and Protect against Metabolic Syndrome. Cell Metab 23, 610-621.

Heinz, S., Benner, C., Spann, N., Bertolino, E., Lin, Y.C., Laslo, P., Cheng, J.X., Murre, C., Singh, H., Glass, C.K. (2010). Simple combinations of lineage-determining transcription factors prime cis-regulatory elements required for macrophage and B cell identities. Mol Cell 38, 576-589.

Hock, M.B., and Kralli, A. (2009). Transcriptional Control of Mitochondrial Biogenesis and Function. Annu Rev Physiol 71, 177-203.

Jacobi, D., Liu, S., Burkewitz, K., Kory, N., Knudsen, N.H., Alexander, R.K., Unluturk, U., Li, X., Kong, X., Hyde, A.L., et al. (2015). Hepatic Bmal1 Regulates Rhythmic Mitochondrial Dynamics and Promotes Metabolic Fitness. Cell Metab 22, 709-720.

Jetten, A.M. (2009). Retinoid-related orphan receptors (RORs): critical roles in development, immunity, circadian rhythm, and cellular metabolism. Nuclear receptor signaling 7, e003.

Kang, H.S., Okamoto, K., Takeda, Y., Beak, J.Y., Gerrish, K., Bortner, C.D., DeGraff, L.M., Wada, T., Xie, W., and Jetten, A.M. (2011). Transcriptional profiling reveals a role for ROR alpha in regulating gene expression in obesity-associated inflammation and hepatic steatosis. Physiol Genomics 43, 818-828.

Katsyuba, E., Mottis, A., Zietak, M., De Franco, F., van der Velpen, V., Gariani, K., Ryu, D., Cialabrini, L., Matilainen, O., Liscio, P., et al. (2018). De novo NAD(+) synthesis enhances mitochondrial function and improves health. Nature 563, 354-359.

Kim, E.J., Choi, Y.K., Han, Y.H., Kim, H.J., Lee, I.K., and Lee, M.O. (2014). RORalpha suppresses proliferation of vascular smooth muscle cells through activation of AMP-activated protein kinase. International journal of cardiology 175, 515-521.

Kim, E.J., Yoon, Y.S., Hong, S., Son, H.Y., Na, T.Y., Lee, M.H., Kang, H.J., Park, J., Cho, W.J., Kim, S.G., et al. (2012). Retinoic acid receptor-related orphan receptor alpha-induced activation of adenosine monophosphate-activated protein kinase results in attenuation of hepatic steatosis. Hepatology 55, 1379-1388.

Kim, K., Boo, K., Yu, Y.S., Oh, S.K., Kim, H., Jeon, Y., Bhin, J., Hwang, D., Kim, K.I., Lee, J.S., et al. (2017). RORalpha controls hepatic lipid homeostasis via negative regulation of PPARgamma transcriptional network. Nature communications 8, 162.

Kim, K.H., and Lee, M.S. (2014). Autophagy--a key player in cellular and body

metabolism. Nat Rev Endocrinol 10, 322-337.

Koek, G.H., Liedorp, P.R., and Bast, A. (2011). The role of oxidative stress in non-alcoholic steatohepatitis. Clin Chim Acta 412, 1297-1305.

Kumaki, Y., Ukai-Tadenuma, M., Uno, K.D., Nishio, J., Masumoto, K.H., Nagano, M., Komori, T., Shigeyoshi, Y., Hogenesch, J.B., and Ueda, H.R. (2008). Analysis and synthesis of high-amplitude Cis-elements in the mammalian circadian clock. Proc Natl Acad Sci U S A 105, 14946-14951.

Langmead, B., Trapnell, C., Pop, M., Salzberg, S.L. (2009). Ultrafast and memory-efficient alignment of short DNA sequences to the human genome. Genome Biol 10, R25.

Lau, P., Bailey, P., Dowhan, D.H., and Muscat, G.E.O. (1999). Exogenous expression of a dominant negative ROR alpha 1 vector in muscle cells impairs differentiation: ROR alpha 1 directly interacts with p300 and MyoD. Nucleic Acids Res 27, 411-420.

Lau, P., Fitzsimmons, R.L., Pearen, M.A., Watt, M.J., and Muscat, G.E.O. (2011). Homozygous staggerer (sg/sg) mice display improved insulin sensitivity and enhanced glucose uptake in skeletal muscle. Diabetologia 54, 1169-1180.

Lau, P., Fitzsimmons, R.L., Raichur, S., Wang, S.C.M., Lechtken, A., and Muscat, G.E.O. (2008). The orphan nuclear receptor, ROR alpha, regulates gene expression that controls lipid metabolism - Staggerer (sg/sg) mice are resistant to diet-induced obesity. J Biol Chem 283, 18411-18421.

Lee, J.M., Wagner, M., Xiao, R., Kim, K.H., Feng, D., Lazar, M.A., and Moore, D.D. (2014). Nutrient-sensing nuclear receptors coordinate autophagy. Nature 516, 112-115.

Liu, C., Li, S.M., Liu, T.H., Borjigin, J., and Lin, J.D. (2007). Transcriptional coactivator PGC-1a integrates the mammalian clock and energy metabolism. Nature 447, 477-U474.

Lu, Y., Liu, X., Jiao, Y., Xiong, X., Wang, E., Wang, X., Zhang, Z., Zhang, H., Pan, L., Guan, Y., et al. (2014). Periostin promotes liver steatosis and hypertriglyceridemia through downregulation of PPARα. The Journal of

Clinical Investigation 124, 3501-3513.

Mao, P.Z., and Reddy, P.H. (2010). Is multiple sclerosis a mitochondrial disease? Bba-Mol Basis Dis 1802, 66-79.

Martin, O.J., Lai, L., Soundarapandian, M.M., Leone, T.C., Zorzano, A., Keller, M.P., Attie, A.D., Muoio, D.M., and Kelly, D.P. (2014). Role for Peroxisome Proliferator-Activated Receptor. Coactivator-1 in the Control of Mitochondrial Dynamics During Postnatal Cardiac Growth. Circ Res 114, 626-636.

Neuschwander-Tetri, B.A., Loomba, R., Sanyal, A.J., Lavine, J.E., Van Natta, M.L., Abdelmalek, M.F., Chalasani, N., Dasarathy, S., Diehl, A.M., Hameed, B., et al. (2015). Farnesoid X nuclear receptor ligand obeticholic acid for non-cirrhotic, non-alcoholic steatohepatitis (FLINT): a multicentre, randomised, placebo-controlled trial. Lancet (London, England) 385, 956-965.

Oseini, A.M., and Sanyal, A.J. (2017). Therapies in non-alcoholic steatohepatitis (NASH). Liver international : official journal of the International Association for the Study of the Liver 37 Suppl 1, 97-103.

Ou, Z.M., Shi, X.J., Gilroy, R.K., Kirisci, L., Romkes, M., Lynch, C., Wang, H.B., Xu, M.S., Jiang, M.X., Ren, S.R., et al. (2013). Regulation of the Human Hydroxysteroid Sulfotransferase (SULT2A1) by ROR alpha and ROR gamma and Its Potential Relevance to Human Liver Diseases. Mol Endocrinol 27, 106-115.

Palikaras, K., and Tavernarakis, N. (2014). Mitochondrial homeostasis: The interplay between mitophagy and mitochondrial biogenesis. Exp Gerontol 56, 182-188.

Perez-Carreras, M., Del Hoyo, P., Martin, M.A., Rubio, J.C., Martin, A., Castellano, G., Colina, F., Arenas, J., and Solis-Herruzo, J.A. (2003). Defective hepatic mitochondrial respiratory chain in patients with nonalcoholic steatohepatitis. Hepatology 38, 999-1007.

Puertollano, R. (2014). mTOR and lysosome regulation. F1000prime reports 6, 52.

Raspe, E., Mautino, G., Duval, C., Fontaine, C., Duez, H., Barbier, O., Monte, D., Fruchart, J., Fruchart, J.C., and Staels, B. (2002). Transcriptional regulation

of human Rev-erb alpha gene expression by the orphan nuclear receptor retinoic acid-related orphan receptor alpha. J Biol Chem 277, 49275-49281.

Robinson, J.T., Thorvaldsdóttir, H., Winckler, W., Guttman, M., Lander, E.S., Getz, G., Mesirov, J.P. (2011). Integrative genomics viewer. Nat Biotechnol 29, 24-26.

Sanyal, A.J., Campbell-Sargent, C., Mirshahi, F., Rizzo, W.B., Contos, M.J., Sterling, R.K., Luketic, V.A., Shiffman, M.L., and Clore, J.N. (2001). Nonalcoholic steatohepatitis: Association of insulin resistance and mitochondrial abnormalities. Gastroenterology 120, 1183-1192.

Scarpulla, R.C. (2008). Transcriptional paradigms in mammalian mitochondrial biogenesis and function. Physiol Rev 88, 611-638.

Schattenberg, J.M., and Schuppan, D. (2011). Nonalcoholic steatohepatitis: the therapeutic challenge of a global epidemic. Curr Opin Lipidol 22, 479-488.

Schreiber, S.N., Emter, R., Hock, M.B., Knutti, D., Cardenas, J., Podvinec, M., Oakeley, E.J., and Kralli, A. (2004). The estrogen-related receptor alpha (ERR alpha) functions in PPAR gamma coactivator 1 alpha (PGC-1 alpha)-induced mitochondrial biogenesis. P Natl Acad Sci USA 101, 6472-6477.

Seok, S., Fu, T., Choi, S.E., Li, Y., Zhu, R., Kumar, S., Sun, X., Yoon, G., Kang, Y., Zhong, W., et al. (2014). Transcriptional regulation of autophagy by an FXR-CREB axis. Nature 516, 108-111.

Shi, X., Cheng, Q., Xu, L., Yan, J., Jiang, M., He, J., Xu, M., Stefanovic-Racic, M., Sipula, I., O'Doherty, R.M., et al. (2014). Cholesterol sulfate and cholesterol sulfotransferase inhibit gluconeogenesis by targeting hepatocyte nuclear factor 4alpha. Mol Cell Biol 34, 485-497.

Silveira, A.C., Morrison, M.A., Ji, F., Xu, H.Y., Reinecke, J.B., Adams, S.M., Arneberg, T.M., Janssian, M., Lee, J.E., Yuan, Y., et al. (2010). Convergence of linkage, gene expression and association data demonstrates the influence of the RAR-related orphan receptor alpha (RORA) gene on neovascular AMD: A systems biology based approach. Vision Res 50, 698-715.

Solt, L.A., and Burris, T.P. (2012). Action of RORs and their ligands in (patho)physiology. Trends Endocrin Met 23, 619-627.

Soriano, F.X., Liesa, M., Bach, D., Chan, D.C., Palacin, M., and Zorzano, A. (2006). Evidence for a mitochondrial regulatory pathway defined by peroxisome proliferator-activated receptor-gamma coactivator-1 alpha, estrogen-related receptor-alpha, and mitofusin 2. Diabetes 55, 1783-1791.

Steinmayr, M., Andre, E., Conquet, F., Rondi-Reig, L., Delhaye-Bouchaud, N., Auclair, N., Daniel, H., Crepel, F., Mariani, J., Sotelo, C., et al. (1998). staggerer phenotype in retinoid-related orphan receptor alpha-deficient mice. P Natl Acad Sci USA 95, 3960-3965.

Sumida, Y., and Yoneda, M. (2018). Current and future pharmacological therapies for NAFLD/NASH. Journal of gastroenterology 53, 362-376.

Todkar, K., Ilamathi, H.S., and Germain, M. (2017). Mitochondria and Lysosomes: Discovering Bonds. Frontiers in cell and developmental biology 5, 106.

Vega, R.B., Huss, J.M., and Kelly, D.P. (2000). The coactivator PGC-1 cooperates with peroxisome proliferator-activated receptor alpha in transcriptional control of nuclear genes encoding mitochondrial fatty acid oxidation enzymes. Mol Cell Biol 20, 1868-1876.

Velikkakath, A.K., Nishimura, T., Oita, E., Ishihara, N., and Mizushima, N. (2012). Mammalian Atg2 proteins are essential for autophagosome formation and important for regulation of size and distribution of lipid droplets. Molecular biology of the cell 23, 896-909.

Wang, X., Zhang, X., Chu, E.S.H., Chen, X., Kang, W., Wu, F., To, K.F., Wong, V.W.S., Chan, H.L.Y., Chan, M.T.V., et al. (2018). Defective lysosomal clearance of autophagosomes and its clinical implications in nonalcoholic steatohepatitis. FASEB journal : official publication of the Federation of American Societies for Experimental Biology 32, 37-51.

Wang, Y.M., Zhang, B., Xue, Y., Li, Z.J., Wang, J.F., Xue, C.H., and Yanagita, T. (2010). The mechanism of dietary cholesterol effects on lipids metabolism

in rats. Lipids in health and disease 9, 4.

Westermann, B. (2010). Mitochondrial fusion and fission in cell life and death. Nat Rev Mol Cell Bio 11, 872-884.

Yamada, T., Murata, D., Adachi, Y., Itoh, K., Kameoka, S., Igarashi, A., Kato, T., Araki, Y., Huganir, R.L., Dawson, T.M., et al. (2018). Mitochondrial Stasis Reveals p62-Mediated Ubiquitination in Parkin-Independent Mitophagy and Mitigates Nonalcoholic Fatty Liver Disease. Cell Metab 28, 588-604.e585.

Youle, R.J., and van der Bliek, A.M. (2012). Mitochondrial Fission, Fusion, and Stress. Science 337, 1062-1065.

Zhang, Y., Papazyan, R., Damle, M., Fang, B., Jager, J., Feng, D., Peed, L.C., Guan, D., Sun, Z., and Lazar, M.A. (2017). The hepatic circadian clock fine-tunes the lipogenic response to feeding through RORalpha/gamma. Genes Dev 31, 1202-1211.

Zolezzi, J.M., Silva-Alvarez, C., Ordenes, D., Godoy, J.A., Carvajal, F.J., Santos, M.J., and Inestrosa, N.C. (2013). Peroxisome Proliferator-Activated Receptor (PPAR) gamma and PPAR alpha Agonists Modulate Mitochondrial Fusion-Fission Dynamics: Relevance to Reactive Oxygen Species (ROS)-Related Neurodegenerative Disorders? Plos One 8.

Some of the contents of this thesis were published in the following journal.

Kim, H.J., Han, Y.H., Na, H., Kim, J.Y., Kim, T., Kim, H.J., Shin, C., Lee, J.W., Lee, M.O. (2017). Liver-specific deletion of RORα aggravates diet-induced nonalcoholic steatohepatitis by inducing mitochondrial dysfunction. Sci Rep 7, 16041.

초 록

비알콜성 지방간염 질환은 과도한 식이 섭취, 약물, 유전자적 원인으로 인하여 발생하는 대사성 질환으로 비만, 고지질혈증, 당뇨 등의 질환과 연관이 깊다. 비알콜성 지방간염은 지질 축적이 일어난 지방간의 상태에서 세포 손상, 염증이 동반되어 진행된 질환이다. 산화 스트레스, 지질 독성, 세포 사멸로 인한 분자적 매개체로 인해 일어나는데 이들 현상은 모두 미토콘드리아의 기능 손상에 의해 일어난다. 실제로 비알콜성 지방간염 질환을 가진 환자들의 간 내 미토콘드리아는 구조적 이상 및 기능적 이상을 나타내는 것이 알려져 있다. 미토콘드리아의 기능은 분열, 생합성, 미토콘드리아-특이적 자가포식이라는 다양한 작용을 통해 조절된다. 비알콜성 지방간염 발병에서의 미토콘드리아 기능조절인자를 밝히고 분자적 기전을 밝힌다면 해당 질환을 치료하는데 기여할 수 있다. 그러나 비알콜성 간염 질환을 치료하는 약물은 부재한 실정이며 현재 임상시험 중인 약물들은 미토콘드리아 기능 상실이라는 병인을 직접적으로 제거하기보다 비알콜성 지방간염에 의해 수반되는 병적 현상을 호전시키는 것에 무게를 두고 있고 이와 더불어 고지질혈증을 유발하는 등의 부작용 또한 보고되고 있다. 따라서 본 연구에서는 비알콜성 지방간염 치료에 있어서 미토콘드리아 기능을 직접 조절하는 인자를 발굴하고자 하며 후보 인자로서 핵 수용체 RORα을 제시하는 바이다. 구체적으로는 간세포 내 미토콘드리아 분열 및 자가포식 작용을 조절하는 분자적 기전을 규명함으로써 RORα를 비알콜성 지방간염 질환의 치료인자로 제시하고자 한다.

먼저 비알콜성 지방간염 질환에서의 RORα의 역할을 규명하고자 간세포 특이적 RORα 결손(RORα-LKO) 마우스를 제작하였고 고지질 식이를 12주간 수행하였을 때 비알콜성 지방간염이 발생한 것을 확인하였다. RORα-LKO 마우스의 간 조직 내 지질 축적과 간 손상 지표가 증가하였고 지질 과산화 및 염증 인자의 발현이 증가한

것을 관찰하였다. 또한 RORα-LKO의 간 조직 내 콜라겐 축적이 증가하였으며 섬유화 관련 인자의 단백질 발현이 증가하였다. 이상의 결과를 통해 RORα-LKO 마우스는 비알콜성 지방간염이 발병하기 쉽다는 것을 알 수 있었다. RORα-LKO 마우스에서 비알콜성 지방간염 병증이 심화된 이유를 전사체 분석을 통해 미토콘드리아 기능 손상에서 찾을 수 있었고, 실제 간 조직 내 미토콘드리아 구성 단백질의 발현과 기능이 RORα-LKO 마우스에서 감소되어 있었다. 전자현미경 분석 결과 RORα-LKO 마우스의 간 내 미토콘드리아가 구조적 이상을 갖거나 비정상적으로 커져 있는 것을 확인하였다. RORα-LKO 마우스에서 일차 배양 간세포를 분리한 후 미토콘드리아 기능의 지표 중 하나인 산소 소비량을 측정하였을 때 대조군에 비하여 감소되어 있음을 확인하였다. 또한 지방산 처리를 하여 미토콘드리아 분열을 유도하였을 때 대조군과 달리 RORα-LKO 마우스의 간세포에서는 분열이 일어나지 않았고 모양도 부풀어있는 등 비정상적인 형태였다. 분자적 기전을 규명하기 위하여 미토콘드리아 분열과 관련된 인자들의 단백질 발현을 확인한 결과, RORα-LKO 마우스의 간세포에서 Bnip3와 Drp1의 인산화가 감소되어 있는 것을 확인하였다.

다음으로, 자가포식 작용이 RORα에 의하여 조절될 수 있는지를 확인하였다. RORα-LKO 마우스의 간 조직 내 오토파고좀(autophagosome)이 감소되어 있는 것을 전자현미경 분석을 통해 확인하였다. p62, LC3-Ⅱ, NBR1의 단백질 축적 현상을 통해 자가포식능이 RORα-LKO 마우스에 감소된 것을 알 수 있었다. RORα-LKO 마우스에서 일차 배양 간세포를 분리하고 바필로마이신(bafilomycin) 약물 처리를 통한 LC3-Ⅱ의 축적을 통해 자가포식능을 확인한 결과 RORα 결손으로 인하여 감소되어 있었다. 선택적 자가포식 작용 중에서 미토콘드리아 기능 조절과 관련된 미토콘드리아-선택적 자가포식능을 확인했을 때 RORα-LKO 마우스의 간 내

미토파고좀(mitophagosome)의 형성이 줄어들어 있었다. 일차 배양 간세포를 분리하고 지방산 처리를 통해 미토콘드리아-선택적 자가포식 현상을 유도하였을 때 RORα-LKO에 의하여 미토콘드리아-선택적 자가포식 작용이 억제되어 있었다. 또한 리소좀에 의한 미토콘드리아의 분해 현상이 RORα 결손에 의해 줄어들었다. 손상된 미토콘드리아의 분해와 함께 자가포식 작용을 통한 지질 분해 현상이 비알콜성 지방간염 완화에 도움을 주는 바, RORα-LKO 마우스에서 지질-특이적 자가포식 작용이 변화되어 있는지 확인하고자 하였다. 그 결과, RORα-LKO 마우스 간 내 리포파고좀(lipophagosome)의 형성이 줄어들었으며 일차 배양 간세포에서 지질-특이적 자가포식 작용과 리소좀에 의한 분해 현상 또한 감소되었음을 확인하였다. RORα을 과발현하였을 때 자가포식능이 증가하였고, 이러한 현상이 mTOR의 비활성화를 통해 일어남을 확인하였다. RORα-LKO 마우스의 간에서 mTOR의 활성이 증가되어 있었다. 뿐만 아니라 RORα의 과발현을 통해 자가포식 및 리소좀 기능과 관련된 유전자 발현이 증가되는 것을 확인하였다.

이상의 연구 결과를 통해 핵 수용체 중 하나인 RORα가 미토콘드리아의 분열뿐만 아니라 자가포식능을 조절함으로써 비알콜성 지방간염을 완화시켰음을 확인하였다. 본 연구를 통해 핵 수용체 RORα를 미토콘드리아 기능조절인자이자 비알콜성 지방간염의 핵심 치료인자로 제시하는 바이다.

주요어 : 비알콜성 지방간염, 미토콘드리아 역동성, 자가포식, RORα

학번 : 2011-21714